Electronic Supplementary Material (ESI) for Inorganic Chemistry Frontiers.

Supporting Information

Different effect of metal-NHC bond cleavage on the Pd/NHC and Ni/NHC catalyzed α-arylation of ketones with aryl halides

Konstantin E. Shepelenko[a], Safarmurod B. Soliev[a], Alexey S. Galushko,[b] Victor M. Chernyshev*[a], Valentine P. Ananikov*[a],[b]

[a] Platov South-Russian State Polytechnic University (NPI), 346428, Novocherkassk, Prosveshcheniya st., 132
E-mail: chern13@yandex.ru
[b] Zelinsky Institute of Organic Chemistry, Russian Academy of Sciences, Leninsky Prospect 47, Moscow, 119991, Russia
E-mail: val@ioc.ac.ru

Table of contents

S1. Additional experimental data

Table S1. Catalytic activities of Pd precatalysts **1a,d**, and $Pd(OAc)_2$ in the arylation of **3a** with bromo- and iodoarenes in the presence of TBAB[a].

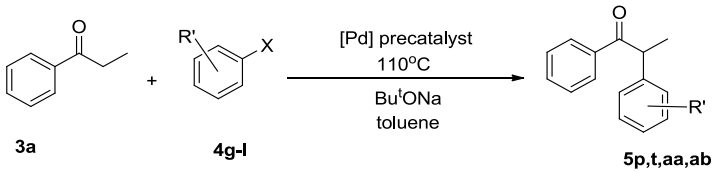

3a **4g-l** **5p,t,aa,ab**

Entry	Precatalyst	Ar-Br	GC-MS yield of 5	Entry	Precatalyst	Ar-I	GC-MS yield of 5
1	**1d**	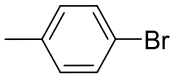 **4g**	**5aa** (99%)	10	**1d**	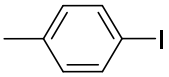 **4j**	**5aa** (99%)
2	**1a**	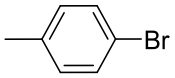 **4g**	**5aa** (90%)	11	**1a**	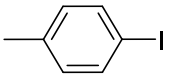 **4j**	**5aa** (92%)
3	$Pd(OAc)_2$ + TBAB	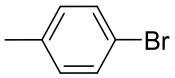 **4g**	**5aa** (98%)	12	$Pd(OAc)_2$ + TBAB	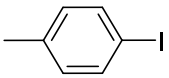 **4j**	**5aa** (98%)
4	**1d**	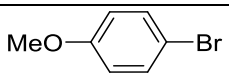 **4h**	**5p** (99%)	13	**1d**	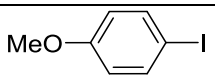 **4k**	**5p** (99%)
5	**1a**	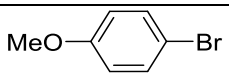 **4h**	**5p** (90%)	14	**1a**	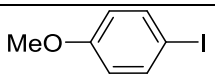 **4k**	**5p** (92%)
6	$Pd(OAc)_2$ + TBAB	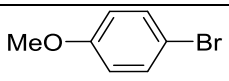 **4h**	**5p** (98%)	15	$Pd(OAc)_2$ + TBAB	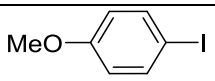 **4k**	**5p** (98%)
7	**1d**	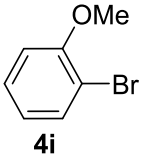 **4i**	**5ab** (98%)	16	**1d**	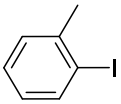 **4l**	**5t** (99%)
8	**1a**	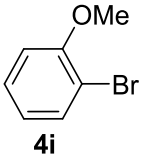 **4i**	**5ab** (90%)	17	**1a**	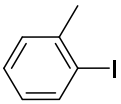 **4l**	**5t** (94%)
9	$Pd(OAc)_2$ + TBAB	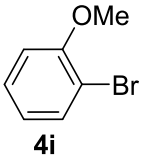 **4i**	**5ab** (98%)	18	$Pd(OAc)_2$ + TBAB	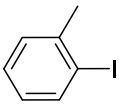 **4l**	**5t** (98%)

[a] Ketone **3a** (60.1 mg, 0.5 mmol), corresponding aryl halide **4g-j** (0.5 mmol), Bu^tONa (1 mmol), toluene (2 mL), precatalyst (1 mol% of Pd compound), TBAB (16.1 mg, 0.05 mmol, 10 mol%) were heated at 110 °C within 5 h.

Table S2. Extended data on catalytic activities of Pd and Ni precatalysts in the arylation of ketones **3a,b** with chlorobenzene **4a**[a].

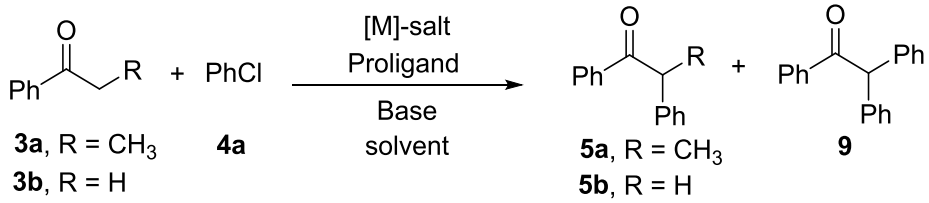

3a, R = CH_3 **4a** **5a**, R = CH_3 **9**

3b, R = H **5b**, R = H

Entry	Ketone	[M]-salt (mol. %)[b,c]	Base	Solvent	Proligand (mol%)[c]	Temp [ºC]	Time [h]	C[d] [%]	GC-MS yield [%]		
									5a	**5b**	**9**
1	**3a**	$Pd(OAc)_2$ (1)	**Bu^{t}ONa**	**toluene**	**IPr · HCl** (2)	110	5	99	94		
2	**3a**	$Ni(OAc)_2$ (5)	**Bu^{t}ONa**	**toluene**	**IPr · HCl** (10)	110	24	89	86		
3	**3a**	$NiSO_4$ (5)	**Bu^{t}ONa**	**toluene**	**IPr · HCl** (10)	110	24	64	52		
4	**3a**	$Ni(Cp)_2$ (5)	**Bu^{t}ONa**	**toluene**	**IPr · HCl** (10)	110	24	2	0		
5	**3a**	$Ni(AcAc)_2$ (5)	**Bu^{t}ONa**	**toluene**	**IPr · HCl** (10)	110	24	91	80		
6	**3a**	$NiCl_2Py_2$ (5)	**Bu^{t}ONa**	**toluene**	**IPr · HCl** (10)	110	24	95	91		
7	**3a**	$NiCl_2Py_2$ (5)	**Bu^{t}ONa**	**1,4-Dioxane**	**IPr · HCl** (10)	100	24	2	trace		
8	**3a**	$NiCl_2Py_2$ (5)	**Bu^{t}ONa**	**THF**	**IPr · HCl** (10)	70	24	3	trace		
9	**3a**	$NiCl_2Py_2$ (5)	**Bu^{t}ONa**	**IPrOH**	**IPr · HCl** (10)	80	24	2	0		
10	**3a**	$NiCl_2Py_2$ (5)	**Bu^{t}ONa**	**DMA**	**IPr · HCl** (10)	110	24	7	trace		
11	**3a**	$NiCl_2Py_2$ (5)	**Bu^{t}OK**	**toluene**	**IPr · HCl** (10)	110	24	84	71		
12	**3a**	$NiCl_2Py_2$ (5)	**KOH**	**toluene**	**IPr · HCl** (10)	110	24	2	0		
13	**3a**	$NiCl_2Py_2$ (5)	**Cs_2CO_3**	**toluene**	**IPr · HCl** (10)	110	24	45	trace		
14	**3a**	$NiCl_2Py_2$ (5)	**K_2CO_3**	**toluene**	**IPr · HCl** (10)	110	24	2	0		
15	**3a**	$NiCl_2Py_2$ (5)	**NaH**	**toluene**	**IPr · HCl** (10)	110	24	5	trace		
16	**3a**	$NiCl_2Py_2$ (5)	**Bu^{t}ONa**	**toluene**	**IPr · HCl** (10)	115	24	98	90		
17	**3a**	$NiCl_2Py_2$ (5)	**Bu^{t}ONa**	**toluene**	**IPr · HCl** (10)	100	24	84	80		
18	**3a**	$NiCl_2Py_2$ (10)	**Bu^{t}ONa**	**toluene**	**IPr · HCl** (20)	110	24	96	91		
19	**3a**	$NiCl_2Py_2$ (5)	**Bu^{t}ONa**	**toluene**	**IPr · HCl** (5)	110	24	62	59		
20	**3a**	$NiCl_2Py_2$ (2.5)	**Bu^{t}ONa**	**toluene**	**IPr · HCl** (5)	110	36	53	49		
21	**3a**	$NiCl_2Py_2$ (5)	**Bu^{t}ONa**	**toluene**	**IPr*OMe · HCl** (10)	110	24	97	92		
22	**3a**	$NiCl_2Py_2$ (2.5)	**Bu^{t}ONa**	**toluene**	**IPr*OMe · HCl** (5)	110	24	84	80		
23	**3b**	$Pd(OAc)_2$ (1)	**Bu^{t}ONa**	**toluene**	**IPr · HCl** (2)	110	5	49		46	1
24	**3b**	$Pd(OAc)_2$ (1)	**Bu^{t}ONa**	**1,4-Dioxane**	**IPr · HCl** (2)	100	5	81		71	3
25	**3b**	$Pd(OAc)_2$ (1)	**Bu^{t}ONa**	**THF**	**IPr · HCl** (2)	70	5	64		62	0
26	**3b**	$Pd(OAc)_2$ (1)	**Bu^{t}ONa**	**toluene**	**IPr · HCl** (2)	80	5	94		87	0
27	**3b**	$Pd(OAc)_2$ (0.1)	**Bu^{t}ONa**	**toluene**	**IPr · HCl** (0.2)	80	24	12		10	0
28	**3b**	$Pd(OAc)_2$ (0.1)	**Bu^{t}ONa**	**toluene**	**IPr*OMe · HCl** (0.2)	80	24	99		90	3
29	**3b**	$Pd(OAc)_2$ (0.1)	**Bu^{t}ONa**	**toluene**	**IPr*OMe · HCl** (0.3)	80	24	99		91	2

30	**3b**	$Pd(OAc)_2$ (0.1)	**Bu^{t}ONa**	**toluene**	**IPr*OMe · HCl** (0.05)	80	36	45		42	0
31	**3b**	$Pd(OAc)_2$ (0.05)	**Bu^{t}ONa**	**toluene**	**IPr*OMe · HCl** (0.1)	80	36	99		84	2
32	**3b**	$Pd(acac)_2$ (1)	**Bu^{t}ONa**	**toluene**	**IPr · HCl** (2)	80	5	49		46	0
33	**3b**	$PdCl_2Py_2$ (1)	**Bu^{t}ONa**	**toluene**	**IPr · HCl** (2)	80	5	41		27	0
34	**3b**	$NiCl_2Py_2$ (5)	**Bu^{t}ONa**	**toluene**	**IPr · HCl** (10)	110	24	10		2	0
35	**3b**	$NiCl_2$Py2 (5)	**Bu^{t}ONa**	**toluene**	**IPr*OMe · HCl** (10)	110	24	8		4	0

[a] Reaction conditions: PhCl (0.5 mmol), propiophenone **3a** (0.5 mmol) or acetophenone **3b** (0.75 mmol), base (1 mmol), solvent (2 mL). [b] OAc – acetate, acac – acetylacetonate, Cp – cyclopentadienyl anion, Py – pyridine. [c] Relative to PhCl. [d] Conversion of **4a**.

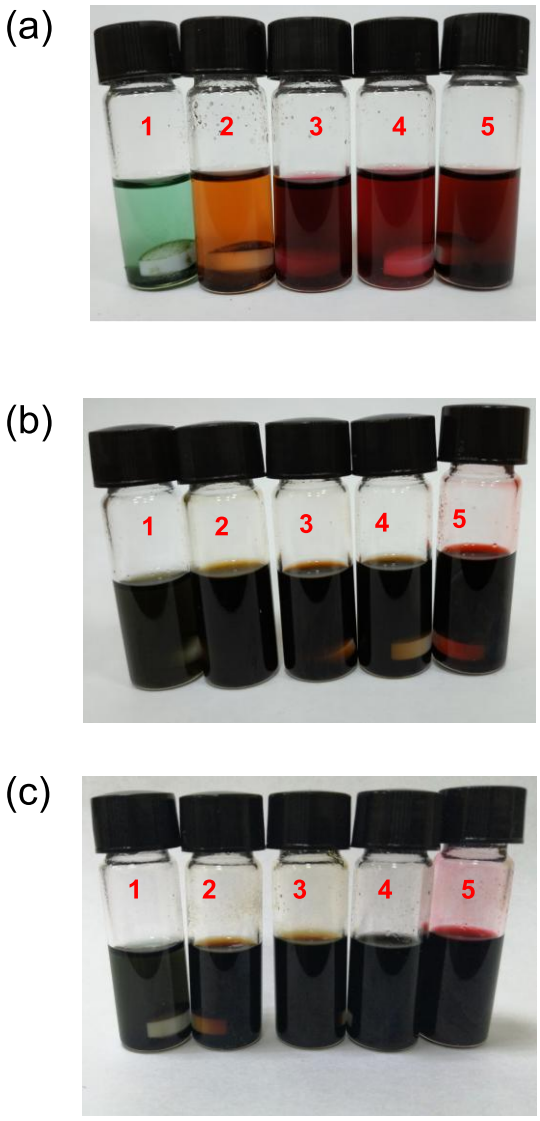

Figure S1. Photos of mixtures of 0.05 mmol of Ni precatalyst [$NiCp_2$ (1), complex **2a** (2), complex **2c** (3), complex **2d** (4), complex **2h** (5)] with Bu^tONa (0.5 mmol) in toluene (2 ml): freshly prepared mixture at room temperature (a); after 5 min of heating at 110°C (b); after 30 min of heating at 110°C (c).

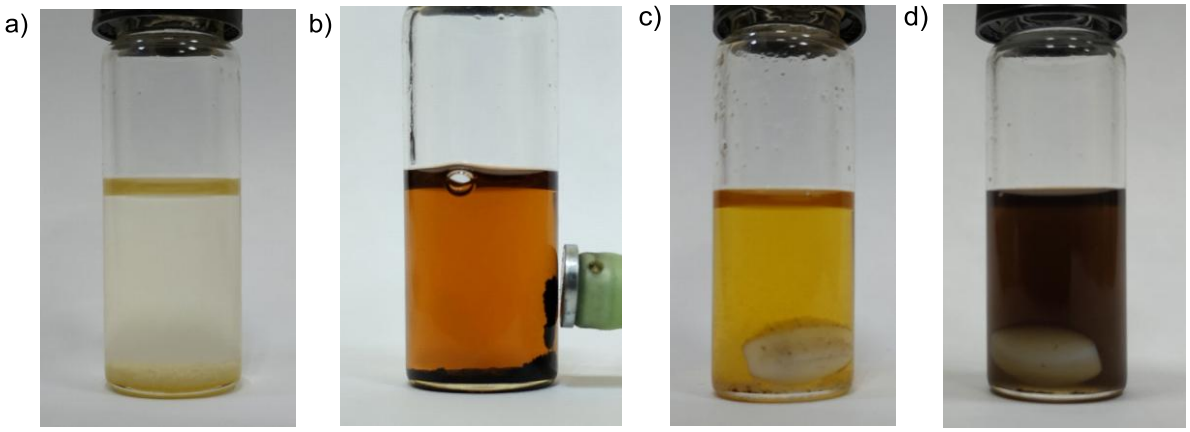

Figure S2. Photos of mixtures of Pd and Ni precatalysts (0.1 mmol) with ButONa (0.5 mmol): $NiCl_2$ before (a) and after (b) heating at 110°C within 10 h; $Pd(OAc)_2$ before (c) and after (d) heating at 110°C within 10 h.

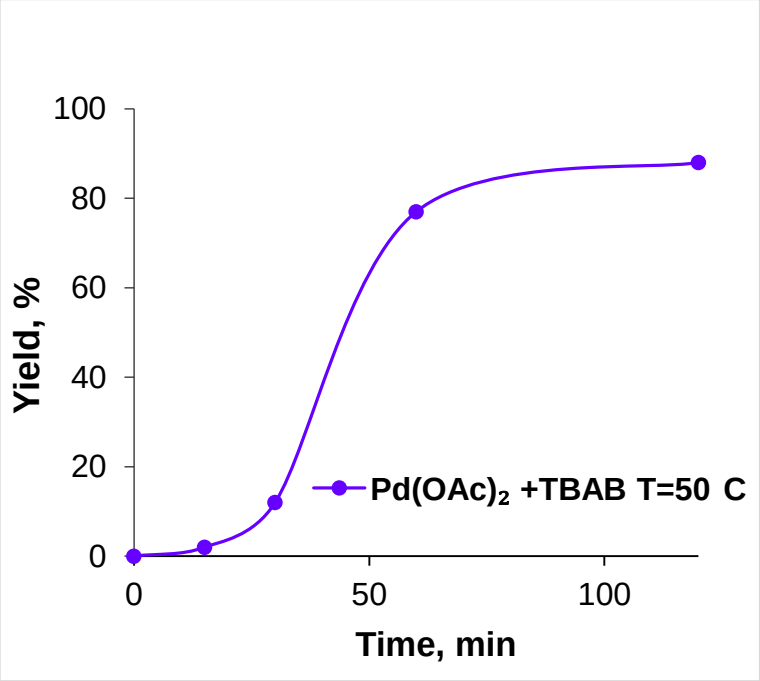

Figure S3. Kinetic plot of the yield of compound **5a** in the reaction of propiophenone **3a** with PhI catalyzed by $Pd(OAc)_2$ at 50 °C. Reaction conditions: ketone **3a** (0.5 mmol), PhI (0.5 mmol), Bu^tONa (1 mmol), toluene (2 mL), $Pd(OAc)_2$ ($0.5 \cdot 10^{-2}$ mmol, 1 mol), TBAB (0.05 mmol).

S2. Hg-poisoning experiments

The Hg poisoning experiments were performed to evaluate the credibility of Hg-poisoning experiments, the so-called mercury test (Hg-drop test), to the ketones α-arylation reaction. The mercury test was widely used for a long time as a rapid method for distinguishing truly homogeneous molecular catalysis from nanoparticle metal catalysis. The method is based on the assumption that metallic mercury should selectively poison M(0) nanoparticles and should be inert toward molecular metal complexes [1-3]. Inhibition of a catalytic reaction in the presence of metallic mercury is typically considered as evidence of a nanoparticle catalysis mechanism. In contrast, the absence of a significant effect of mercury on the metal-catalyzed reaction is accepted as a sign of a homogeneous catalysis mechanism.

One may assume that the mercury test may be used to elucidate the nature of the metal active species (molecular complexes or nanoparticles) in the Pd- and Ni-catalyzed reactions of ketone α-arylation.

However, the credibility of the mercury test was recently subjected to criticism [4-7]. It was found that the mercury test may be generally inadequate as a method for distinguishing between homogeneous and cluster/nanoparticle catalysis mechanisms for the following reasons: (i) the general and facile reactivity of molecular metal complexes toward metallic mercury and (ii) the very high and often unpredictable dependence of the test results on the operational conditions [4].

The effects of Hg loadings, temperature, and solvent on the yields of propiophenone arylation products under Pd and Ni catalysis are presented in Tables S3 and S4, correspondingly.

First of all, let us consider the effect of mercury loadings on the yields of **5a** in the reaction with chlorobenzene in toluene catalyzed by complex **1d** at various temperatures (Table S3, entries 9-11, 20-22, 23-25). The observed effect of mercury poisoning at 110 °C (entries 9-11) is quite low: the yield of **5a** decreases from 99% without Hg to 87% with 300 mol eq Hg loaded and to 85% with 2000 mol eq Hg loaded. Because the effect of Hg is low, the homogeneous molecular Pd/NHC catalysis mechanism can be concluded from the test results. However, at a lower temperature, the effect of mercury is quite high. At 90 °C (entries 20-22) the yield decreases from 93% in the absence of Hg to 35% in the presence of 2000 mol eq Hg. At 70 °C (entries 23-25) the effect of mercury is even higher: the yield decreases from 80% (without Hg) to 41% (300 mol eq Hg) and to 12% (2000 mol eq Hg). So, the opposite conclusion that Pd nanoparticles operate as active centers follows from the experiments performed at 90 °C and 70 °C. It seems to be very doubtful that the homogeneous molecular Pd/NHC catalysis mechanism dominates at 110 °C whereas the heterogeneous Pd nanoparticle catalysis mechanism dominates at 90 °C and 70 °C for the same quite stable Pd/NHC complex **1d** in the reaction of the same reagents in toluene. **These experiments clearly demonstrate the unreliability of the mercury test for distinguishing the nature of Pd active particles in the Pd/NHC catalyzed ketone α-arylation reaction**.

Further, let us consider the effect of the mercury poisoning on the yields of the arylated product in the Pd catalyzed reaction with iodobenzene (Table S3, the rightmost column). The effect of the mercury is very low, regardless of the Pd precatalyst. So, it may be concluded that the same molecular species operate as active centers, whereas very different Pd precatalysts ($Pd(OAc)_2$, low-stable Pd/NHC complex **1a**, and quite stable Pd/NHC complex **1d** with bulky NHC ligand) were used.

Finally, experiments on the Hg poisoning of Ni/NHC catalyzed arylation of propiophenone can be discussed (Table S4). Even small amounts of mercury result in significant inhibition of the reaction both with PhI and PhCl. It should be concluded from the Hg poisoning experiments that the Ni nanoparticle catalysis mechanism dominates in the arylation reactions catalyzed by Ni/NHC complexes containing bulky NHC ligands. This conclusion contradicts the results of experiments with the preliminary decomposition of the precatalysts (see Table 1 in the article, entries 18, 19, Method B) and to experiments with the use of ligandless Ni precatalysts (Table 1 in the article, entries 20, 21), and most of the literature data [8-13].

Overall, the results presented in Tables S3 and S4 demonstrate the general unreliability of the mercury test for distinguishing between homogeneous and nanoparticle catalysis mechanisms in the ketone α-arylation reaction.

Table S3. Effects of Hg loading and other reaction conditions on the yields of propiophenone arylation products under catalysis with various Pd precatalysts.

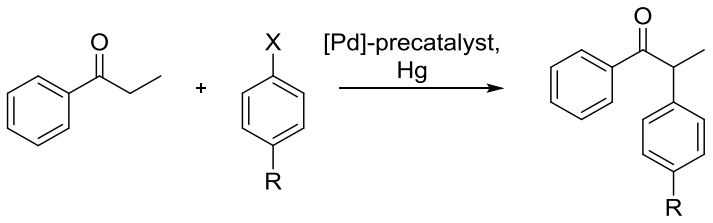

3a **4a,c,g** **5a, 5aa**

Entry	[Pd]-precetalyst	Temp, °C	Solvent	Hg, eq[b]	Time, h	GC-MS Yield, **5**, %		
						X=Cl, R=H	X=Br R=Me	X=I, R=H
1	$Pd(OAc)_2$	110	Toluene	0	2	0	92	99
2	$Pd(OAc)_2$	110	Toluene	300	2	0	22	98
3	$Pd(OAc)_2$	110	Toluene	2000	2	0	20	90
4	**1a**	110	Toluene	0	2	0	87	94
5	**1a**	110	Toluene	50	2	0	60	93
6	**1a**	110	Toluene	100	2	0	52	95
7	**1a**	110	Toluene	300	2	0	18	87
8	**1a**	110	Toluene	2000	2	0	3	89
9	**1d**	110	Toluene	0	2	99	92	99
10	**1d**	110	Toluene	300	2	87	89	98
11	**1d**	110	Toluene	2000	2	85	91	98
12	**1d**	100	Dioxane	0	2	92	94	91
13	**1d**	100	Dioxane	300	2	68	87	94
14	**1d**	100	Dioxane	2000	2	56	81	91
15	$Pd(OAc)_2$	90	Toluene	0	2	0	91	94
16	$Pd(OAc)_2$	90	Toluene	50	2	0	65	91
17	$Pd(OAc)_2$	90	Toluene	100	2	0	48	92
18	$Pd(OAc)_2$	90	Toluene	300	2	0	24	87
19	$Pd(OAc)_2$	90	Toluene	2000	2	0	11	90
20	**1d**	90	Toluene	0	2	93	93	95
21	**1d**	90	Toluene	300	2	86	94	96
22	**1d**	90	Toluene	2000	2	35	92	94
23	**1d**	70	Toluene	0	2	80	91	89
24	**1d**	70	Toluene	300	2	41	93	88
25	**1d**	70	Toluene	2000	2	12	92	89

[a]Reaction conditions: ArX (0.5 mmol), propiophenone (0.5 mmol), Bu^tONa (1 mmol), toluene (2 mL), [Pd]-precatalyst (0.005 mmol), magnetic stirrer rotation rate was 1000 rpm. [b] Mol eq Hg relative to the amount of Pd precatalyst.

Table S4. Effects of Hg loading and other reaction conditions on the yields of propiophenone arylation products under catalysis with Ni/NHC complexes.

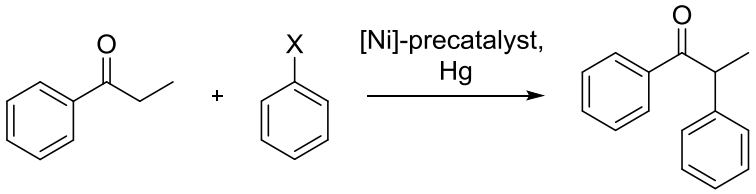

3a **4a,c** **5a**

Entry	[Ni]-precatalyst	Temp, °C	Solvent	Hg, eq[b]	Time, h	GC-MS Yield, **5**, %	
						X=Cl	X=I
1	**2g**	110	Toluene	0	24	63	84
2	**2g**	110	Toluene	300	24	20	18
3	**2g**	110	Toluene	2000	24	12	10
4	**2h**	110	Toluene	0	24	82	91
5	**2h**	110	Toluene	50	24	54	41
6	**2h**	110	Toluene	100	24	20	17
7	**2h**	110	Toluene	300	24	21	25
8	**2h**	110	Toluene	2000	24	18	24

[a]Reaction conditions: ArX (0.5 mmol), propiophenone (0.5 mmol), Bu^tONa (1 mmol), toluene (2 mL), [Ni]-precatalyst (0.015 mmol), magnetic stirrer rotation rate was 1000 rpm. [b] Mol eq Hg relative to amount of Ni/NHC precatalyst.

References

1. Widegren J. A.; Finke R. G. A review of the problem of distinguishing true homogeneous catalysis from soluble or other metal-particle heterogeneous catalysis under reducing conditions *J. Mol. Catal. A: Chem.* **2003**, *198*, p. 317. doi: *10.1016/s1381-1169(02)00728-8*.
2. Crabtree R. H. Resolving heterogeneity problems and impurity artifacts in operationally homogeneous transition metal catalysts *Chem. Rev.* **2012**, *112*, p. 1536. doi: *10.1021/cr2002905*.
3. Sonnenberg J. F.; Morris R. H. Distinguishing homogeneous from nanoparticle asymmetric iron catalysis *Catal. Sci. Technol.* **2014**, *4*, p. 3426. doi: *10.1039/c4cy00468j*.
4. Chernyshev V. M.; Astakhov A. V.; Chikunov I. E.; Tyurin R. V.; Eremin D. B.; Ranny G. S.; Khrustalev V. N.; Ananikov V. P. Pd and Pt Catalyst Poisoning in the Study of Reaction Mechanisms: What Does the Mercury Test Mean for Catalysis? *ACS Catal.* **2019**, *9*, p. 2984. doi: *10.1021/acscatal.8b03683*.
5. Gorunova O. N.; Novitskiy I. M.; Grishin Y. K.; Gloriozov I. P.; Roznyatovsky V. A.; Khrustalev V. N.; Kochetkov K. A.; Dunina V. V. When Applying the Mercury Poisoning Test to Palladacycle-Catalyzed Reactions, One Should Not Consider the Common Misconception of Mercury(0) Selectivity *Organometallics* **2018**, *37*, p. 2842. doi: *10.1021/acs.organomet.8b00363*.
6. Schmidt A. F.; Kurokhtina A. A.; Larina E. V. Analysis of Differential Selectivity Using Phase Trajectories of Catalytic Reactions: New Aspects and Applications *Kinetics and Catalysis* **2019**, *60*, p. 551. doi: *10.1134/S0023158419050100*.
7. Gorunova O. N.; Novitskiy I. M.; Grishin Y. K.; Gloriozov I. P.; Roznyatovsky V. A.; Khrustalev V. N.; Kochetkov K. A.; Dunina V. V. The use of control experiments as the sole route to correct the mechanistic interpretation of mercury poisoning test results: The case of P,C-palladacycle-catalysed reactions *J. Organomet. Chem.* **2020**, *916*, p. 121245. doi: *https://doi.org/10.1016/j.jorganchem.2020.121245*.

8. Matsubara K.; Ueno K.; Koga Y.; Hara K. Nickel–NHC-Catalyzed α-Arylation of Acyclic Ketones and Amination of Haloarenes and Unexpected Preferential N-Arylation of 4-Aminopropiophenone *J. Org. Chem.* **2007**, *72*, p. 5069. doi: *10.1021/jo070313d*.
9. Henrion M.; Chetcuti M. J.; Ritleng V. From acetone metalation to the catalytic α-arylation of acyclic ketones with NHC–nickel(ii) complexes *Chem. Commun.* **2014**, *50*, p. 4624. doi: *10.1039/C4CC00959B*.
10. Fernández-Salas J. A.; Marelli E.; Cordes D. B.; Slawin A. M. Z.; Nolan S. P. General and Mild Ni0-Catalyzed α-Arylation of Ketones Using Aryl Chlorides *Chem. - Eur. J.* **2015**, *21*, p. 3906. doi: *10.1002/chem.201406457*.
11. Marelli E.; Fernández Salas J. A.; Nolan S. P. Synthesis of an Intermediate of Nafoxidine via Nickel-Catalyzed Ketone Arylation *Synthesis* **2015**, *47*, p. 2032. doi: *10.1055/s-0034-1380813*.
12. Li J.; Wang Z.-X. Nickel catalyzed α-arylation of ketones with aryltrimethylammonium triflates *Org. Biomol. Chem.* **2016**, *14*, p. 7579. doi: *10.1039/C6OB01299J*.
13. Li J.; Wang Z.-X. Nickel-Catalyzed Transformation of Aryl 2-Pyridyl Ethers via Cleavage of the Carbon–Oxygen Bond: Synthesis of Mono-α-arylated- Ketones *Synthesis* **2018**, *50*, p. 3217. doi: *10.1055/s-0037-1609963*.

S3. Quantitative poisoning experiments

The methodology of quantitative poisoning (quantitative kinetic poisoning) developed by the Finke group is used for determining the nature of catalyst active species and distinguishing between molecular and cluster/nanoparticle mechanisms in transition metal catalysis [1-6]. The method is based on the use of nonselective poisons capable of strong binding with active centers of various catalyst species. Distinguishing between truly homogeneous and cluster/nanoparticle catalysis is based on the amount of the poison required for complete inhibition of catalytic activity. The quantity of the poison << 1 eq. (usually ~0.02-0.2 eq.) per metal amount signifies cluster/nanoparticle catalysis, whereas quantity ≥ 1 eq. indicates molecular catalysis [7]. The logic of the method is based on the assumption that nanoparticles contain only a fraction of active metal atoms on the surface, whereas molecular complex requires at least a stoichiometric amount of poison to be completely deactivated [5, 8]. Quantitative kinetic poisoning includes determining the catalytic reaction rates in the presence of various amounts of catalyst poison (starting from the substoichiometric amounts) and building plots of the relative rate (rate in the presence of poison/rate in the absence of poison) vs equiv of added poison in which the x-intercept of the linear extrapolated portion of the data implies the amount of poison required to totally poison the active catalyst.

To the best of our knowledge, quantitative kinetic poisoning was never used before for studying Pd/NHC-catalyzed ketone α-arylation. Therefore, we tested several typical catalyst poisons to find the poison suitable for quantitative kinetic poisoning experiments (Table S5). Among the studied poisons, only CS_2 demonstrated reasonable results, whereas other poisons were inefficient (Table S5). Therefore, CS_2 was selected as the poison for quantitative kinetic poisoning experiments.

The quantitative kinetic poisoning experiments were performed for the reaction of propiophenone **3a** arylation by iodobenzene **4c** catalyzed with complex **1a** and $Pd(OAc)_2$ (Figure S4). The plots "relative rate versus relative CS_2 loading" are quite similar and show that only ~0.2 mol eq of CS_2 is required for almost complete suppressing of the arylation reaction. These results point to the high probability that small Pd aggregates (more probably, Pd clusters) play an important role of active centers in the studied catalytic systems. It is noteworthy that a flatter graph is observed in the case of Pd/NHC precatalyst **1a** (Figure S4, a) than in the case of palladium acetate (Figure S4, b). This can speak in favor of the cocktail-type character of the Pd/NHC catalytic system and the slight contribution of molecular NHC-connected Pd complexes into catalysis.

Of course, these results can be considered as preliminary only. This question deserves a special in-depth study, which is beyond the scope of this work.

Table S5. Effect of various catalytic poisons on the yield of compound **5a**[a].

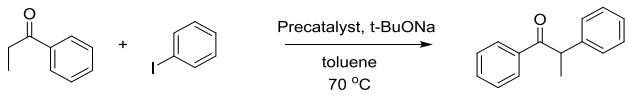

3a **4c** **5a**

Precatalyst, (1 mol%)	Poison, (eq)	GC-MS Yield, **5a**, %
1a	none	99
1a	CS_2 (0.1)	65
1a	CS_2 (0.5)	0
1a	CS_2 (1.0)	0
1a	PPh_3(1.0)	30
1a	1,10-Phenantroline (0.5)	99
1a	1,10-Phenantroline (1)	99
1a	$N(Et)_3$ (0.5)	99
1a	$N(Et)_3$ (1.0)	99
1a	PhSH (0.5)	99
1a	PhSH (1.0)	99
$Pd(OAc)_2$	CS_2 (0.5)	0

[a]Reaction conditions: PhI (0.75 mmol), propiophenone (0.5 mmol), Bu^tONa (1 mmol), toluene (2 mL), [Pd]-precatalyst (0.005 mmol), 70 °C, within 2 h, Mol eq of poison relative to the amount of Pd precatalyst.

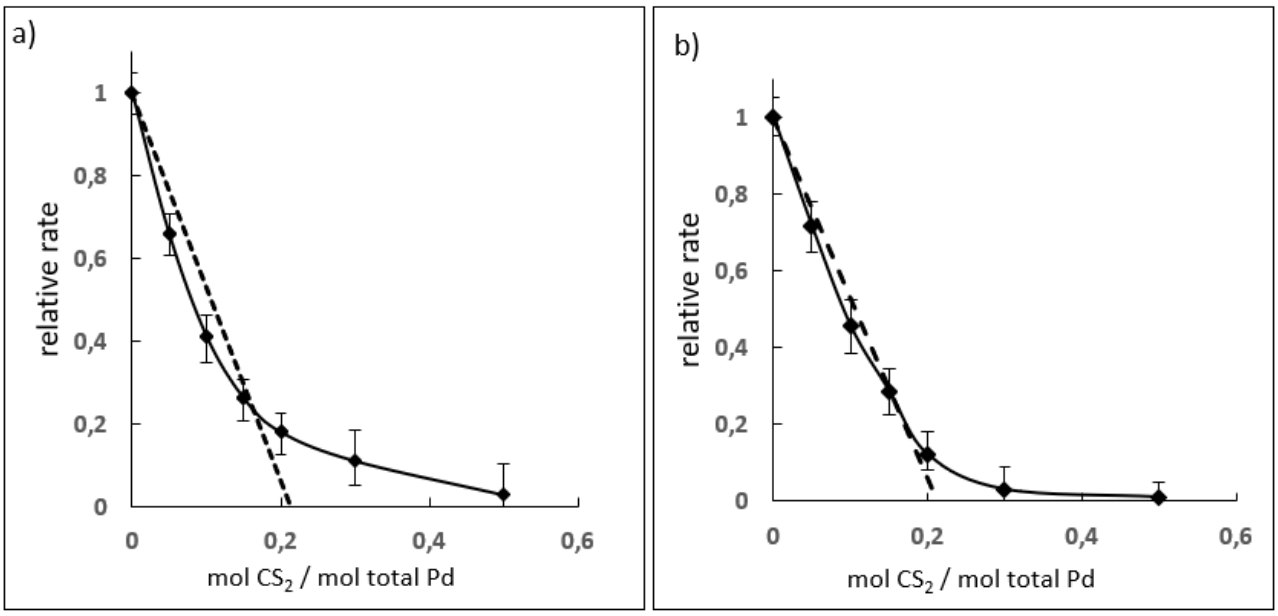

Figure S4. The plots of relative rate of compound **5a** formation *vs* relative quantity of CS_2 loaded (mol CS_2 per a mol of Pd catalyst) in the reaction between propiophenone (**3a**) and iodobenzene (**4c**) catalyzed by the complex **1a** (a) and $Pd(OAc)_2$ (b). The reaction rates were determined by the initial-rate method over the course of 0.5 h; the $x_{intercept}$ is 0.21 ± 0.01 (a), 0.21 ± 0.01 (b). Reaction conditions: PhI (5 mmol), propiophenone (0.5 mmol), Bu^tONa (1 mmol), toluene (2 mL), [Pd]-precatalyst (0.005 mmol), 70 °C.

References

1. Hornstein B. J.; Aiken J. D.; Finke R. G. Nanoclusters in Catalysis: A Comparison of CS_2 Catalyst Poisoning of Polyoxoanion- and Tetrabutylammonium-Stabilized 40 ± 6 Å Rh(0) Nanoclusters to 5% Rh/Al_2O_3, Including an Analysis of the Literature Related to the CS_2 to Metal Stoichiometry Issue *Inorg. Chem.* **2002**, *41*, p. 1625. doi: *10.1021/ic010920y*.
2. Bayram E.; Linehan J. C.; Fulton J. L.; Roberts J. A. S.; Szymczak N. K.; Smurthwaite T. D.; Özkar S.; Balasubramanian M.; Finke R. G. Is It Homogeneous or Heterogeneous Catalysis Derived from [RhCp*Cl2]2? In Operando XAFS, Kinetic, and Crucial Kinetic Poisoning Evidence for Subnanometer Rh4 Cluster-Based Benzene Hydrogenation Catalysis *J. Am. Chem. Soc.* **2011**, *133*, p. 18889. doi: *10.1021/ja2073438*.
3. Bayram E.; Finke R. G. Quantitative 1,10-Phenanthroline Catalyst-Poisoning Kinetic Studies of Rh(0) Nanoparticle and Rh_4 Cluster Benzene Hydrogenation Catalysts: Estimates of the Poison Kassociation Binding Constants, of the Equivalents of Poison Bound and of the Number of Catalytically Active Sites for Each Catalyst *ACS Catal.* **2012**, *2*, p. 1967. doi: *10.1021/cs300330c*.
4. Bayram E.; Lu J.; Aydin C.; Uzun A.; Browning N. D.; Gates B. C.; Finke R. G. Mononuclear Zeolite-Supported Iridium: Kinetic, Spectroscopic, Electron Microscopic, and Size-Selective Poisoning Evidence for an Atomically Dispersed True Catalyst at 22 °C *ACS Catal.* **2012**, *2*, p. 1947. doi: *10.1021/cs300366w*.
5. Stracke J. J.; Finke R. G. Distinguishing homogeneous from heterogeneous water oxidation catalysis when beginning with polyoxometalates *ACS Catal.* **2014**, *4*, p. 909. doi: *10.1021/cs4011716*.
6. Bayram E.; Linehan J. C.; Fulton J. L.; Szymczak N. K.; Finke R. G. Determination of the Dominant Catalyst Derived from the Classic $[RhCp^*Cl_2]_2$ Precatalyst System: Is it Single-Metal Rh_1Cp^*-Based, Subnanometer Rh_4 Cluster-Based, or $Rh(0)_n$ Nanoparticle-Based Cyclohexene Hydrogenation Catalysis at Room Temperature and Mild Pressures? *ACS Catal.* **2015**, *5*, p. 3876. doi: *10.1021/acscatal.5b00315*.
7. Sonnenberg J. F.; Morris R. H. Distinguishing homogeneous from nanoparticle asymmetric iron catalysis *Catal. Sci. Technol.* **2014**, *4*, p. 3426. doi: *10.1039/c4cy00468j*.
8. Widegren J. A.; Finke R. G. A review of the problem of distinguishing true homogeneous catalysis from soluble or other metal-particle heterogeneous catalysis under reducing conditions *J. Mol. Catal. A: Chem.* **2003**, *198*, p. 317. doi: *10.1016/s1381-1169(02)00728-8*.

S4. ESI-MS study of reaction mixtures

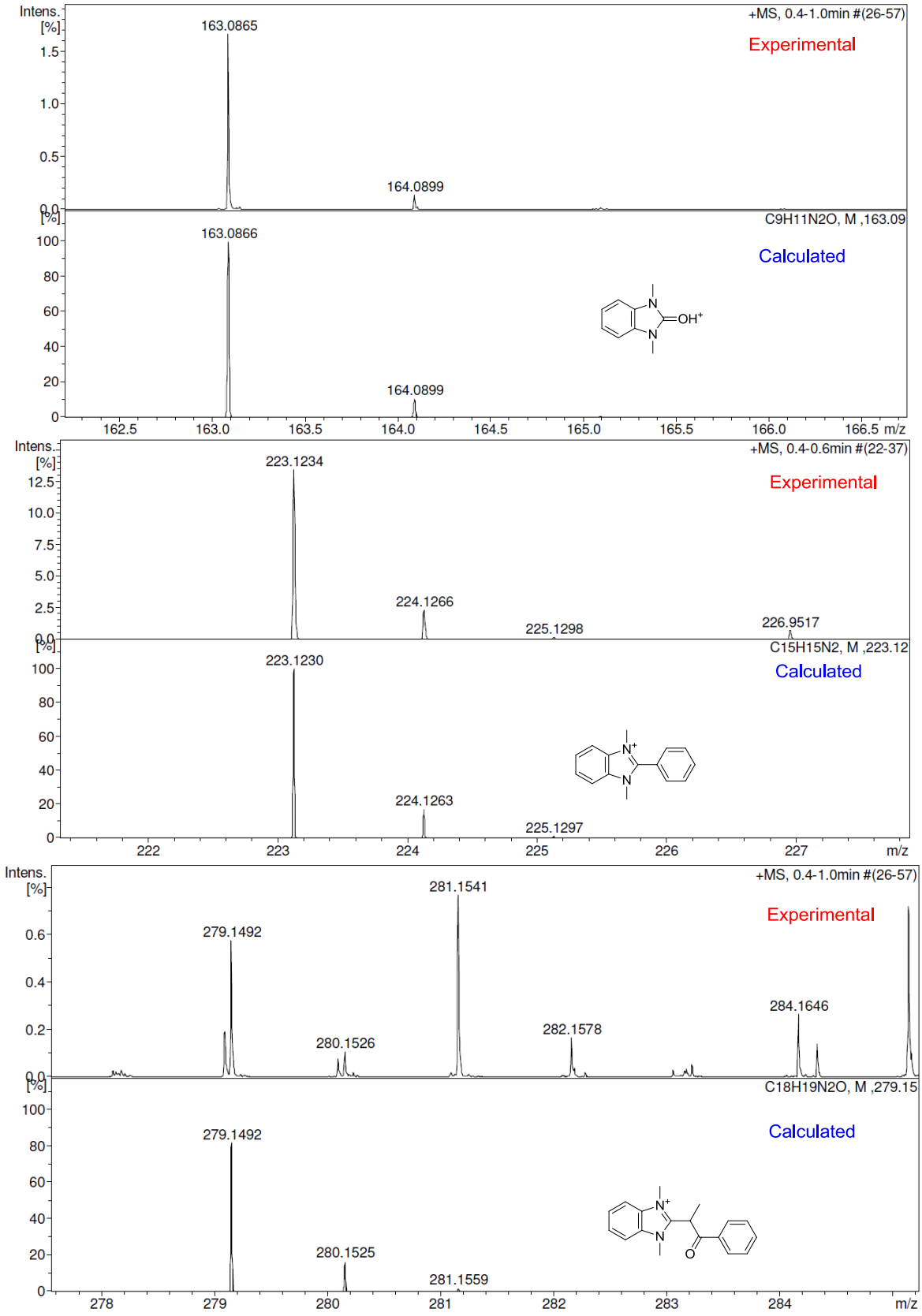

Figure S5. ESI-MS spectra of complex **1a** decomposition products formed in the reaction of arylation of propiophenone with chlorobenzene (for all ESI-MS spectra in the present study, in case of signal overlap or low intensity, only plausible identification of the ions may be suggested).

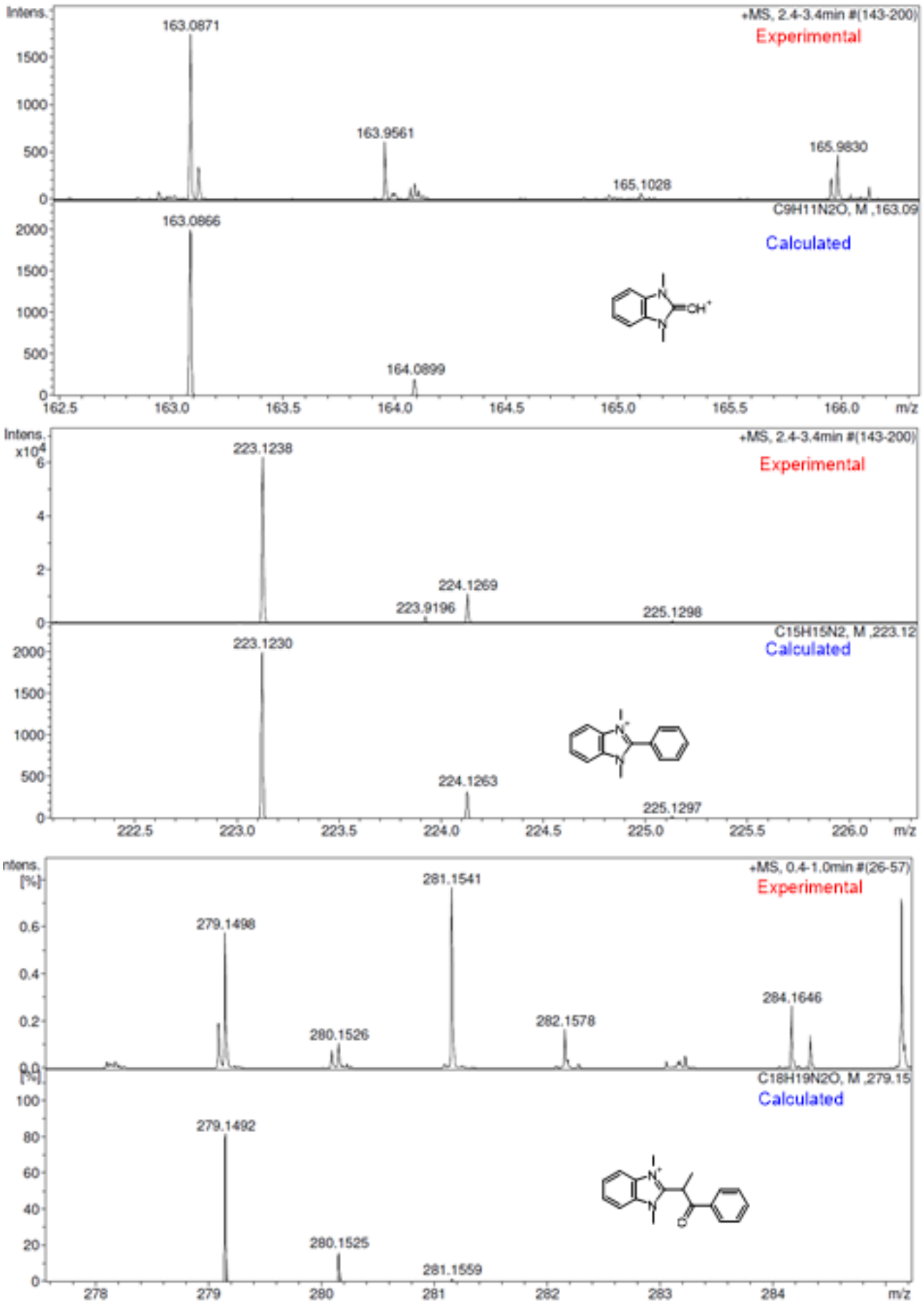

Figure S6. ESI-MS spectra of complex **1b** decomposition products formed in the reaction of arylation of propiophenone with chlorobenzene.

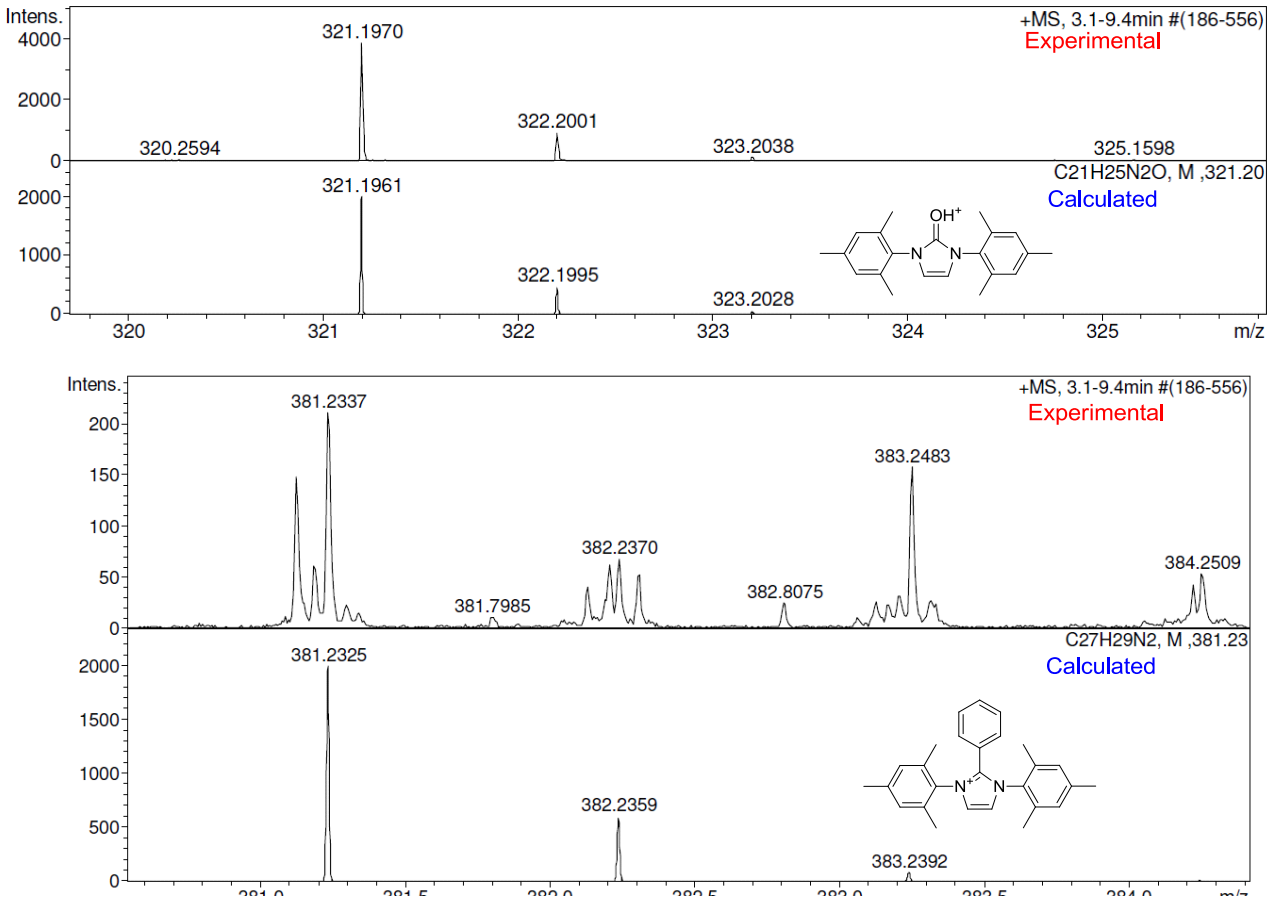

Figure S7. ESI-MS spectra of complex **1c** decomposition products formed in the reaction of arylation of propiophenone with chlorobenzene.

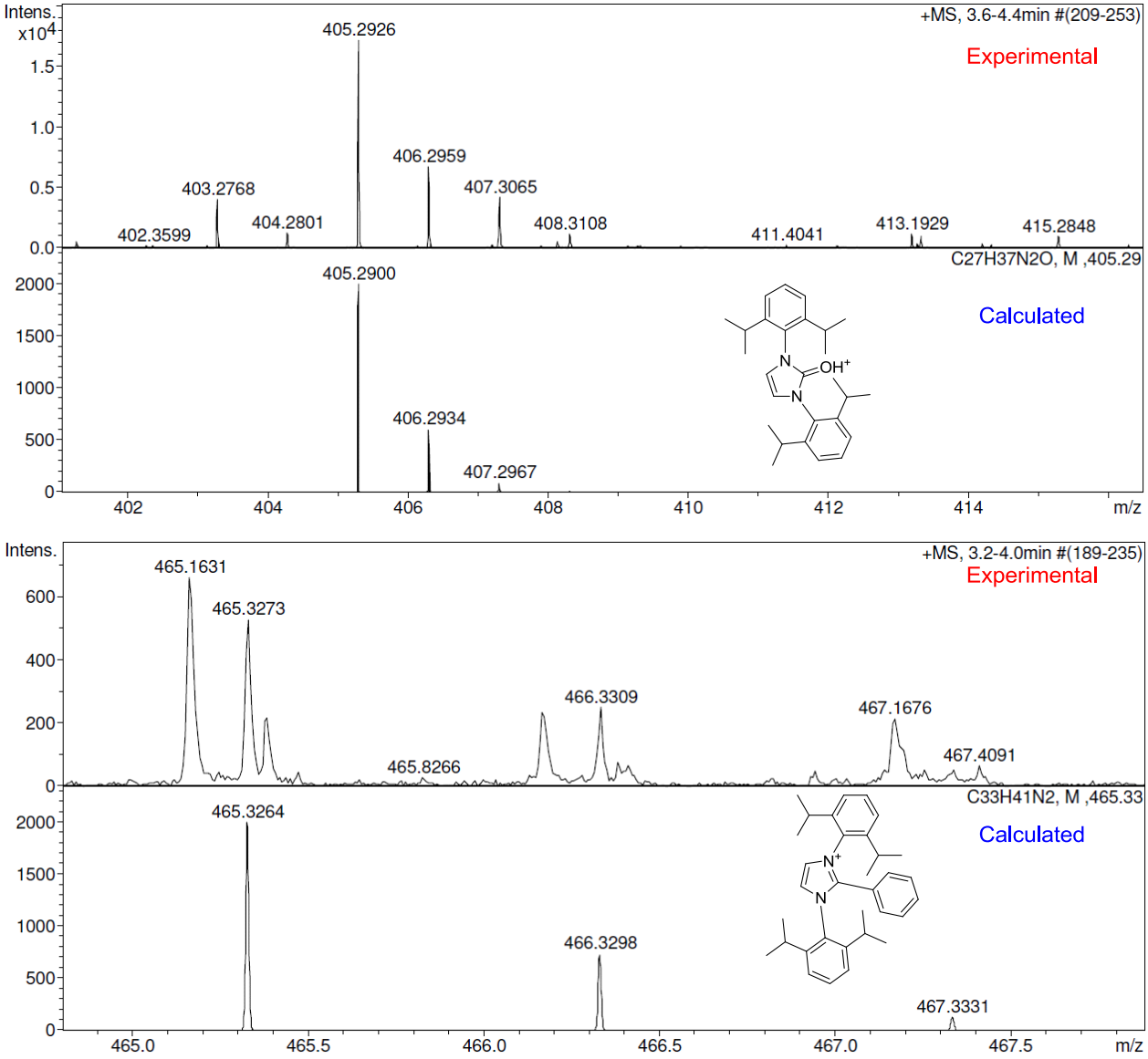

Figure S8. ESI-MS spectra of complex **1d** decomposition products formed in the reaction of arylation of propiophenone with chlorobenzene.

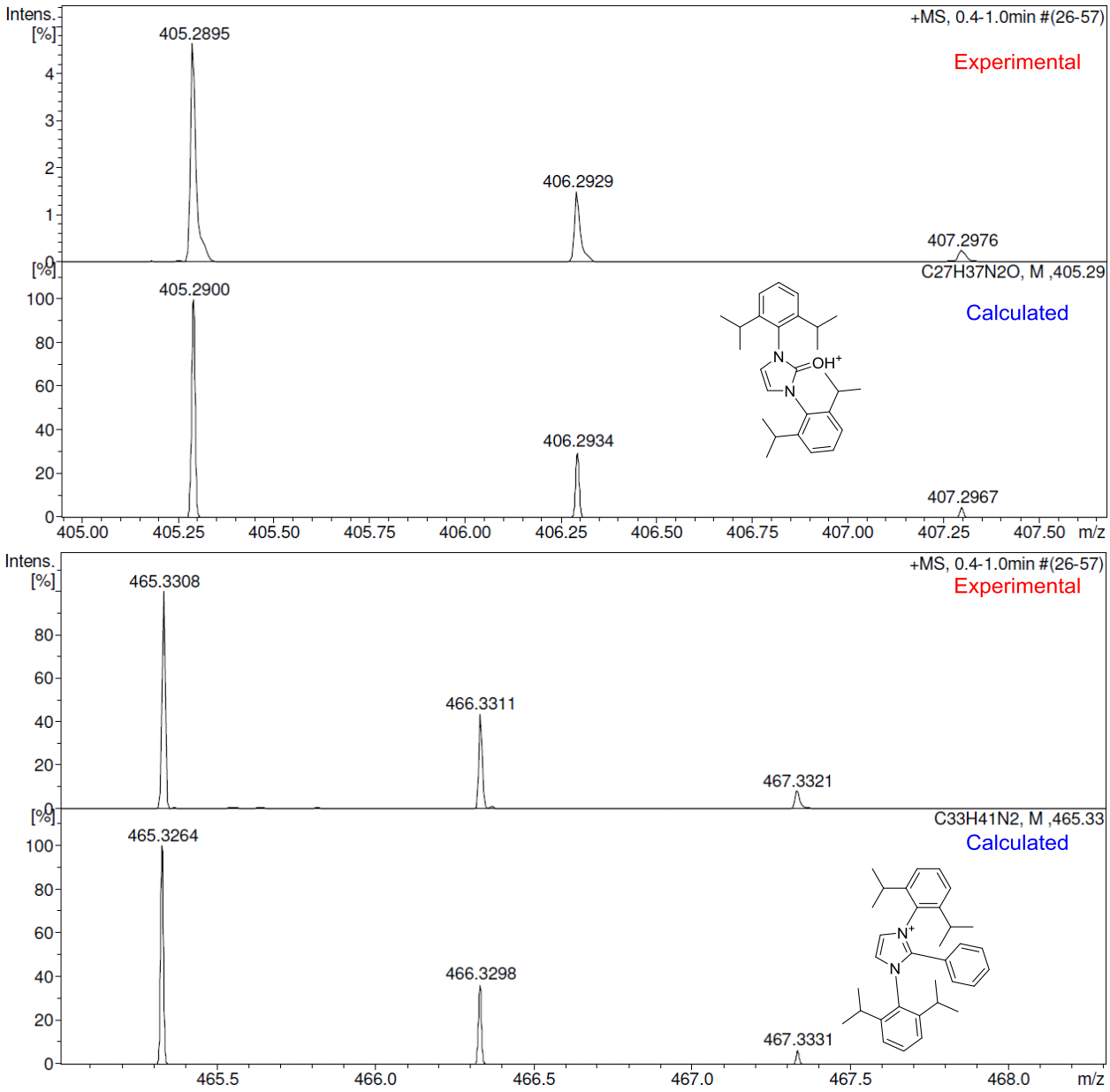

Figure S9. ESI-MS spectra of complex **1e** decomposition products formed in the reaction of arylation of propiophenone with chlorobenzene.

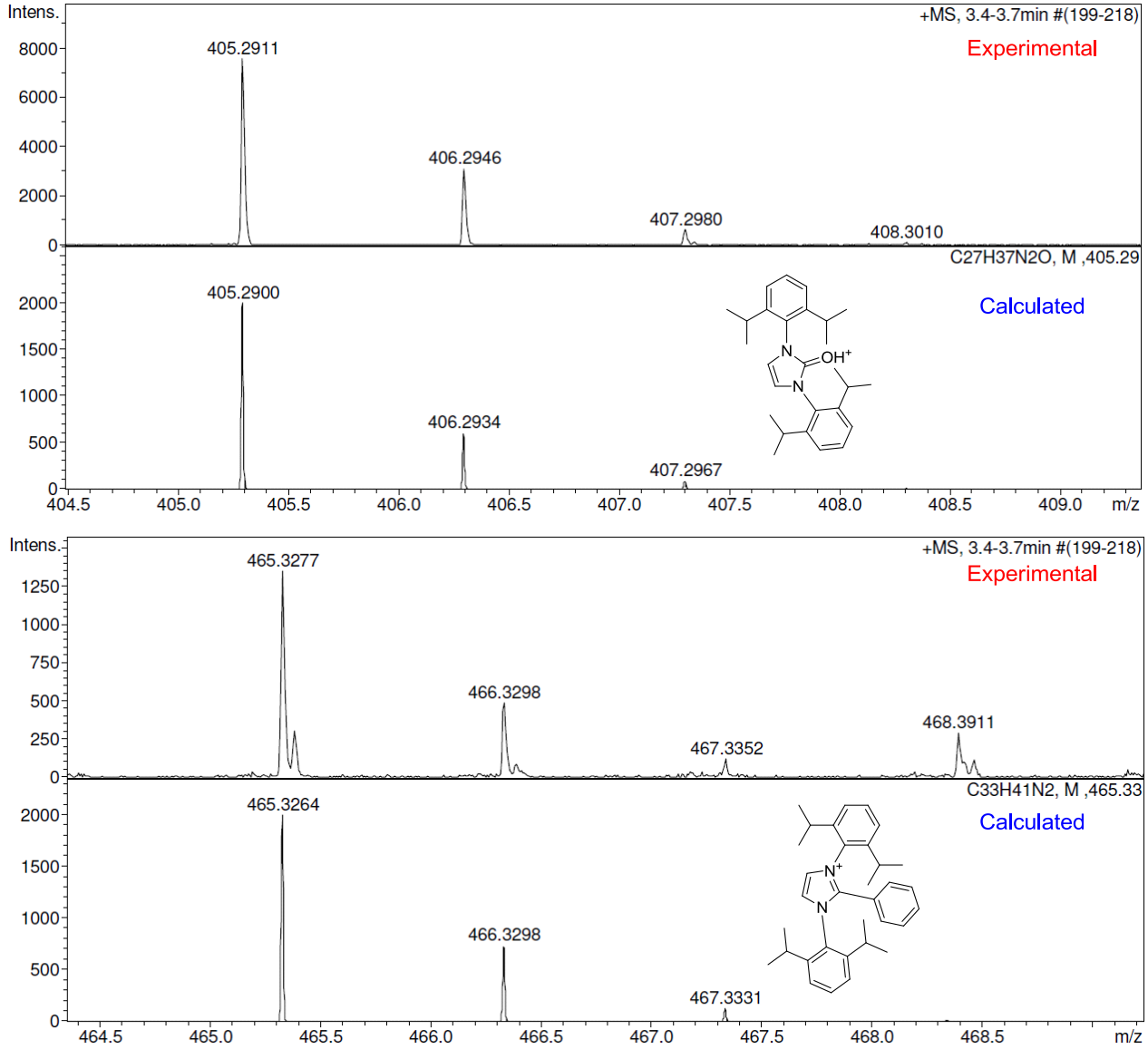

Figure S10. ESI-MS spectra of complex **1f** decomposition products formed in the reaction of arylation of propiophenone with chlorobenzene.

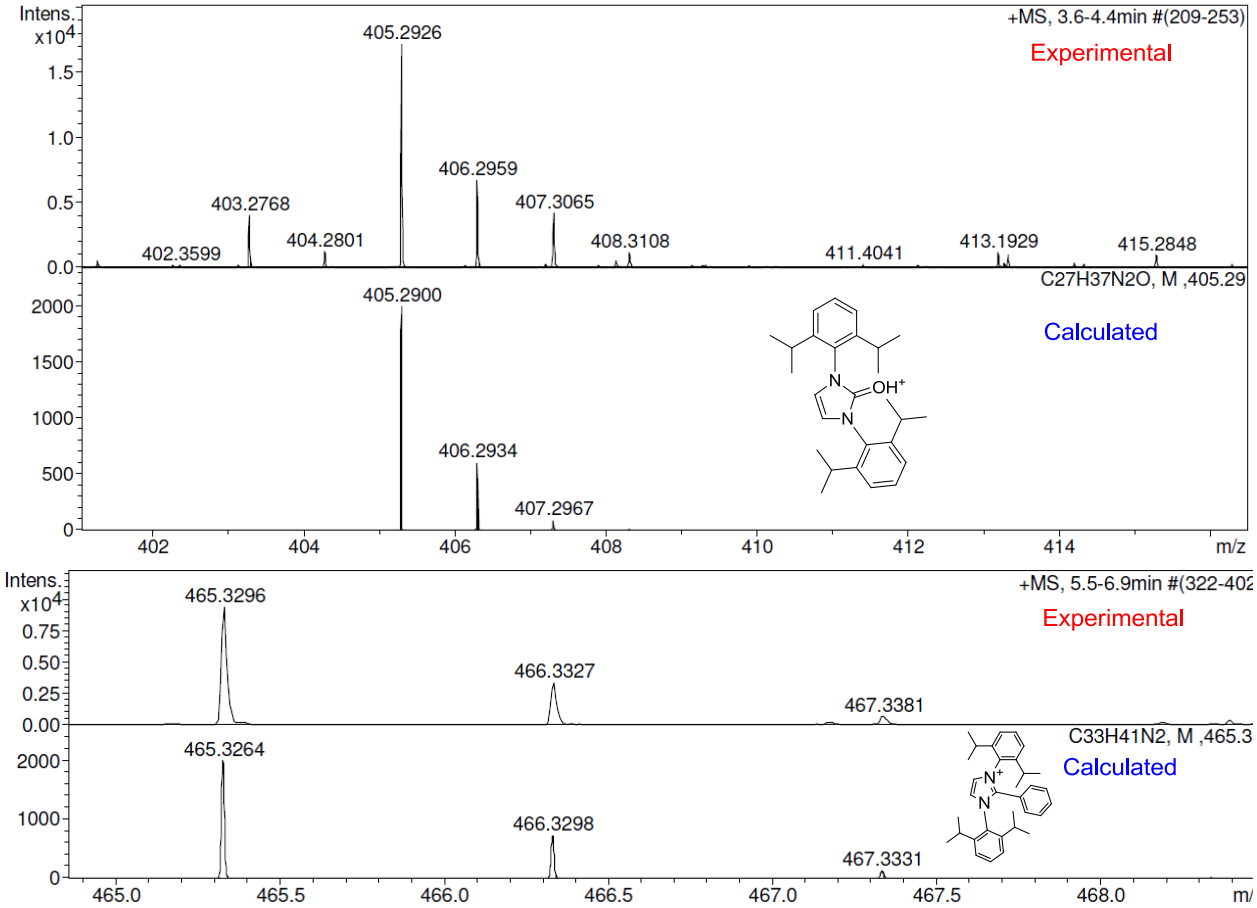

Figure S11. ESI-MS spectra of complex **1g** decomposition products formed in the reaction of arylation of propiophenone with chlorobenzene.

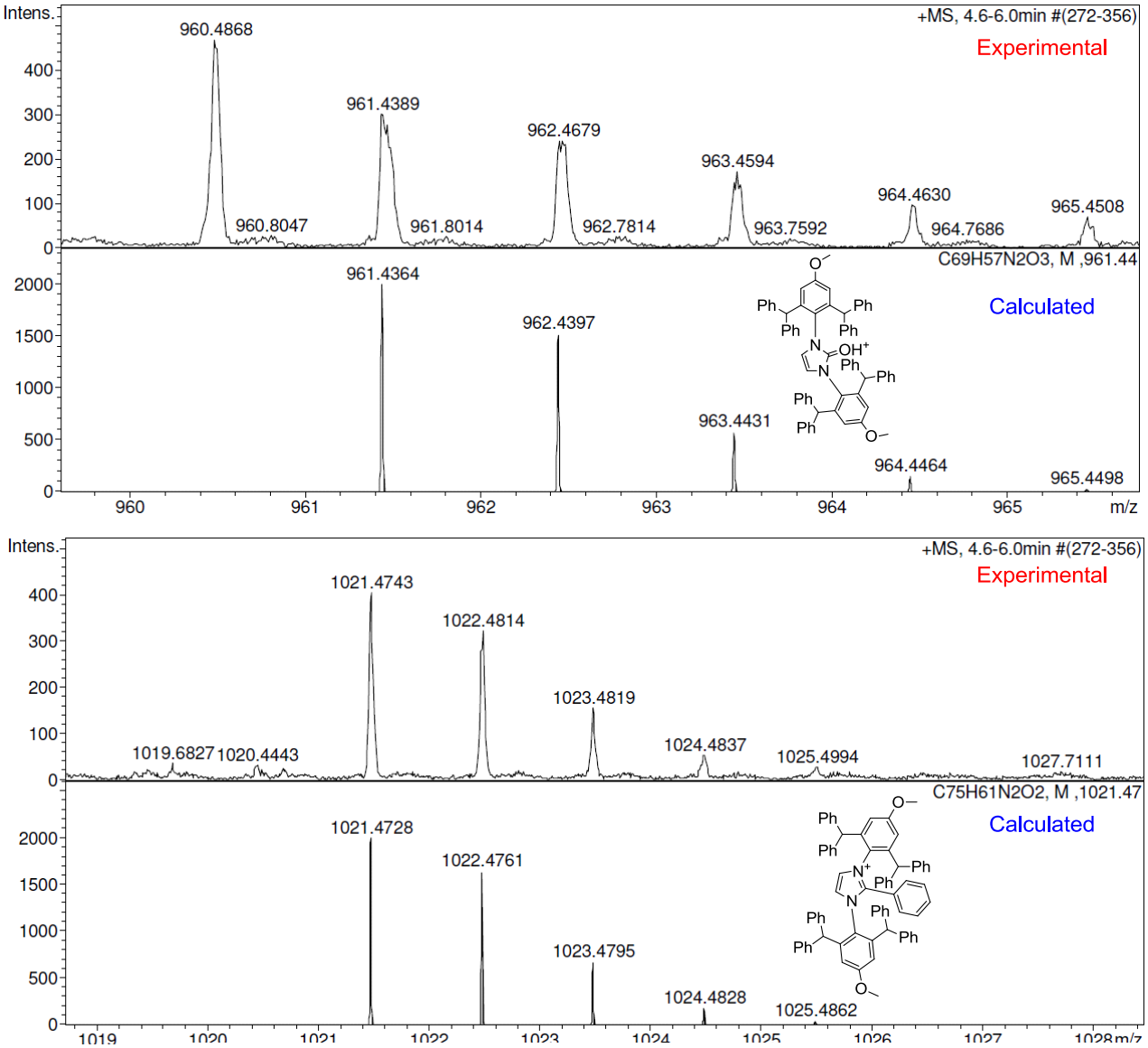

Figure S12. ESI-MS spectra of complex **1h** decomposition products formed in the reaction of arylation of propiophenone with chlorobenzene.

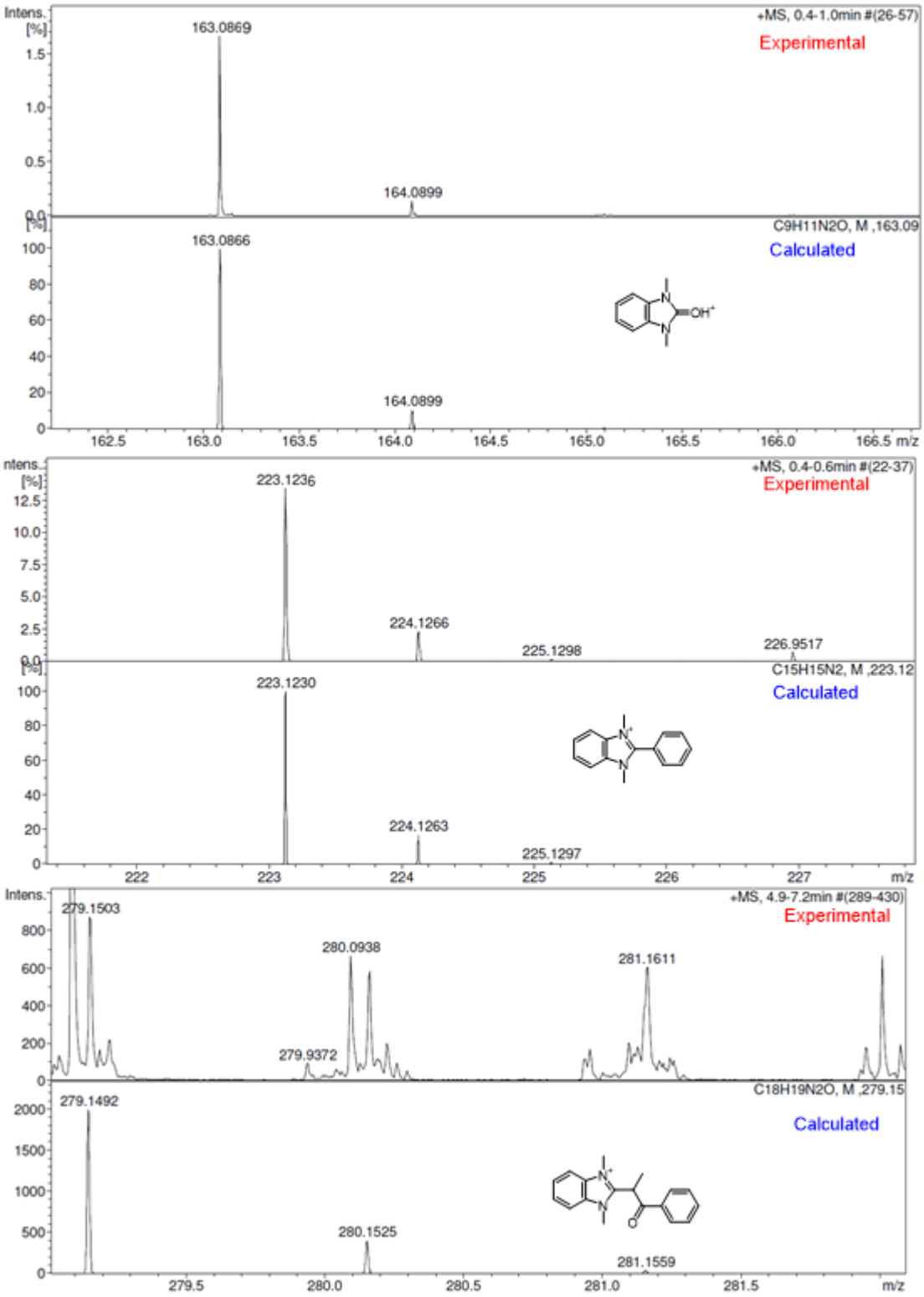

Figure S13. ESI-MS spectra of complex **2a** decomposition products formed in the reaction of arylation of propiophenone with chlorobenzene.

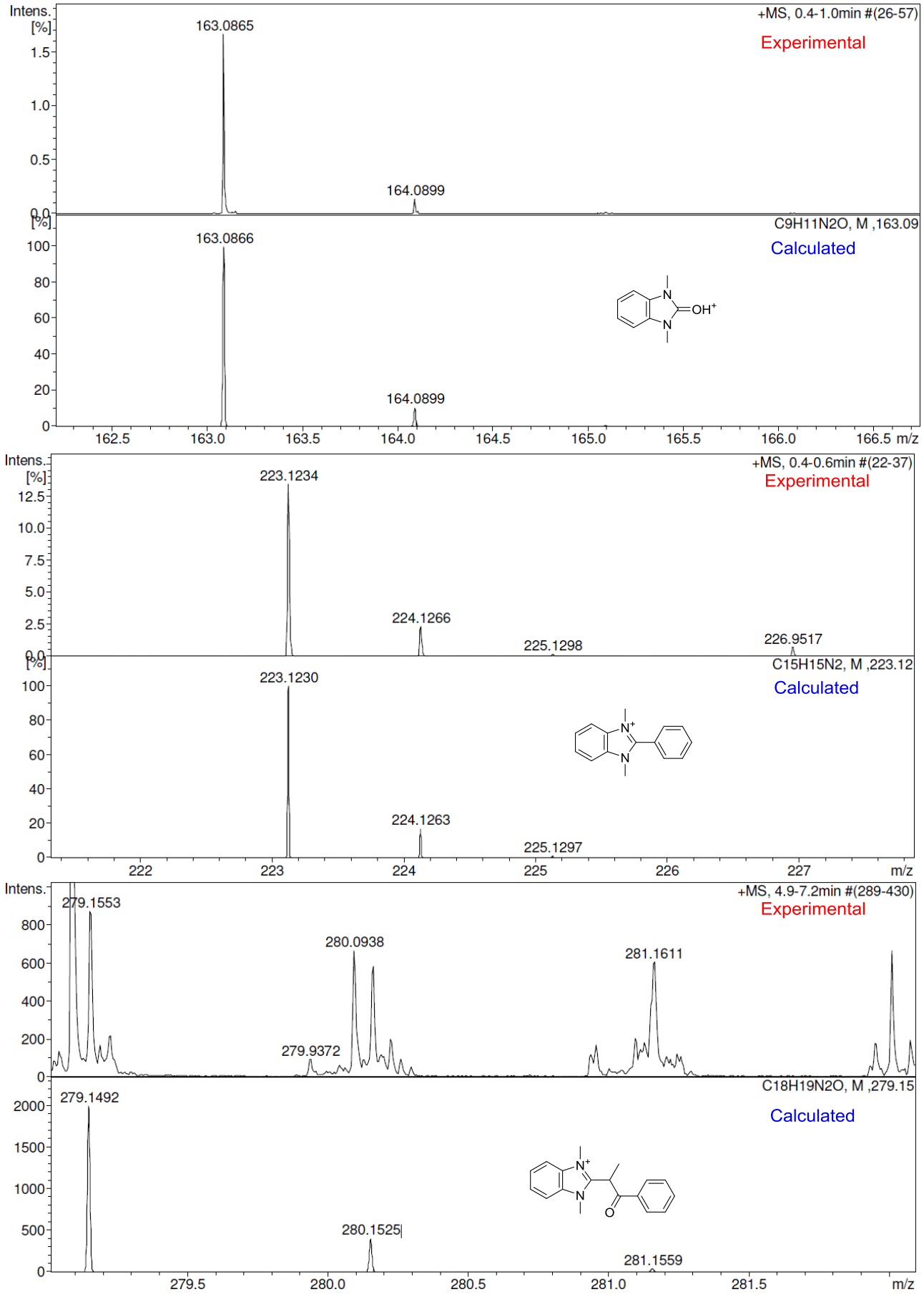

Figure S14. ESI-MS spectra of complex **2b** decomposition products formed in the reaction of arylation of propiophenone with chlorobenzene.

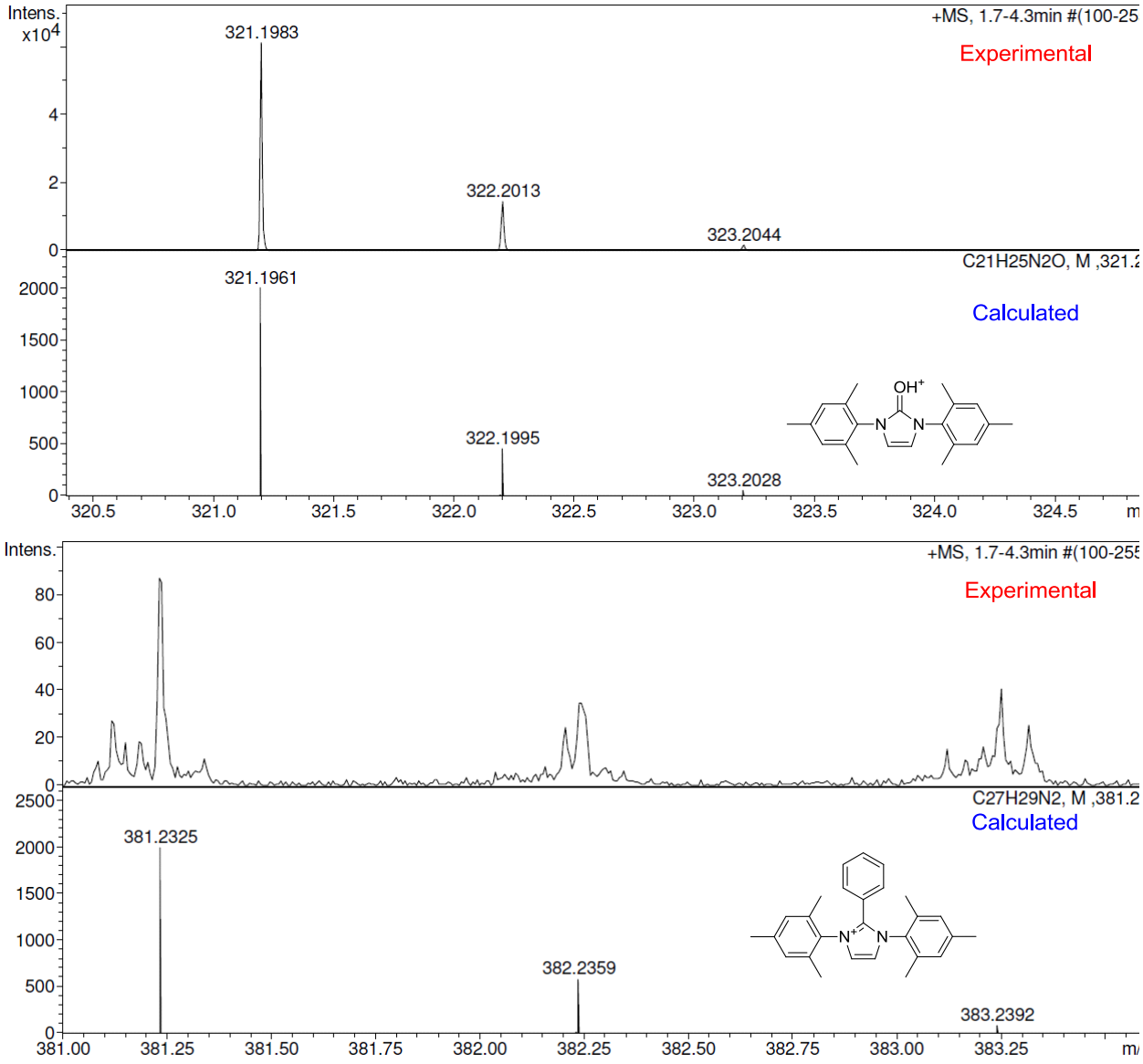

Figure S15. ESI-MS spectra of complex **2c** decomposition products formed in the reaction of arylation of propiophenone with chlorobenzene.

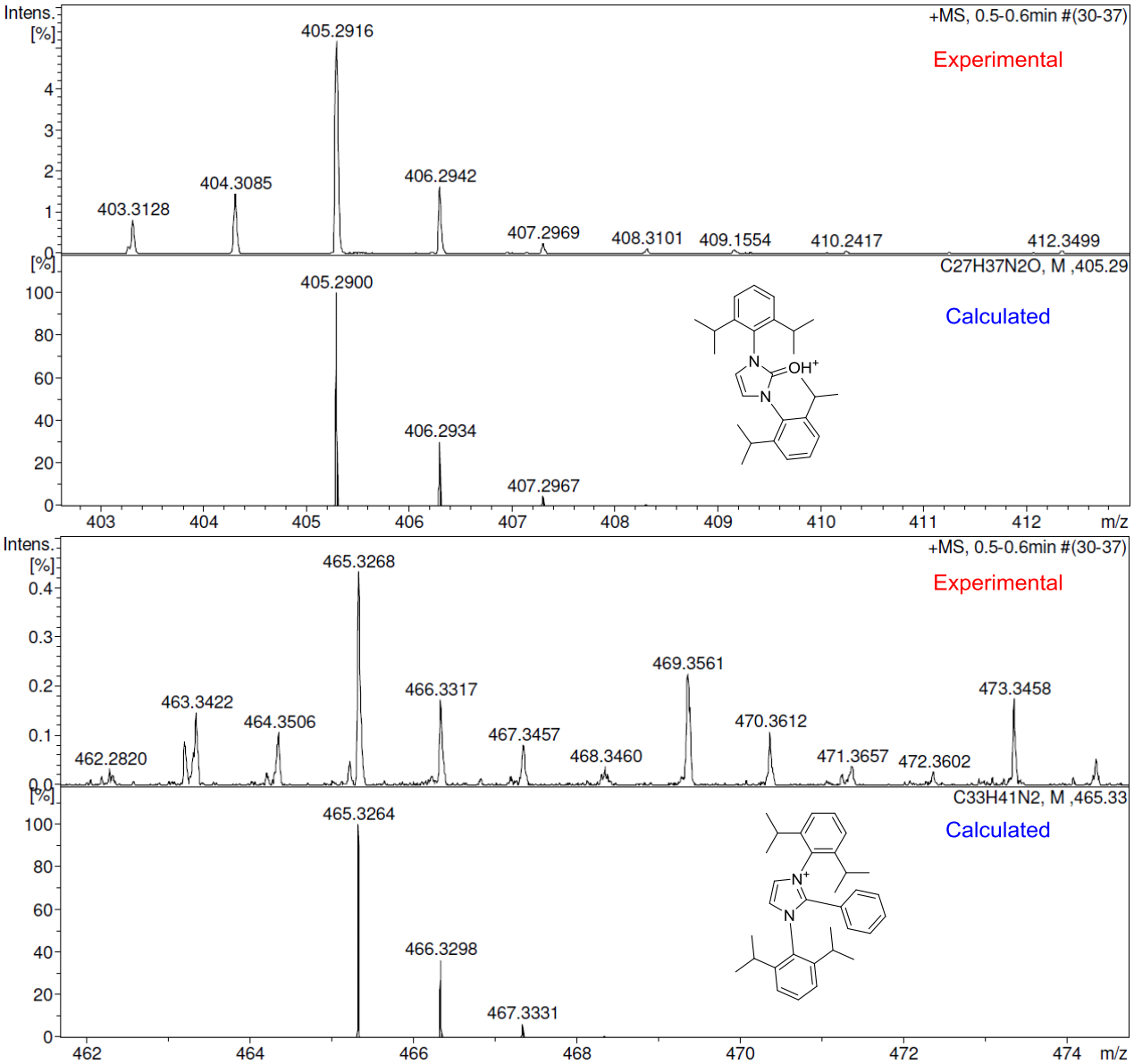

Figure S16. ESI-MS spectra of complex **2d** decomposition products formed in the reaction of arylation of propiophenone with chlorobenzene.

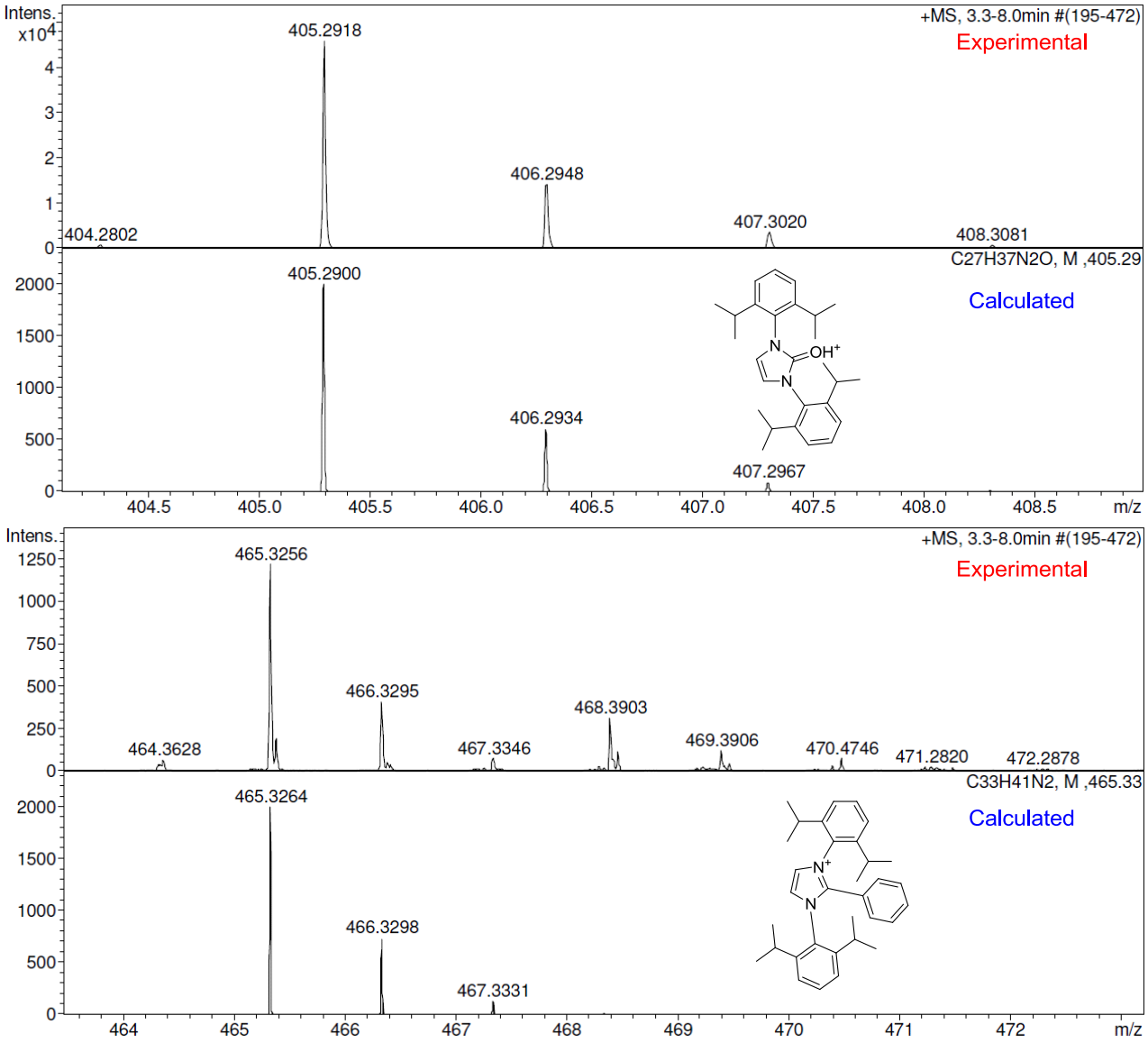

Figure S17. ESI-MS spectra of complex **2e** decomposition products formed in the reaction of arylation of propiophenone with chlorobenzene.

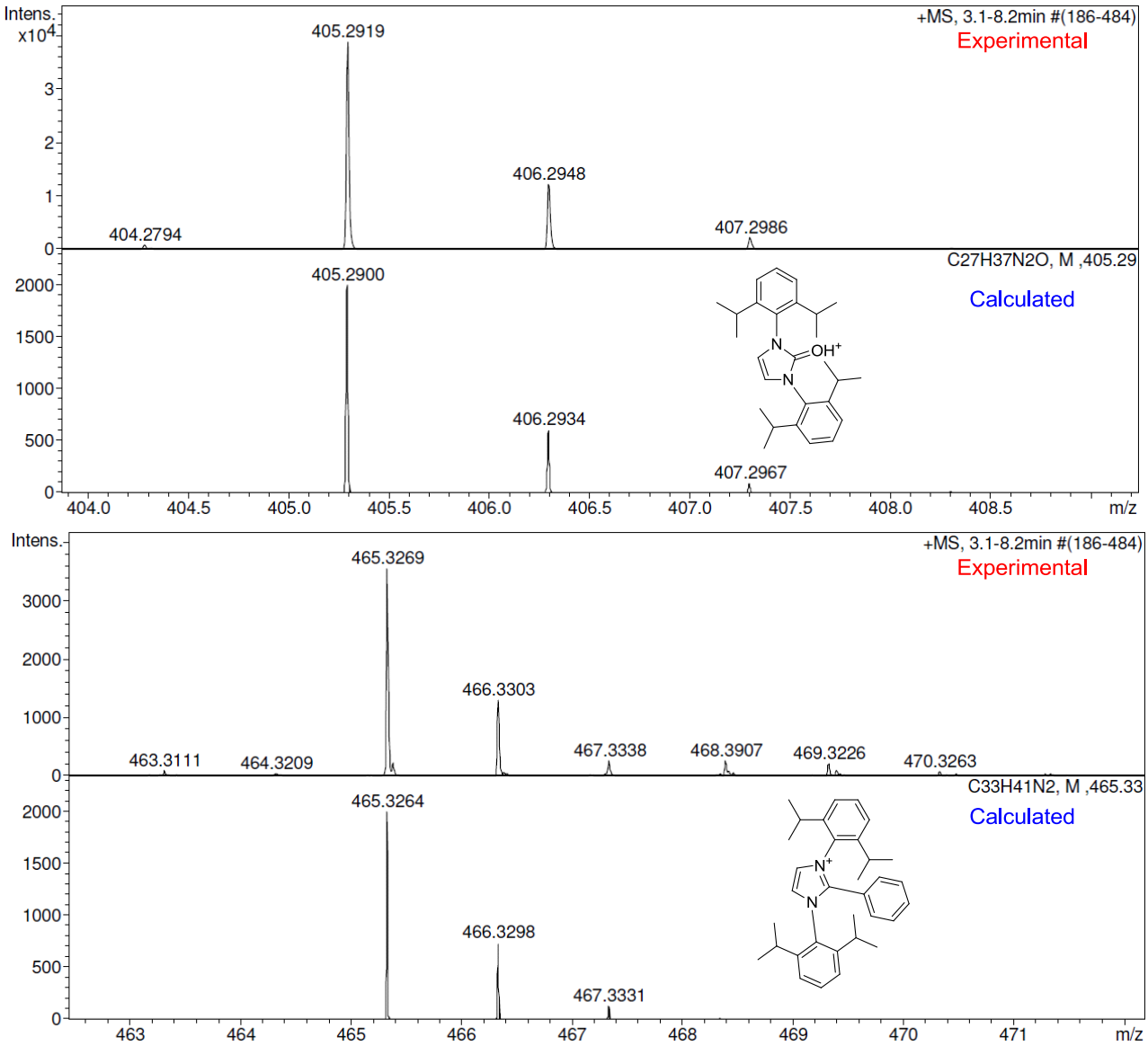

Figure S18. ESI-MS spectra of complex **2f** decomposition products formed in the reaction of arylation of propiophenone with chlorobenzene.

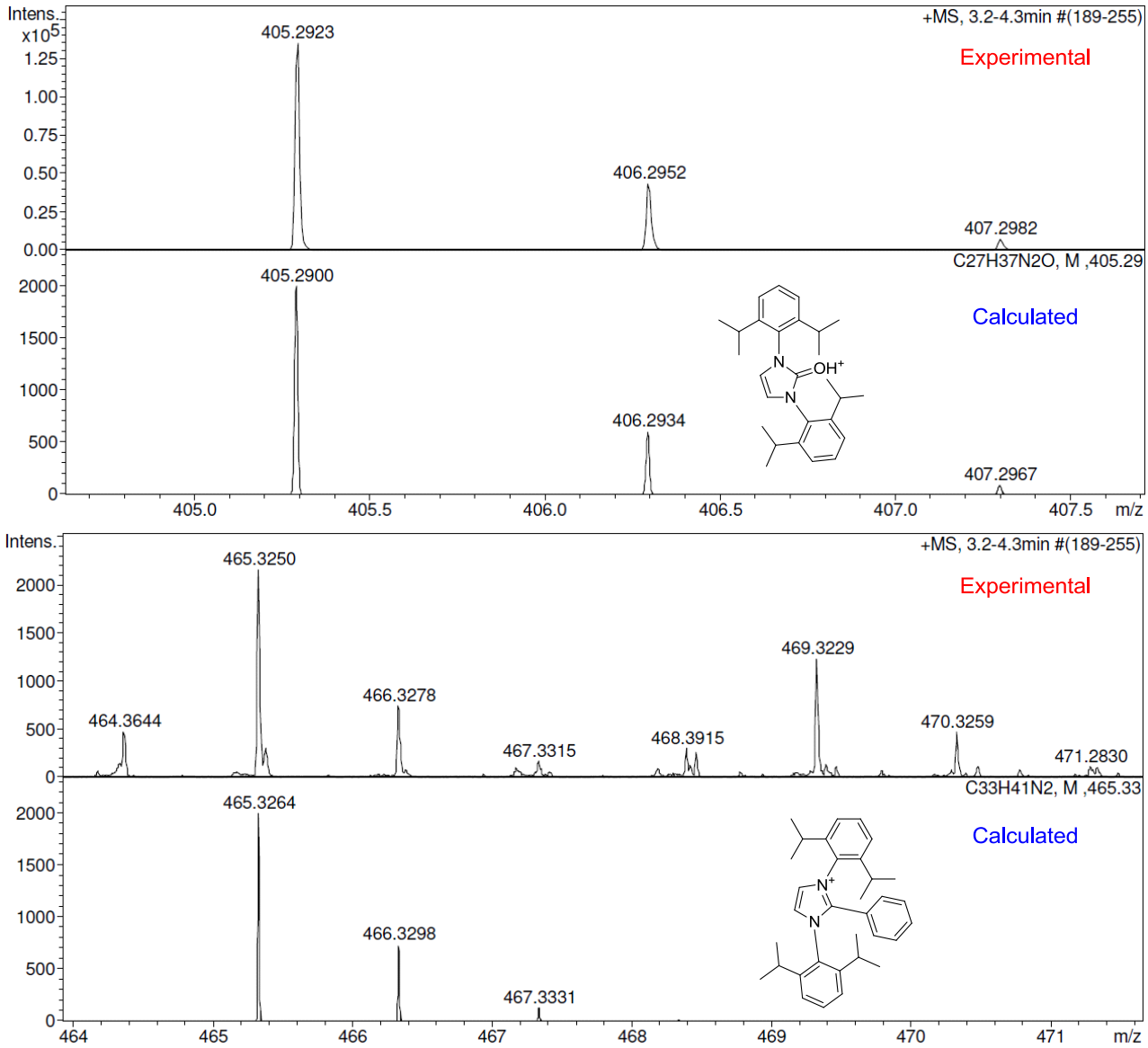

Figure S19. ESI-MS spectra of complex **2g** decomposition products formed in the reaction of arylation of propiophenone with chlorobenzene.

S5. Electronic microscopy study

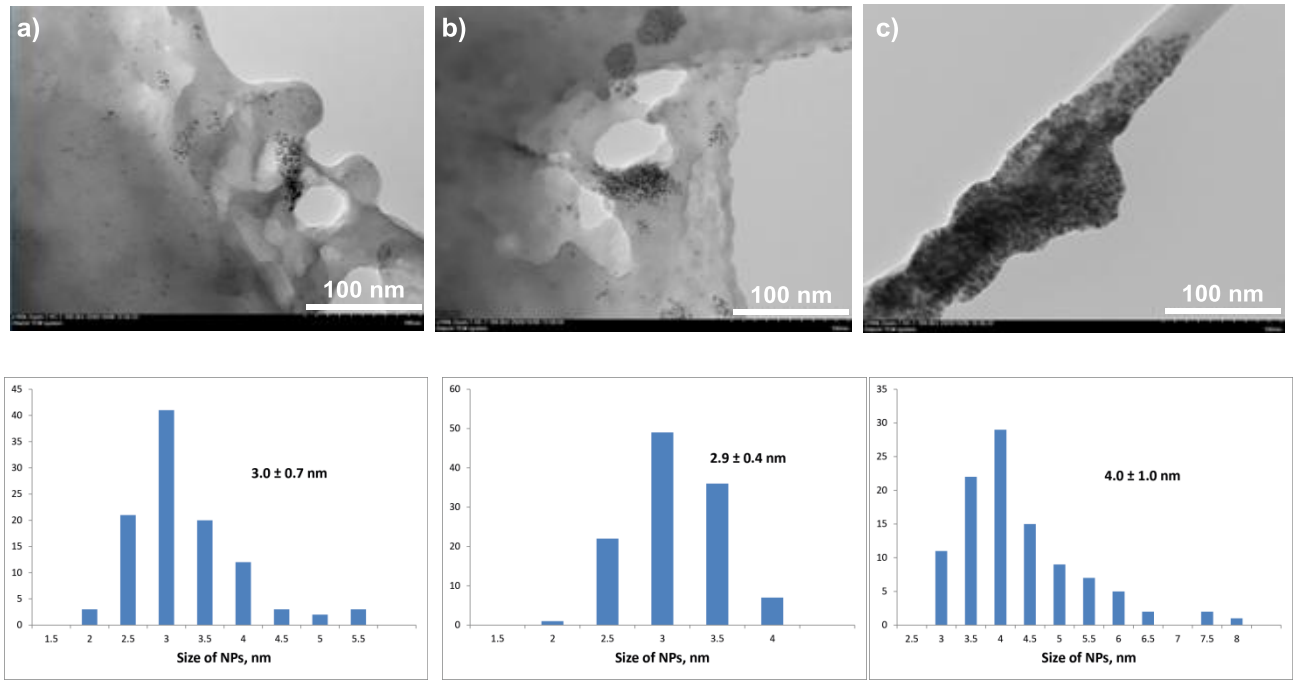

Figure S20. TEM images of Pd particles and their size distribution (below) trapped from reaction mixtures 15 min after reaction start (a), 60 min after reaction start (b), 180 min after reaction start (c). Reaction conditions: precatalyst **1a** (0.005 mmol), chlorobenzene (0.5 mmol), propiophenone (0.5 mmol), Bu^{t}ONa (1 mmol), toluene (2 mL), 110 °C.

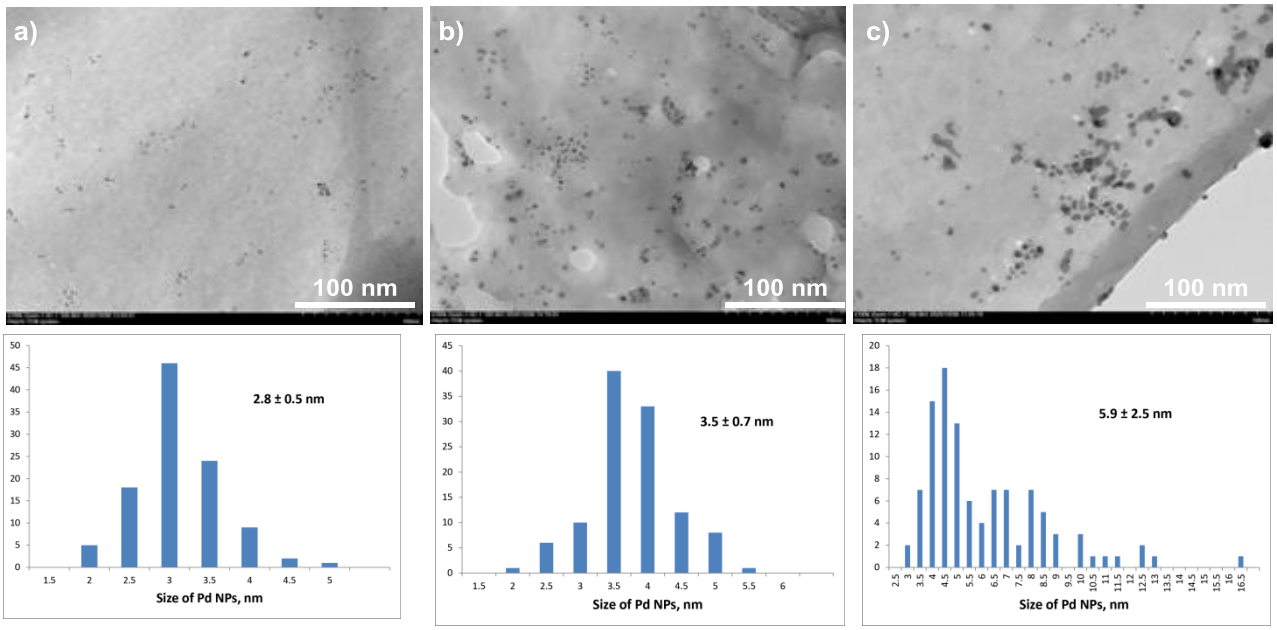

Figure S21. TEM images of Pd particles and their size distribution (below) trapped from reaction mixtures 15 min after reaction start (a), 60 min after reaction start (b), 180 min after reaction start (c). Reaction conditions: precatalyst **1d** (0.005 mmol), chlorobenzene (0.5 mmol), propiophenone (0.5 mmol), Bu^{t}ONa (1 mmol), toluene (2 mL), 110 °C.

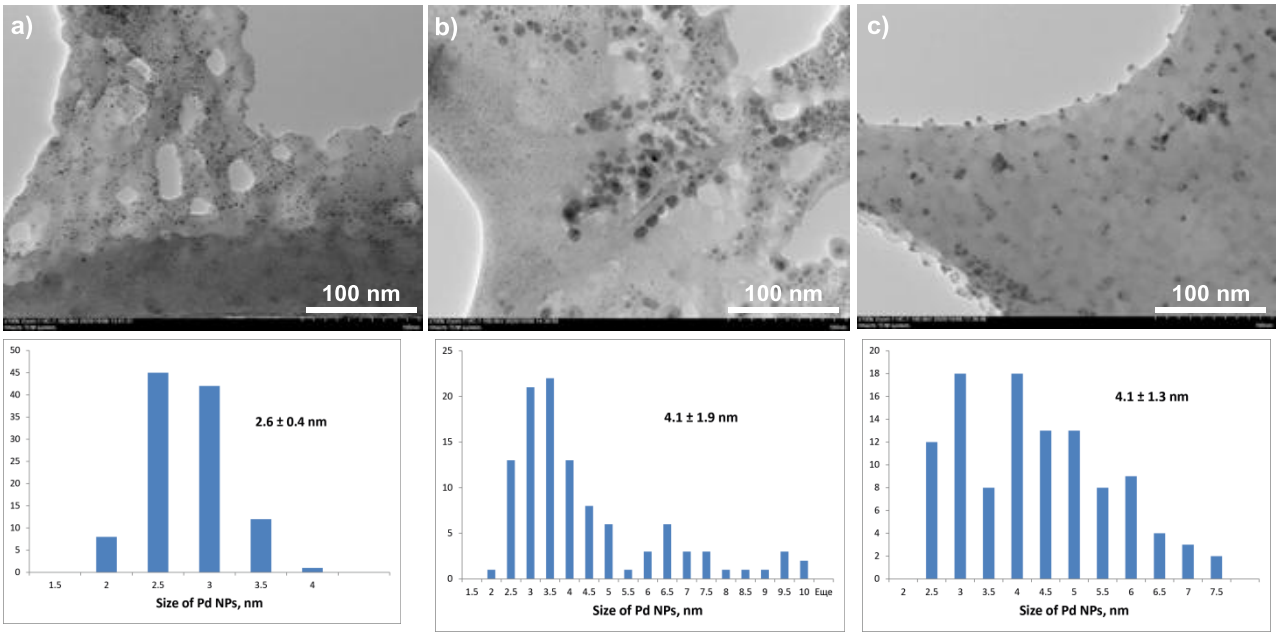

Figure S22. TEM images of Pd particles and their size distribution (below) trapped from reaction mixtures 15 min after reaction start (a), 60 min after reaction start (b), 180 min after reaction start (c). Reaction conditions: **$Pd(OAc)_2$** (0.005 mmol), TBAB (0.05 mmol), chlorobenzene (0.5 mmol), propiophenone (0.5 mmol), Bu^tONa (1 mmol), toluene (2 mL), 110 °C.

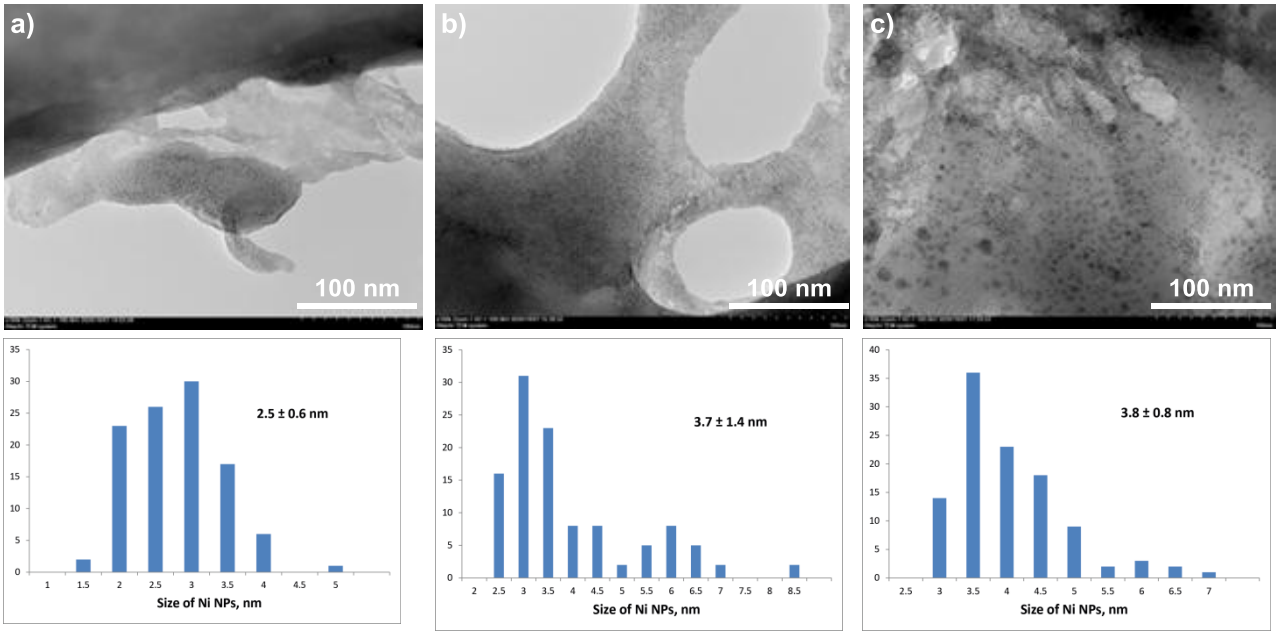

Figure S23. TEM images of nanoparticles and their size distribution (below) trapped from reaction mixtures 15 min after reaction start (a), 60 min after reaction start (b), 180 min after reaction start (c). Reaction conditions: precatalyst **2a** (0.015 mmol), chlorobenzene (0.5 mmol), propiophenone (0.5 mmol), Bu^tONa (1 mmol), toluene (2 mL), 110 °C.

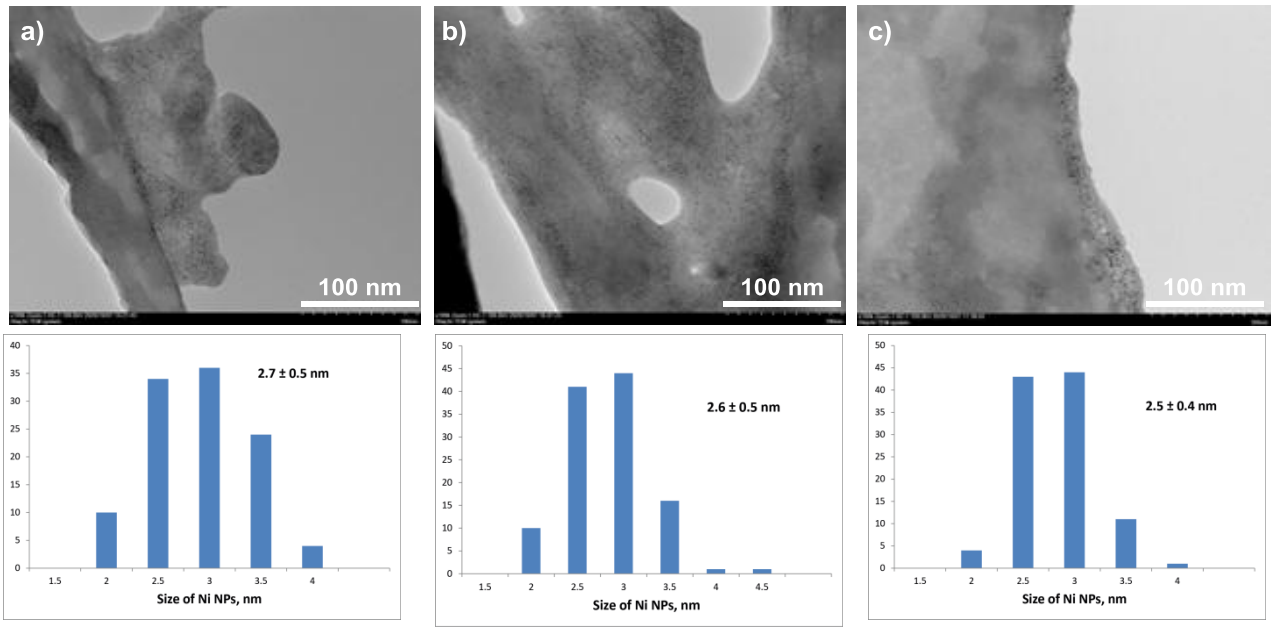

Figure S24. TEM images of nanoparticles and their size distribution (below) trapped from reaction mixtures 15 min after reaction start (a), 60 min after reaction start (b), 180 min after reaction start (c). Reaction conditions: precatalyst **2h** (0.015 mmol), chlorobenzene (0.5 mmol), propiophenone (0.5 mmol), Bu^{t}ONa (1 mmol), toluene (2 mL), 110 °C.

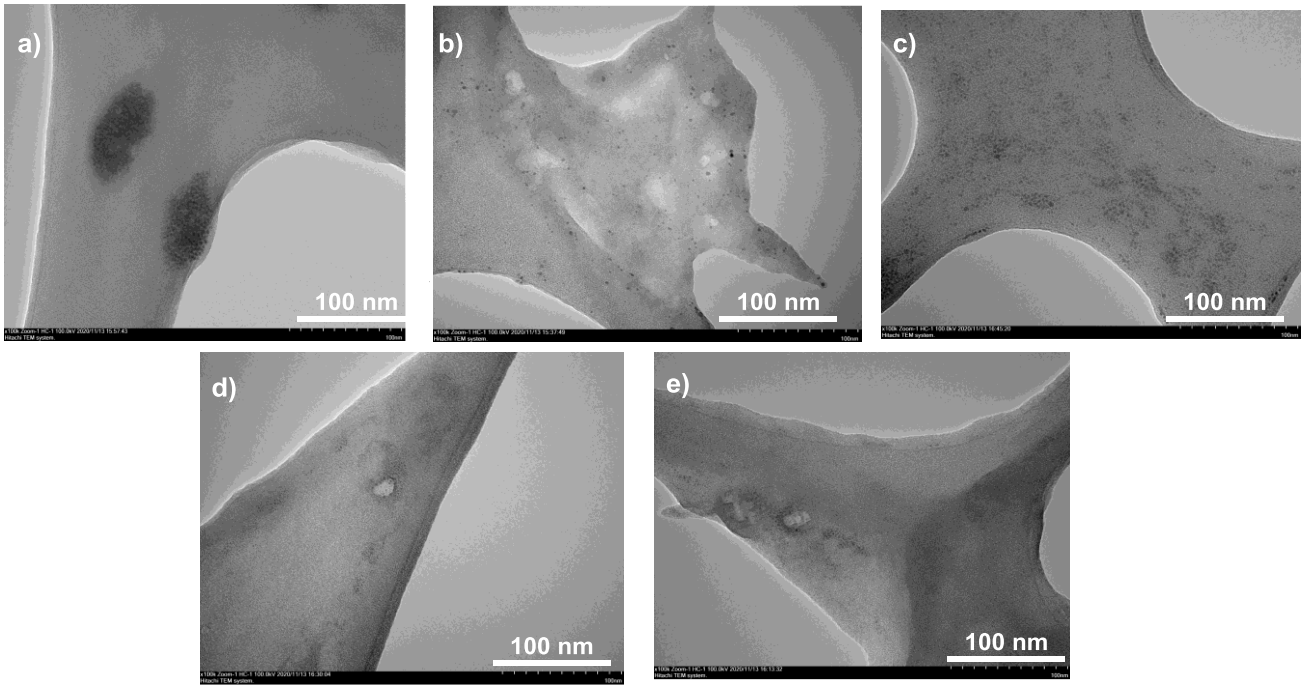

Figure S25. TEM images of nanoparticles trapped from reaction mixtures 1 min after reaction start, using **1a**(a), **1d**(b), **Pd(OAc)$_2$**(c) **2a**(d), **2h**(e) as precatalyst. Reaction conditions: 0.005 mmol of Pd-precatalyst or 0.015 mmol of Ni-precatalyst, chlorobenzene (0.5 mmol), propiophenone (0.5 mmol), Bu^{t}ONa (1 mmol), toluene (2 mL), 110 °C.

S6. NMR spectra

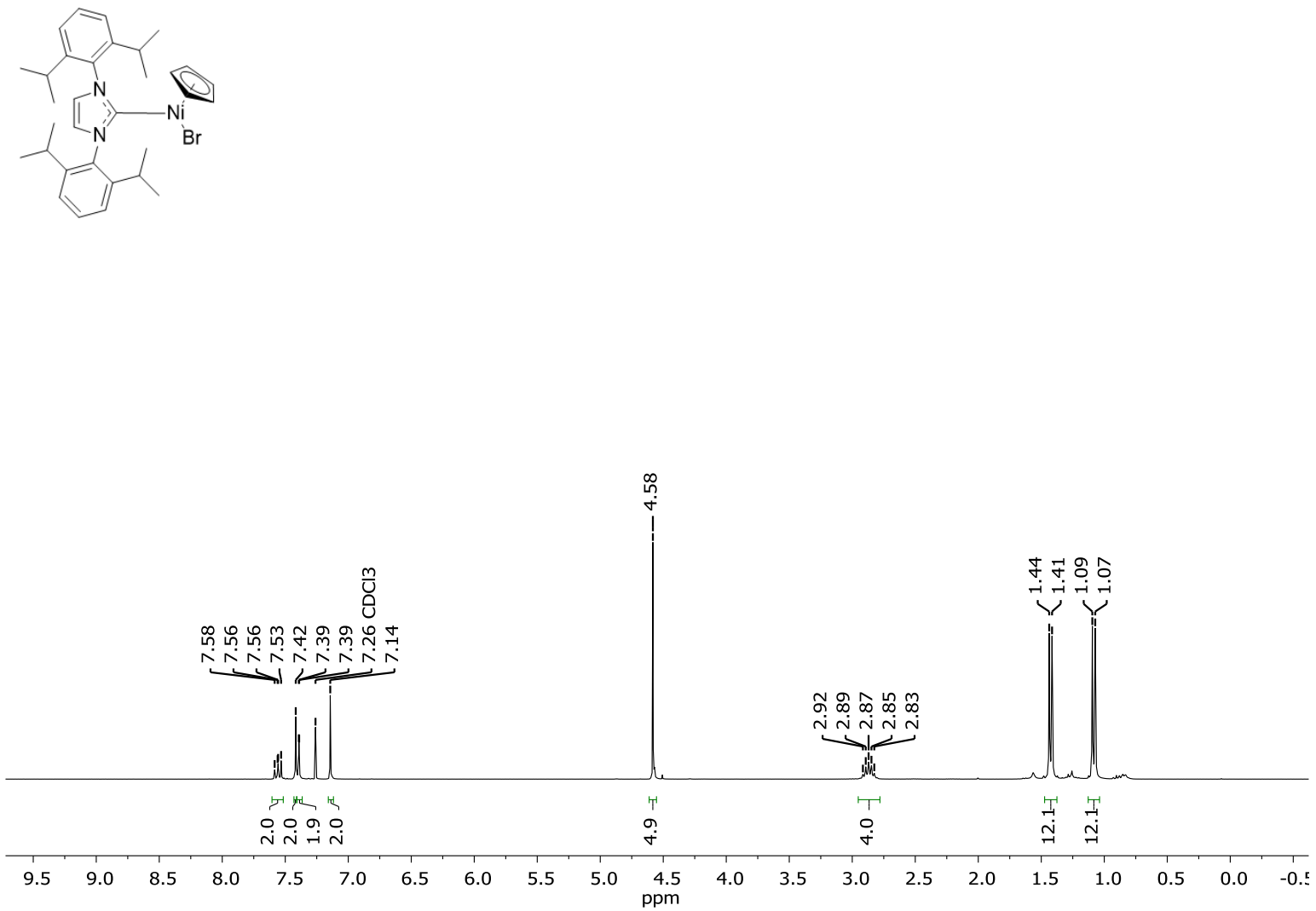

Figure S26. ^{1}H NMR spectrum of compound **2e** ($CDCl_3$, 300 MHz)

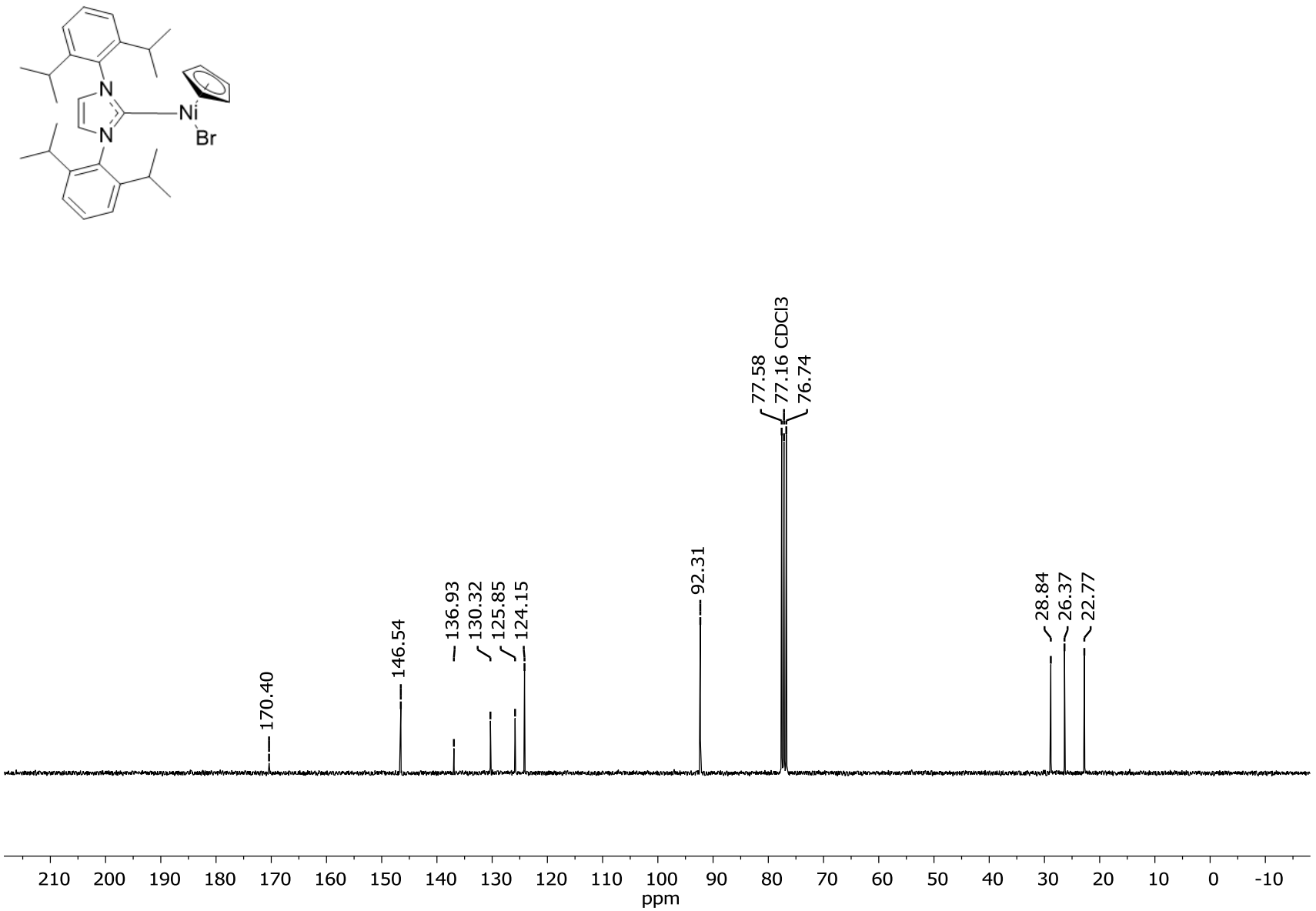

Figure S27. ^{13}C NMR spectrum of compound **2e** ($CDCl_3$, 75 MHz)

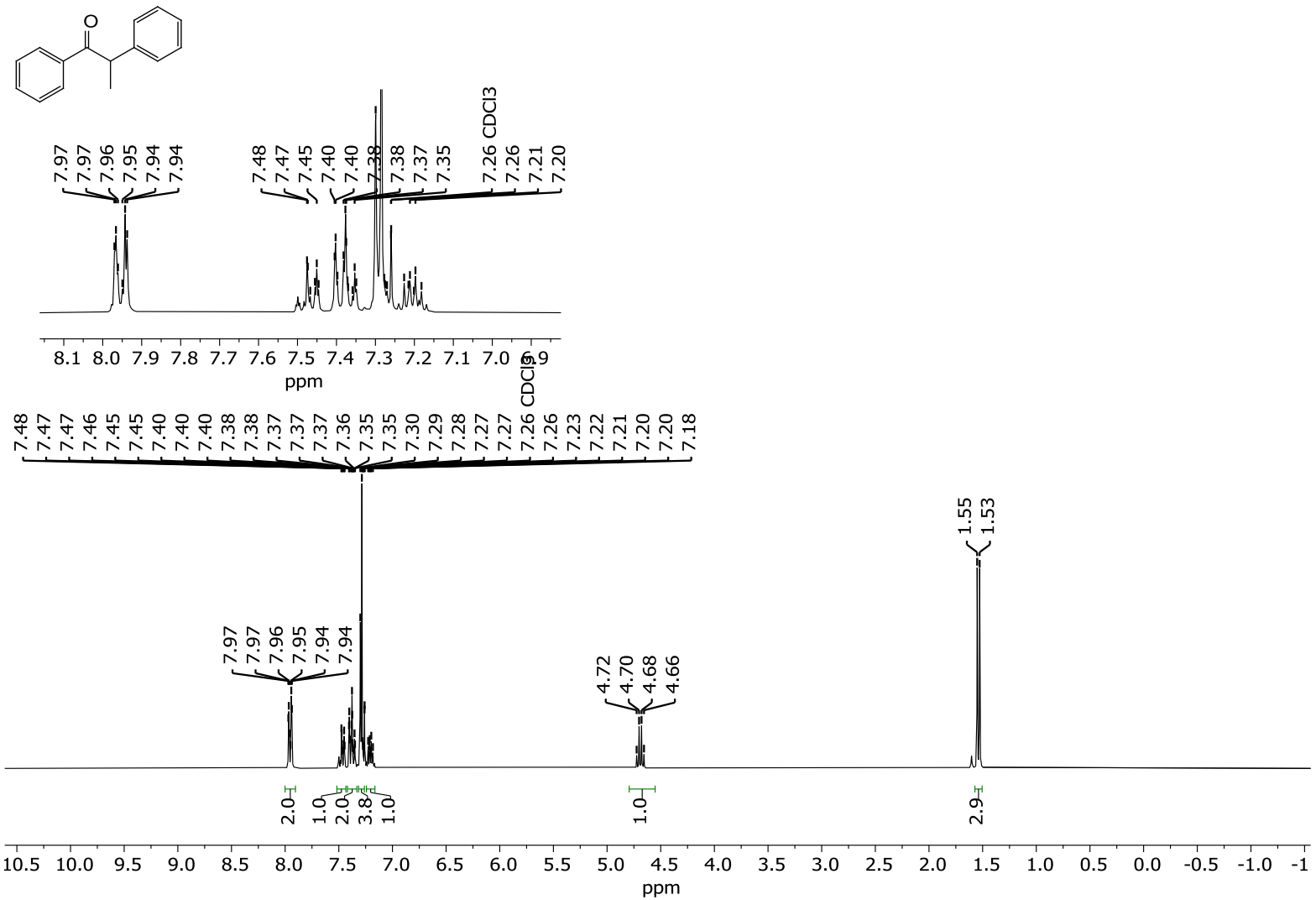

Figure S28. ^{1}H NMR spectrum of compound **5a** ($CDCl_3$, 300 MHz)

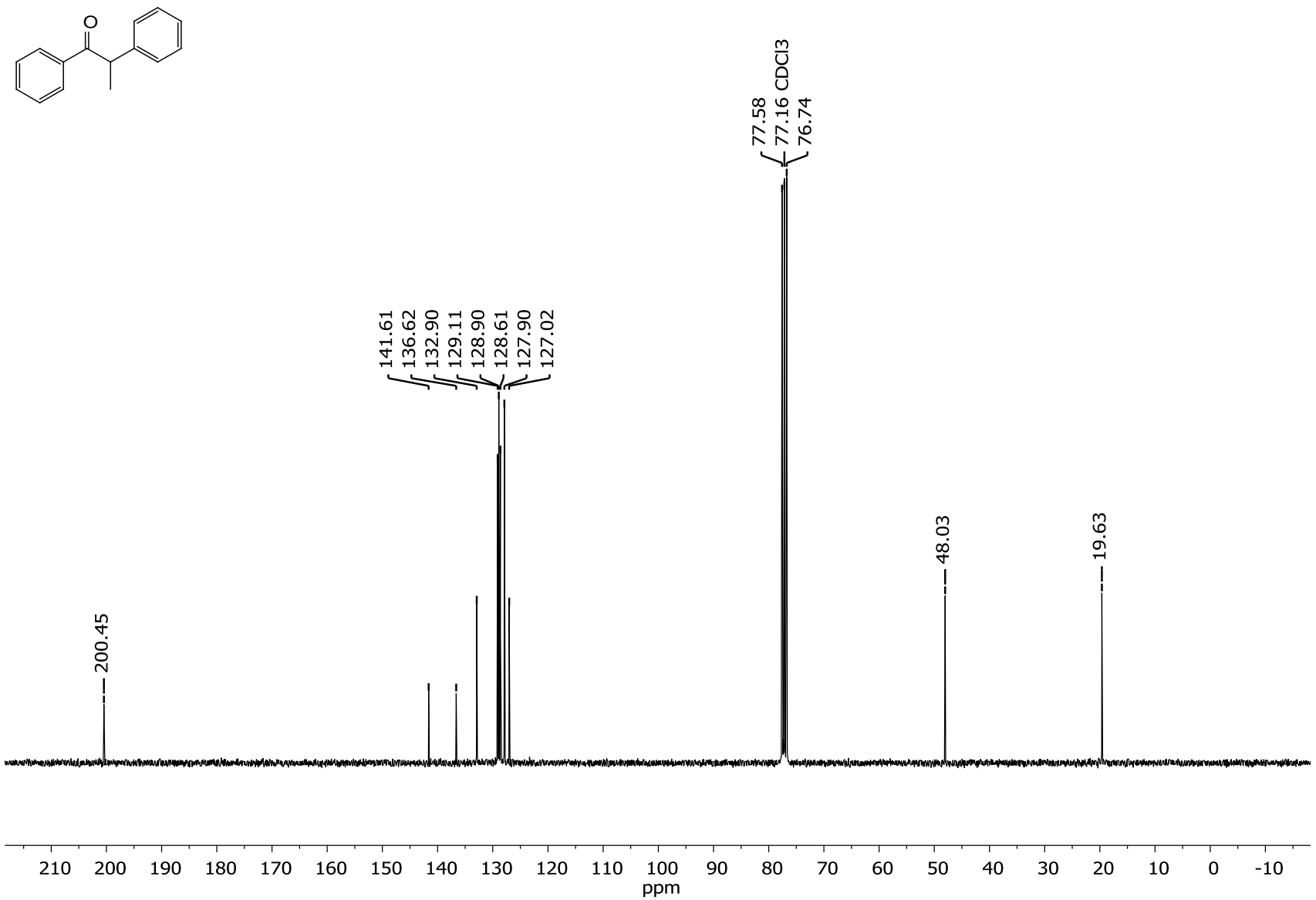

Figure S29. ^{13}C NMR spectrum of compound **5a** ($CDCl_3$, 75 MHz)

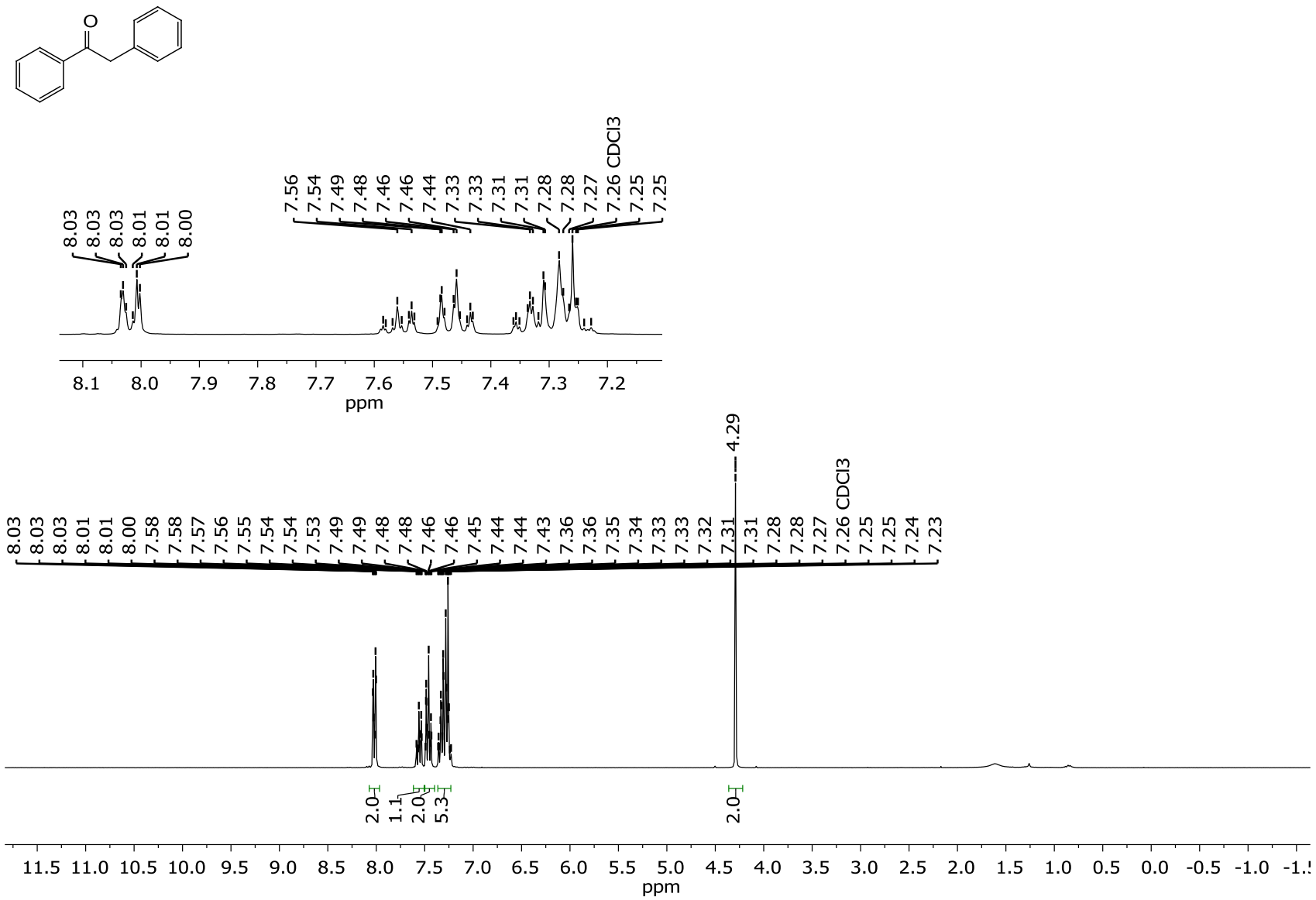

Figure S30. ^{1}H NMR spectrum of compound **5b** ($CDCl_3$, 300 MHz)

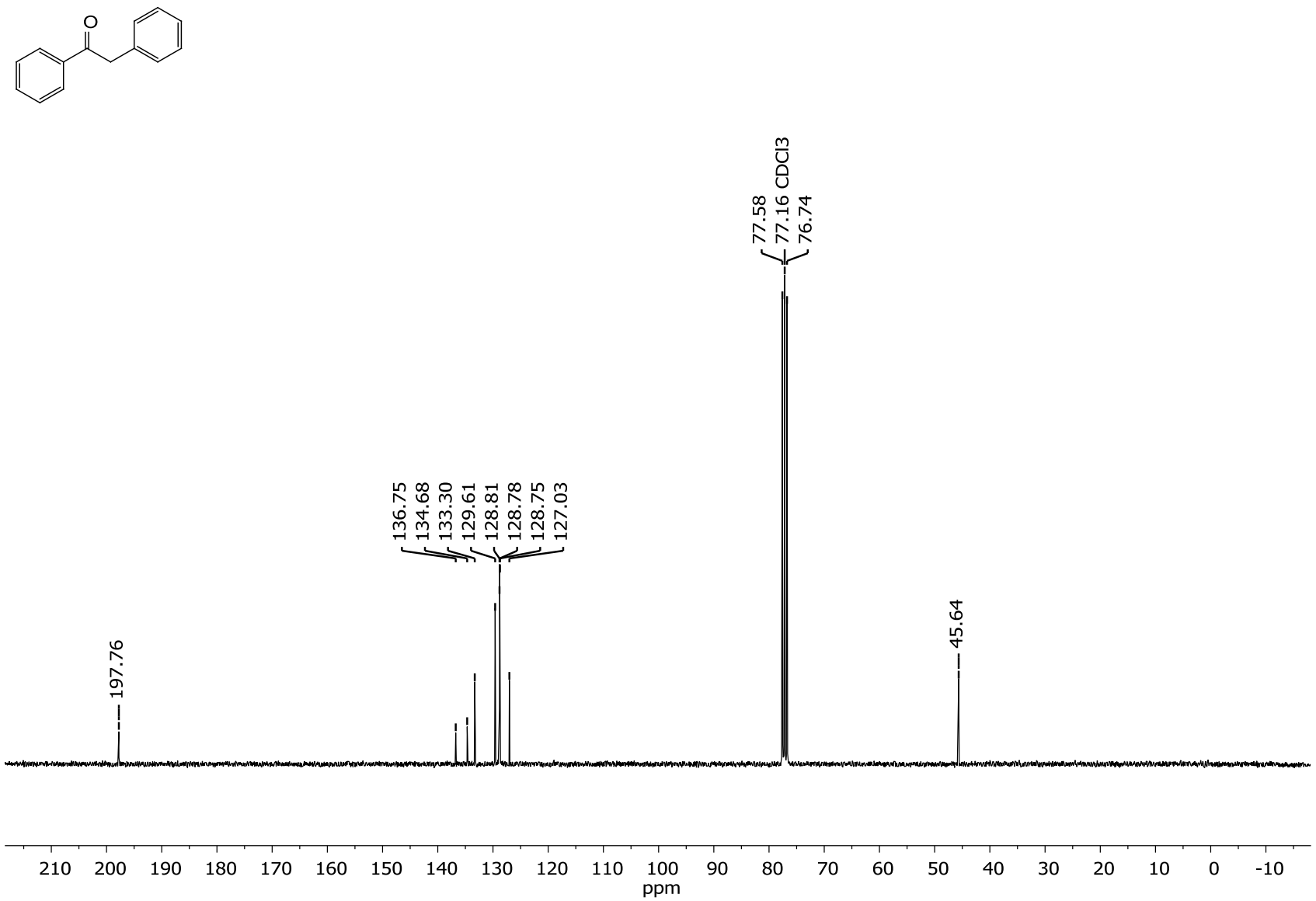

Figure S31. ^{13}C NMR spectrum of compound **5b** ($CDCl_3$, 75 MHz)

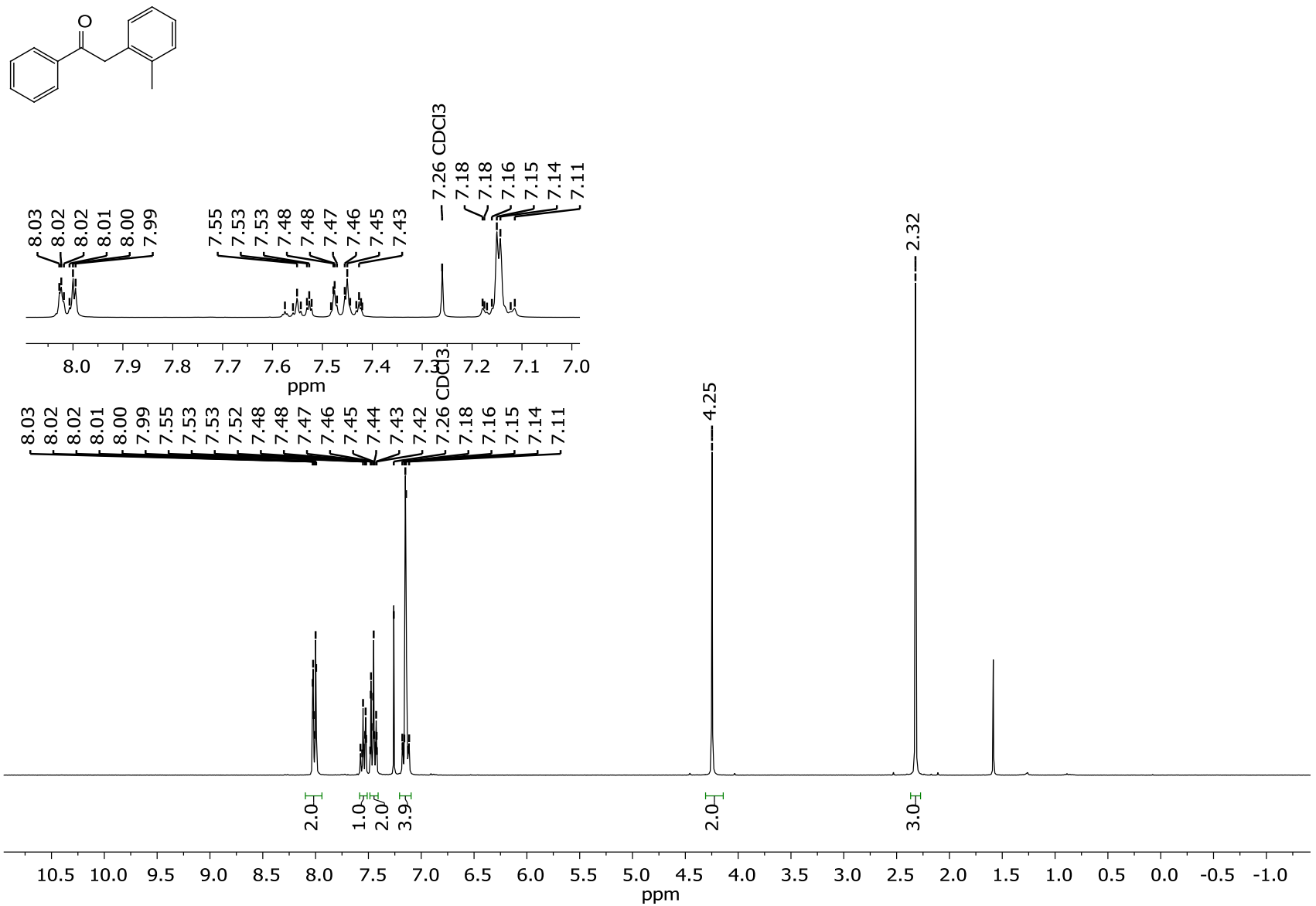

Figure S32. ^{1}H NMR spectrum of compound **5c** ($CDCl_3$, 300 MHz)

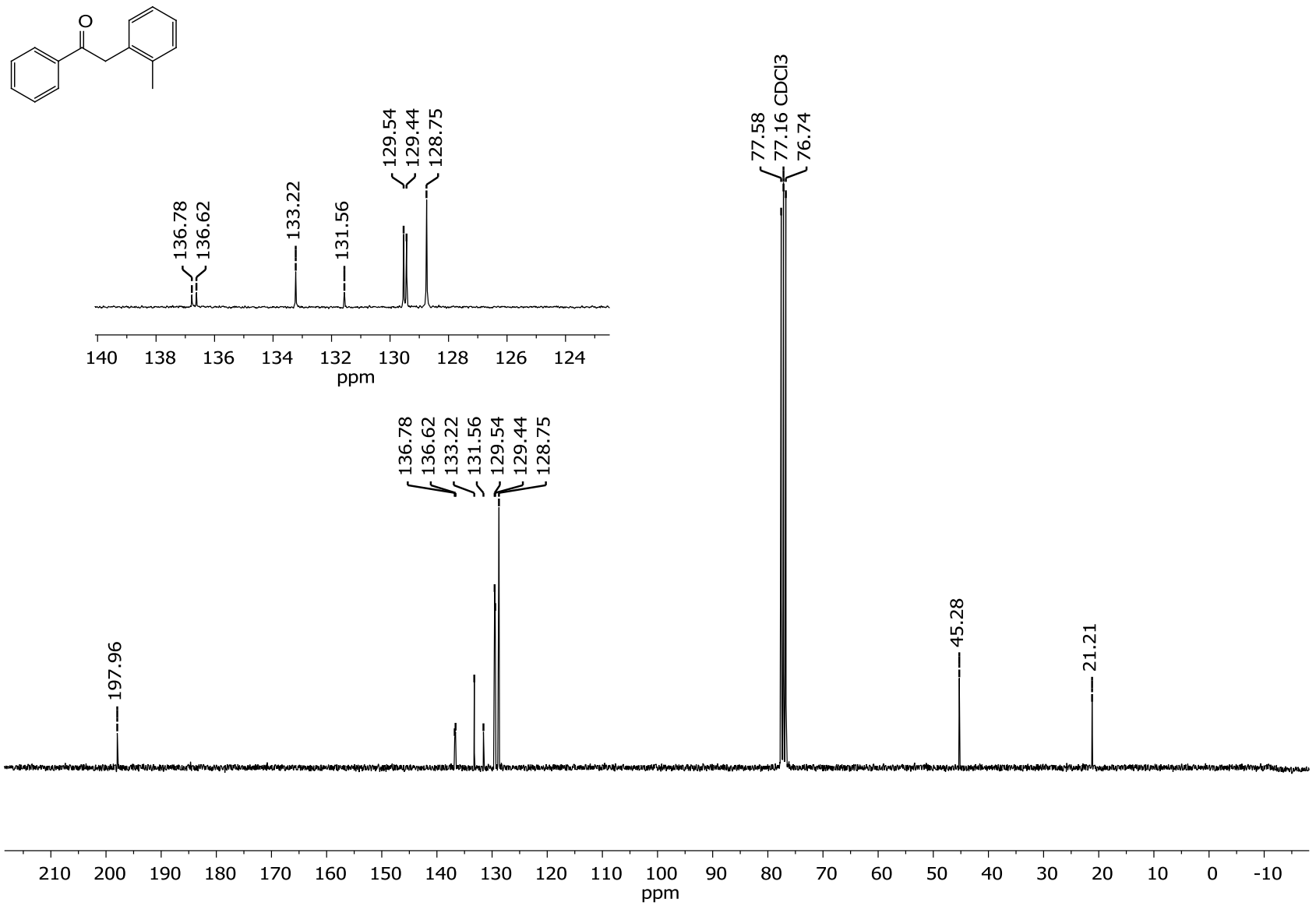

Figure S33. ^{13}C NMR spectrum of compound **5c** ($CDCl_3$, 75 MHz)

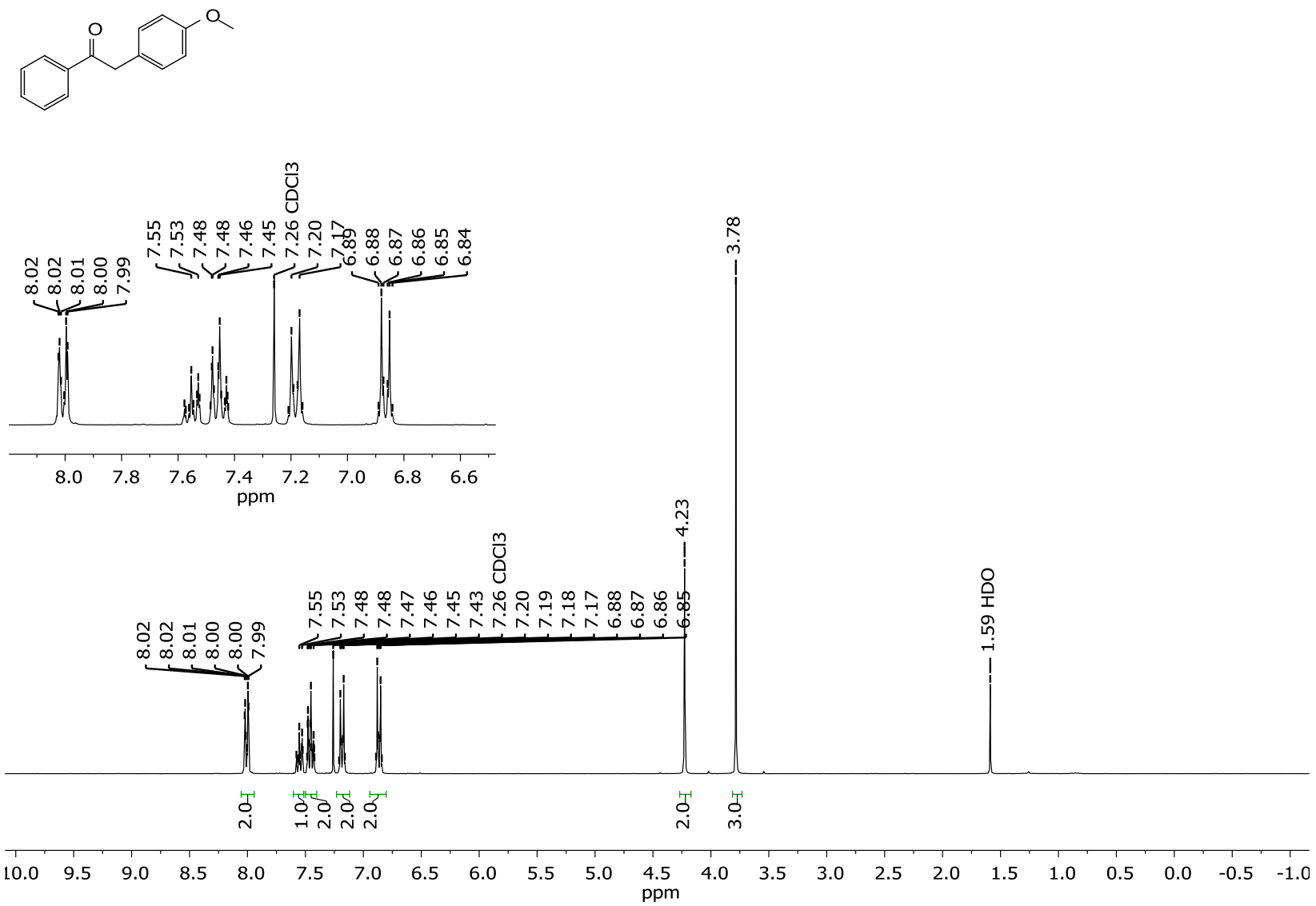

Figure S34. ^{1}H NMR spectrum of compound **5d** ($CDCl_3$, 300 MHz)

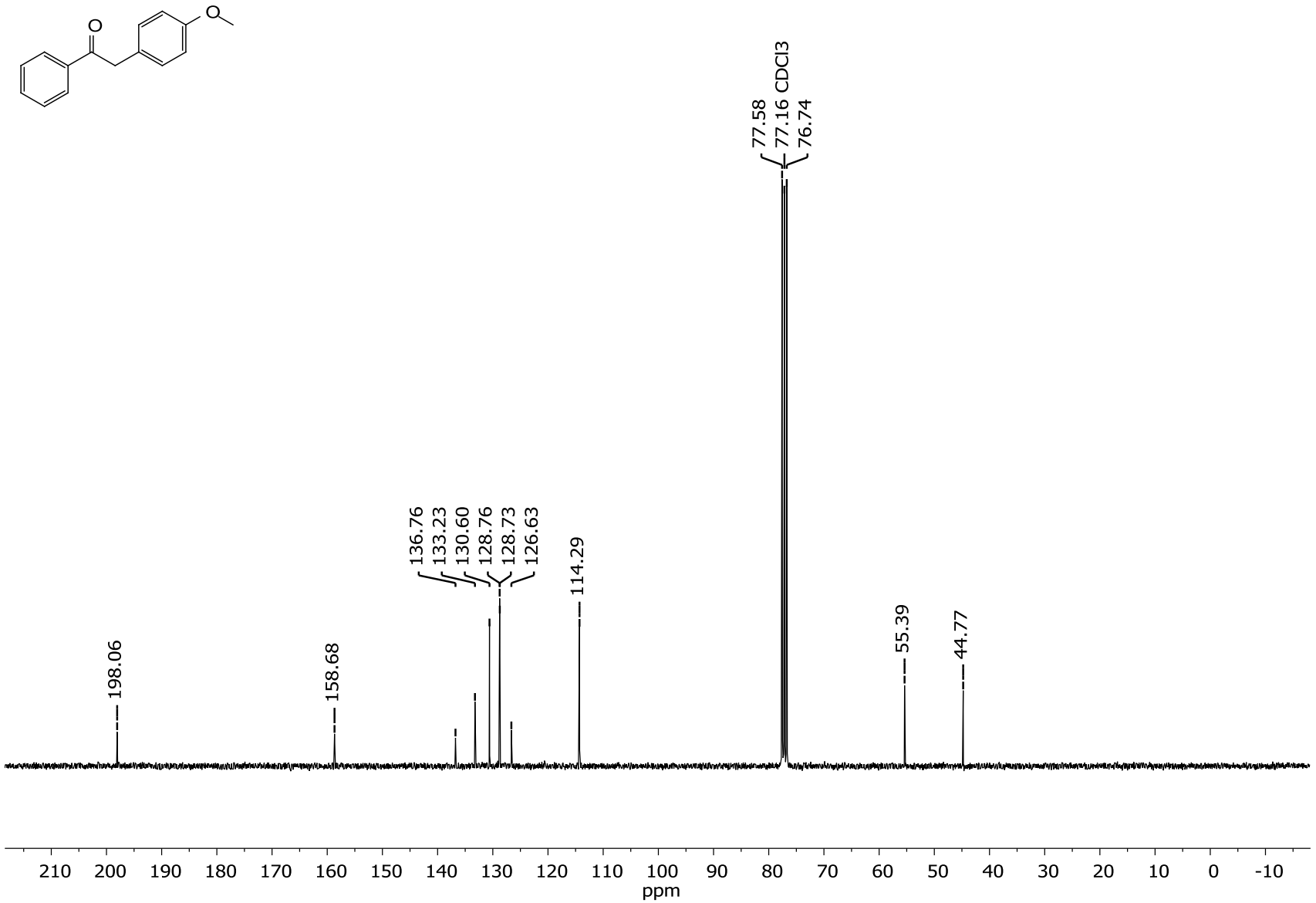

Figure S35. ^{13}C NMR spectrum of compound **5d** ($CDCl_3$, 75 MHz)

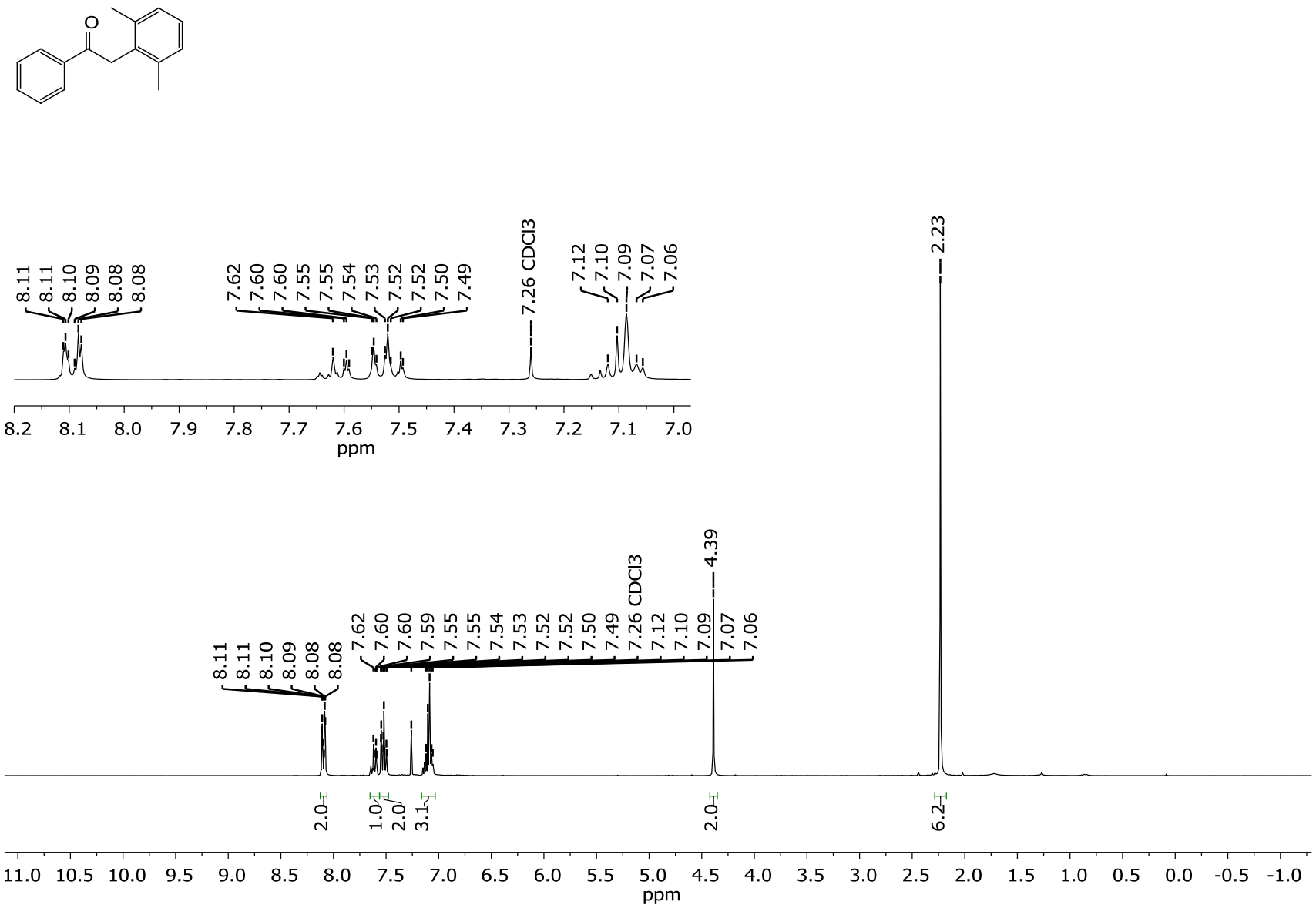

Figure S36. ^{1}H NMR spectrum of compound **5e** ($CDCl_3$, 300 MHz)

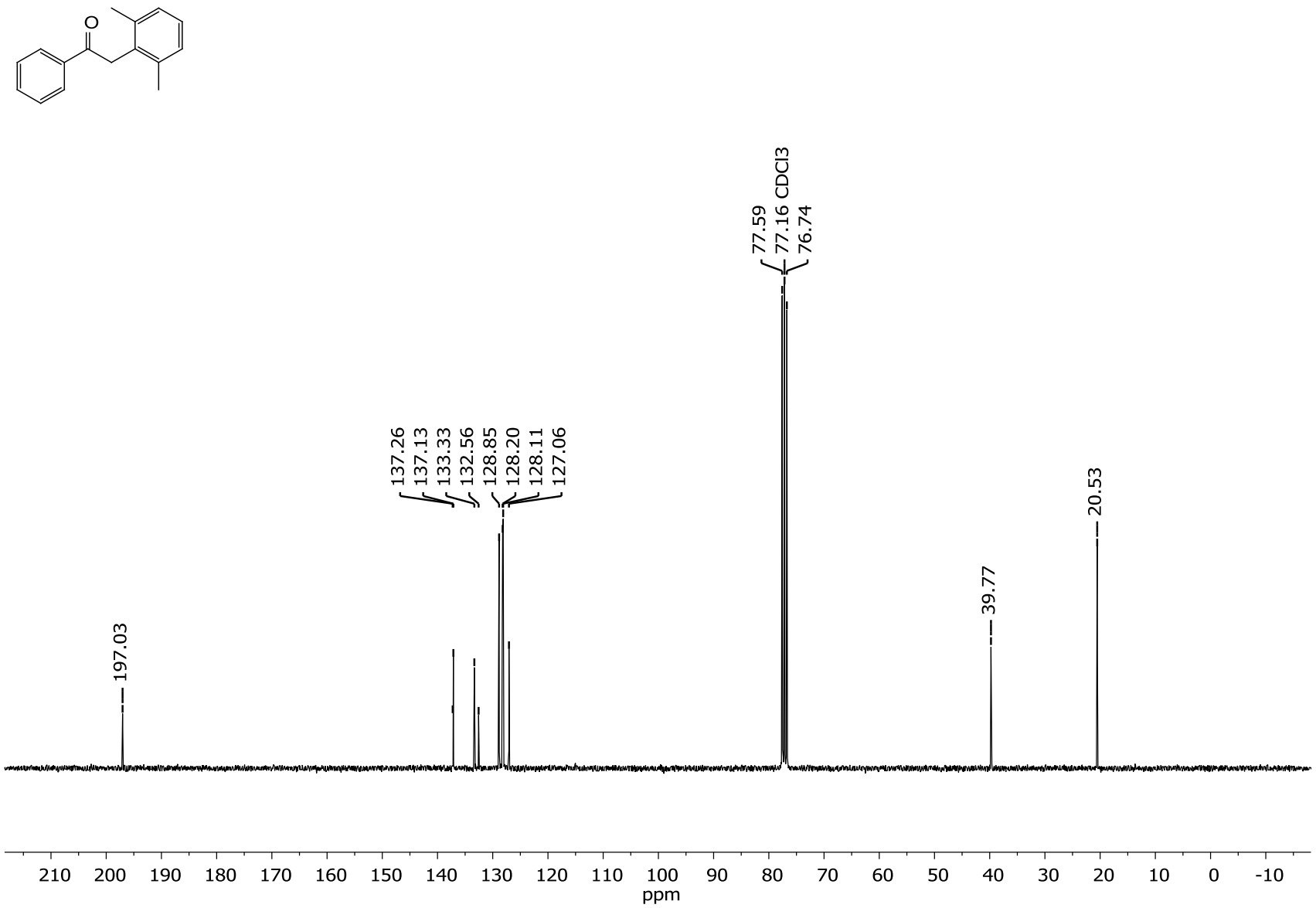

Figure S37. ^{13}C NMR spectrum of compound **5e** ($CDCl_3$, 75 MHz)

Figure S38. ^{1}H NMR spectrum of compound **5f** ($CDCl_3$, 300 MHz)

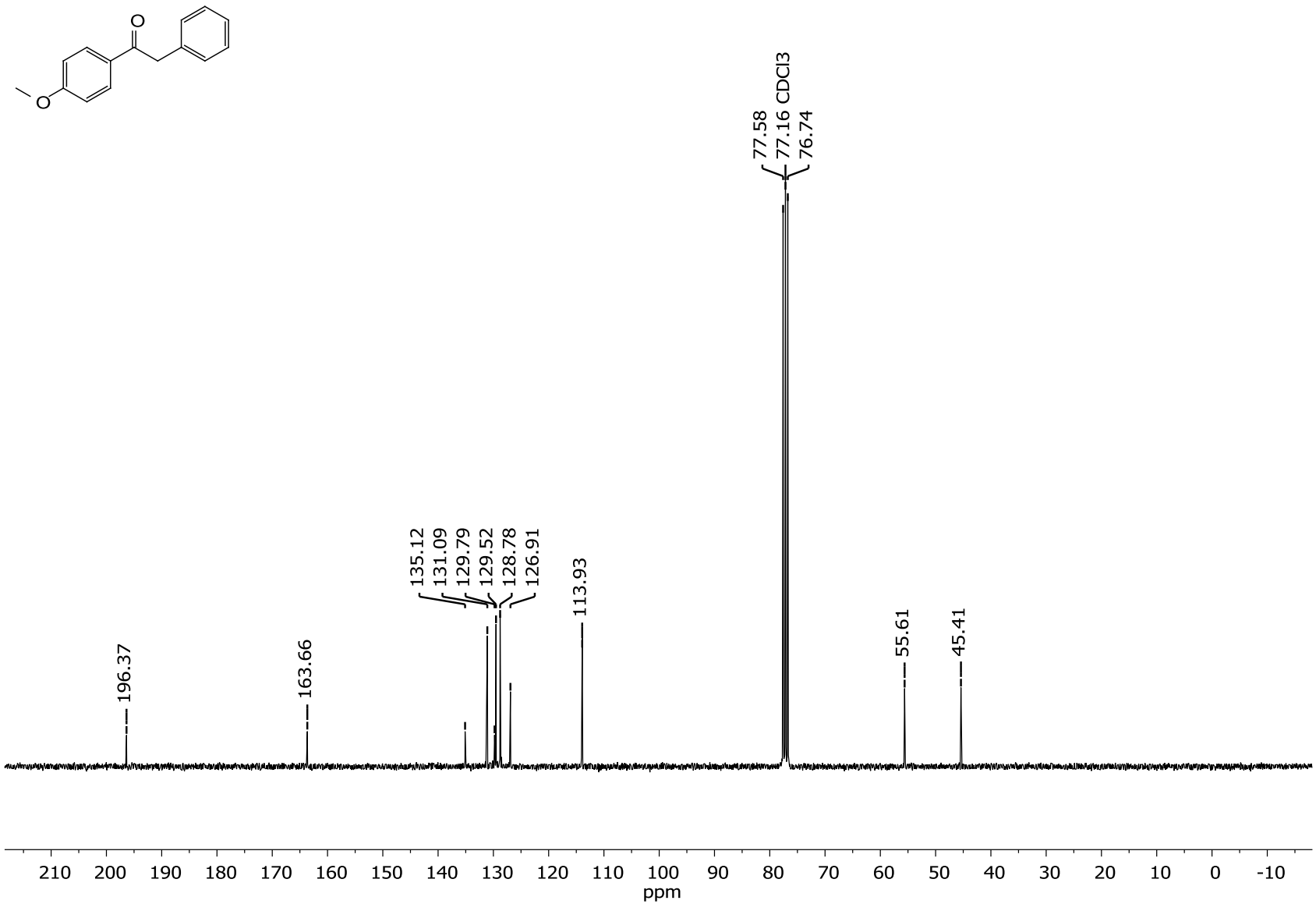

Figure S39. ^{13}C NMR spectrum of compound **5f** ($CDCl_3$, 75 MHz)

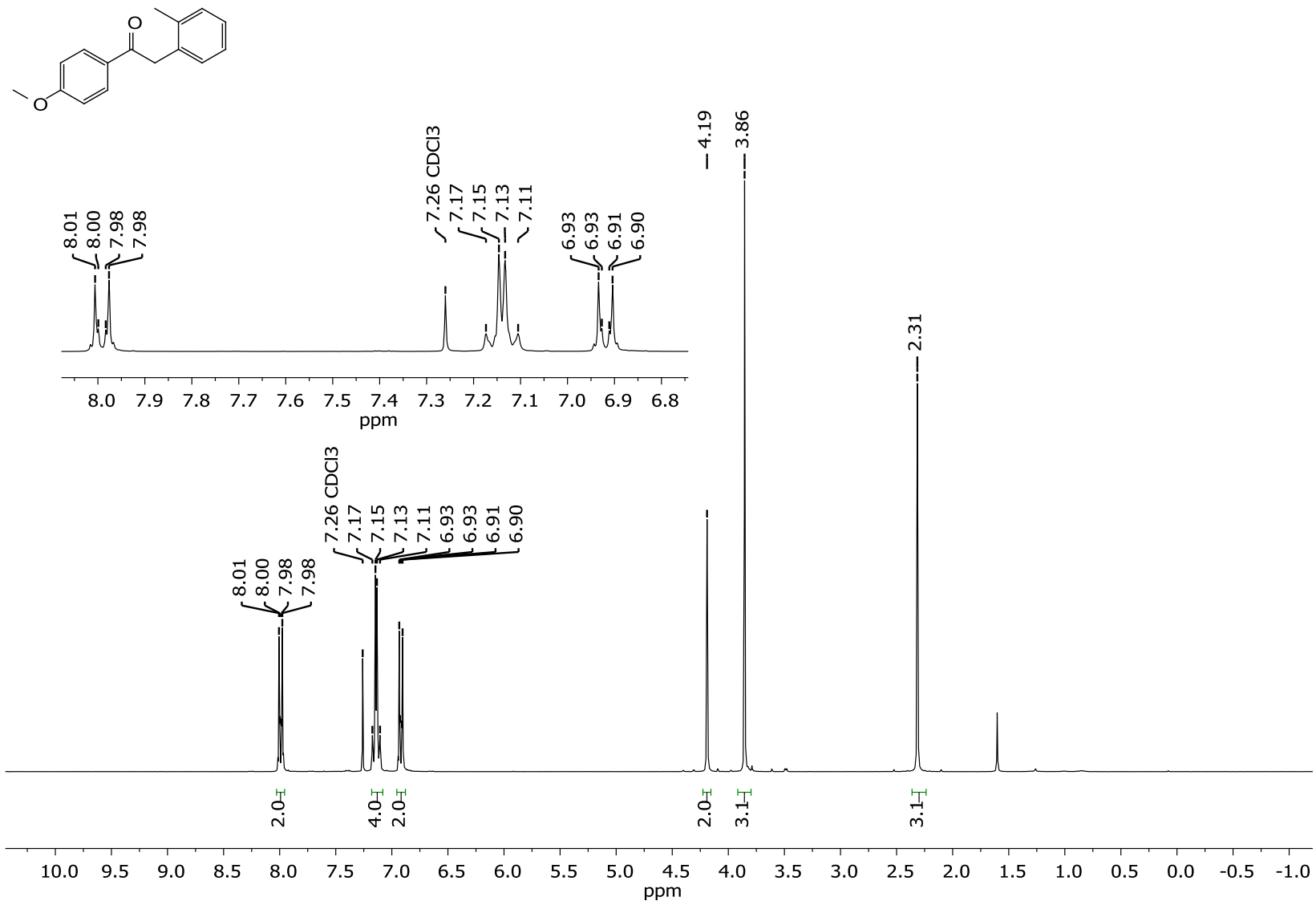

Figure S40. ^{1}H NMR spectrum of compound **5g** ($CDCl_3$, 300 MHz)

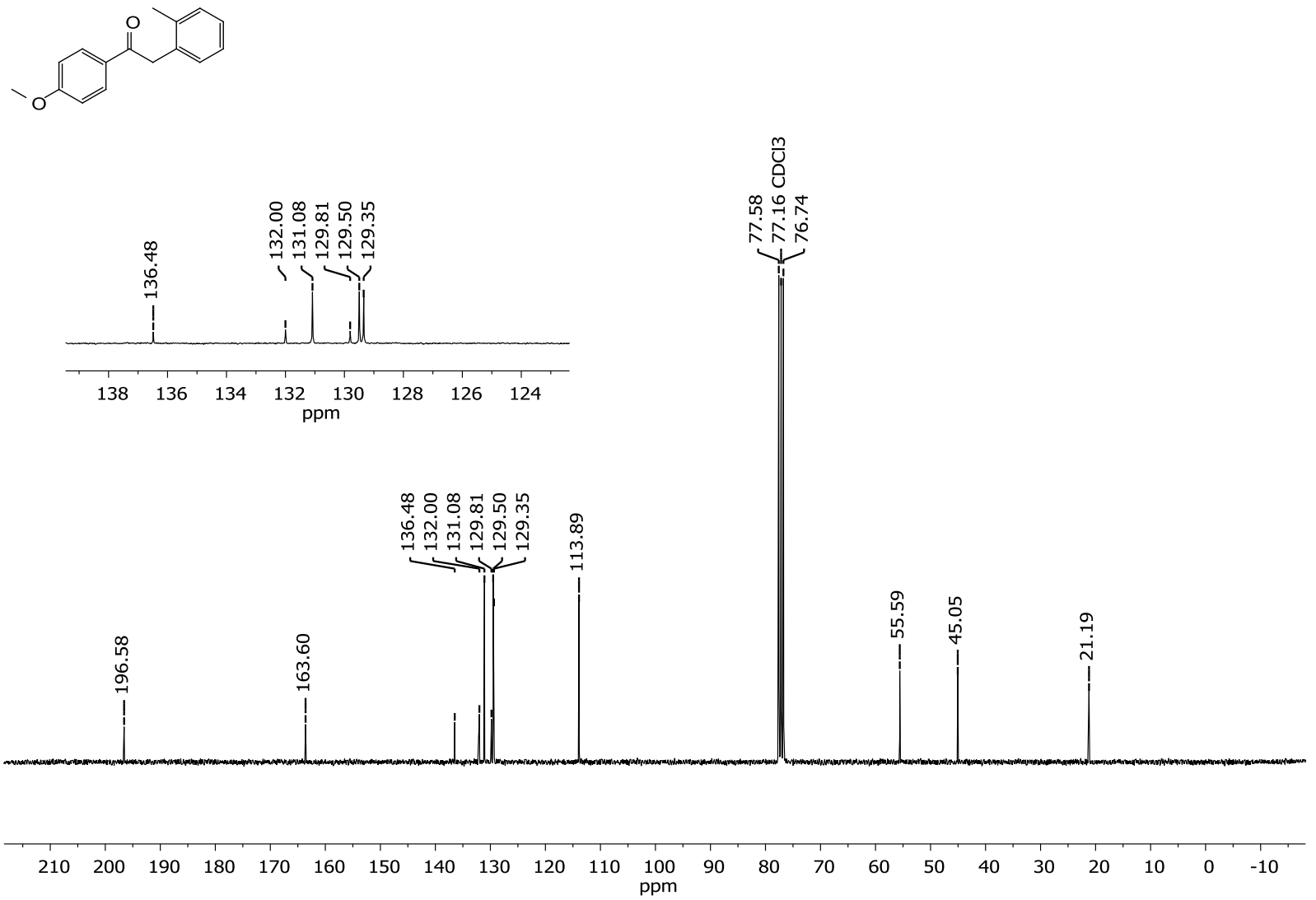

Figure S41. ^{13}C NMR spectrum of compound **5g** ($CDCl_3$, 75 MHz)

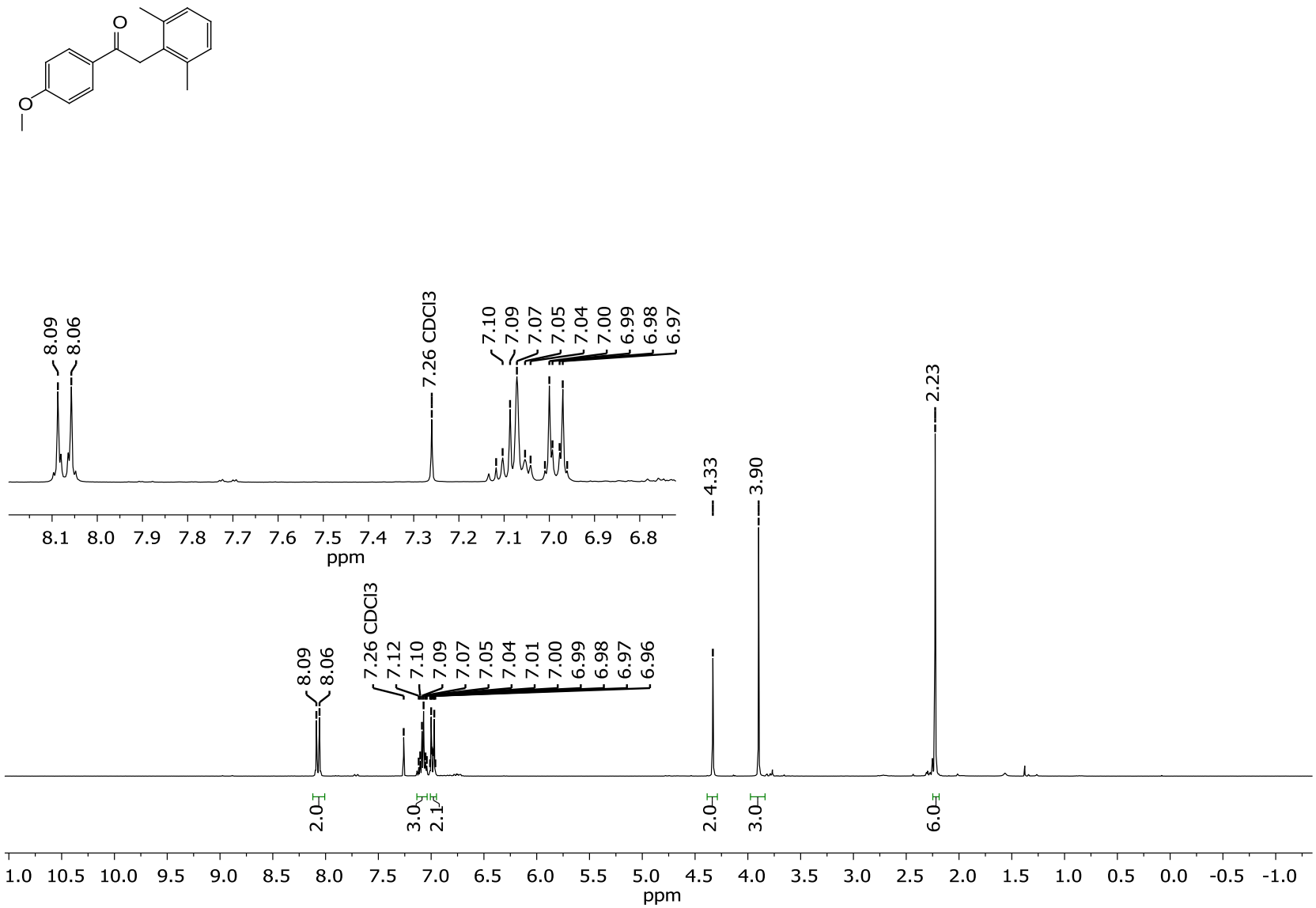

Figure S42. ^{1}H NMR spectrum of compound **5h** ($CDCl_3$, 300 MHz)

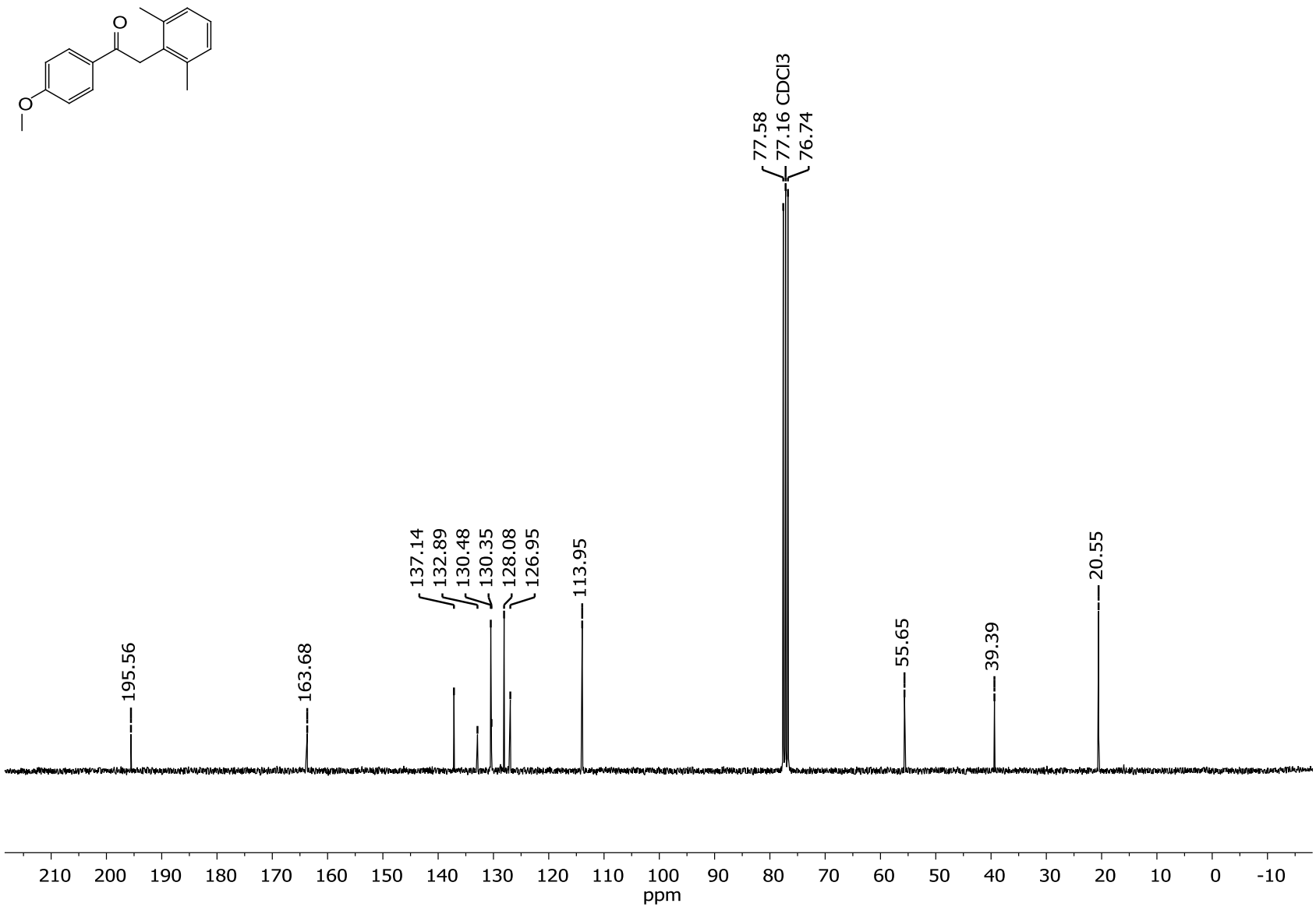

Figure S43. ^{13}C NMR spectrum of compound **5h** ($CDCl_3$, 75 MHz)

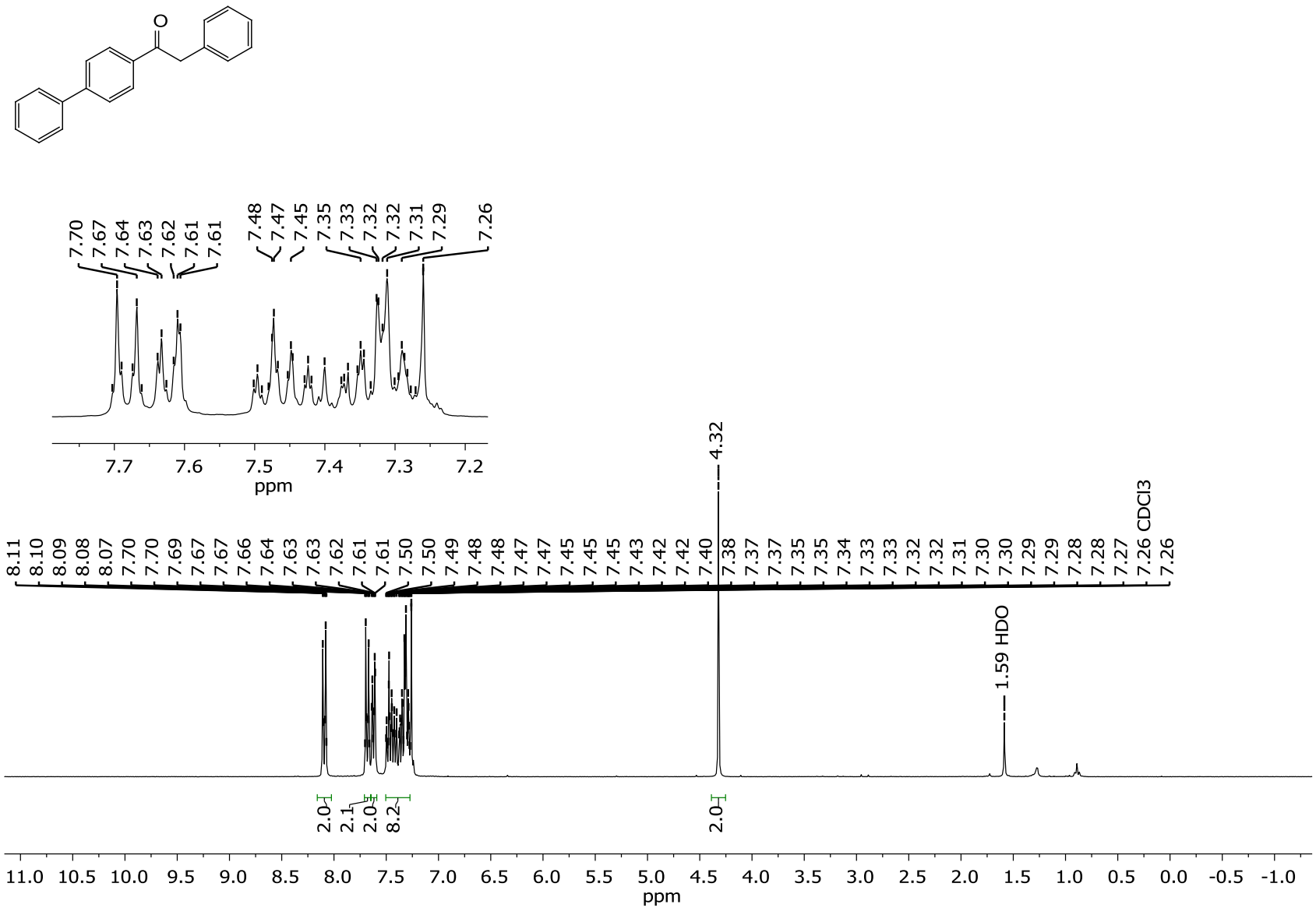

Figure S44. ^{1}H NMR spectrum of compound **5i** ($CDCl_3$, 300 MHz)

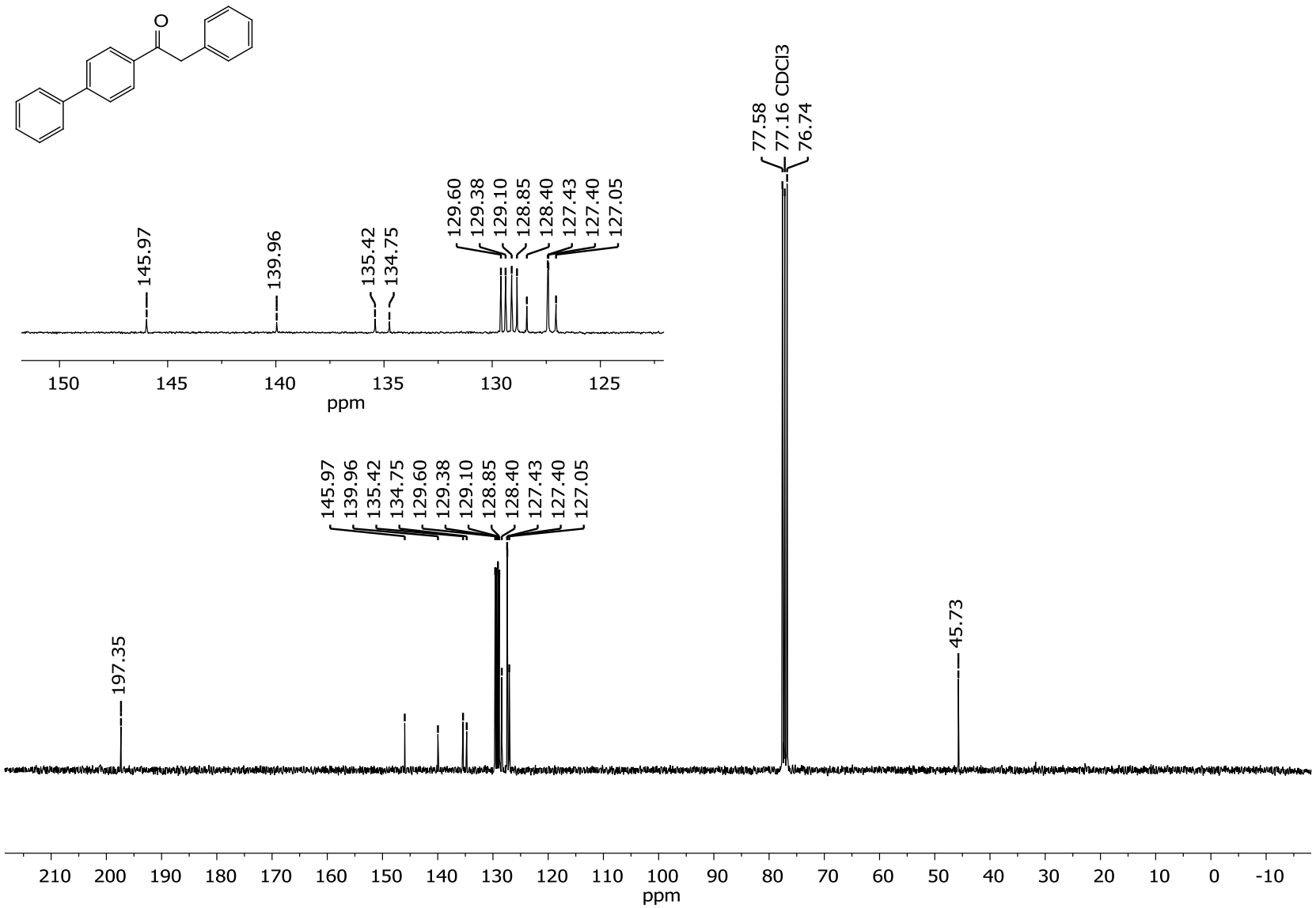

Figure S45. ^{13}C NMR spectrum of compound **5i** ($CDCl_3$, 75 MHz)

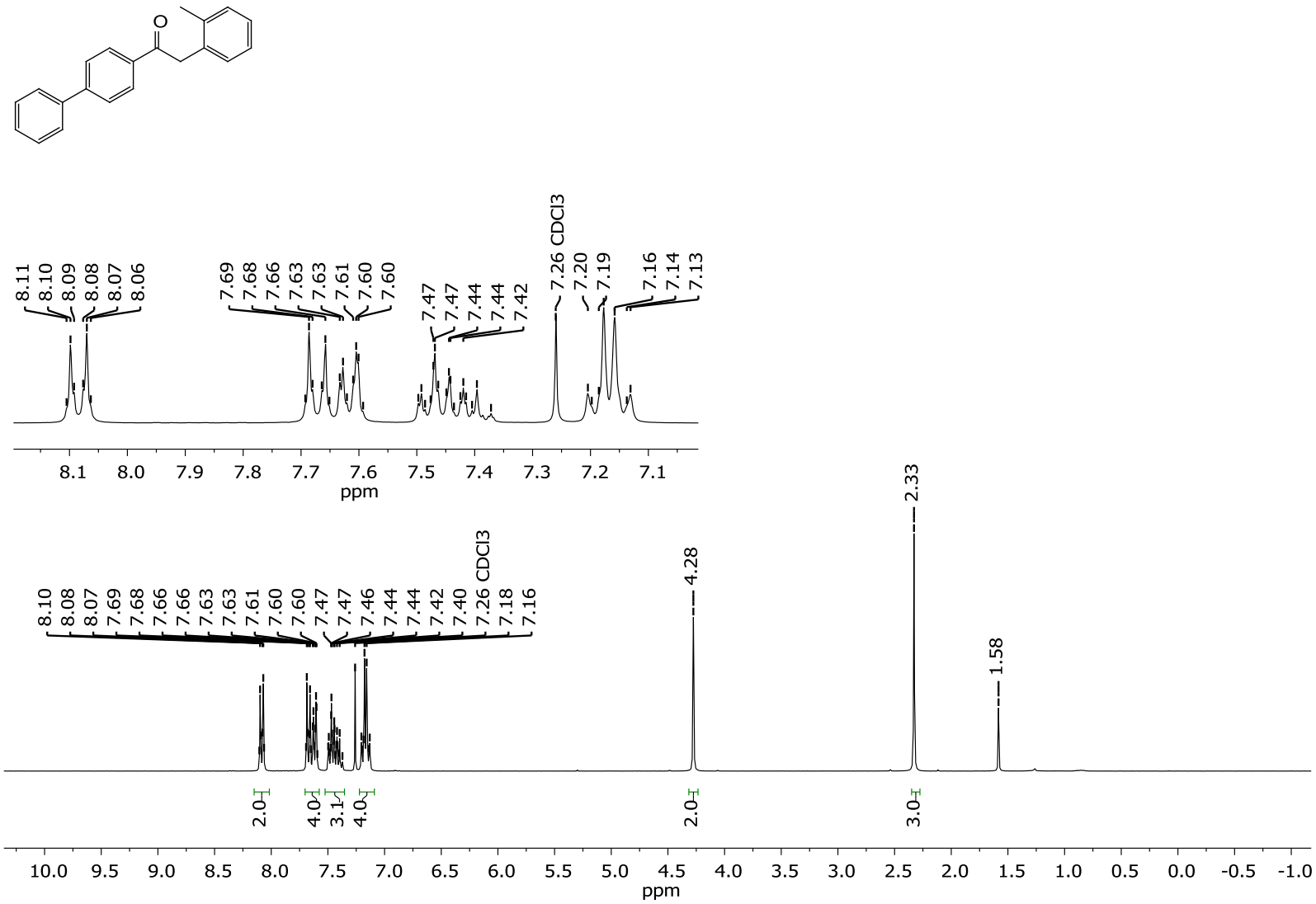

Figure S46. ^{1}H NMR spectrum of compound **5j** ($CDCl_3$, 300 MHz)

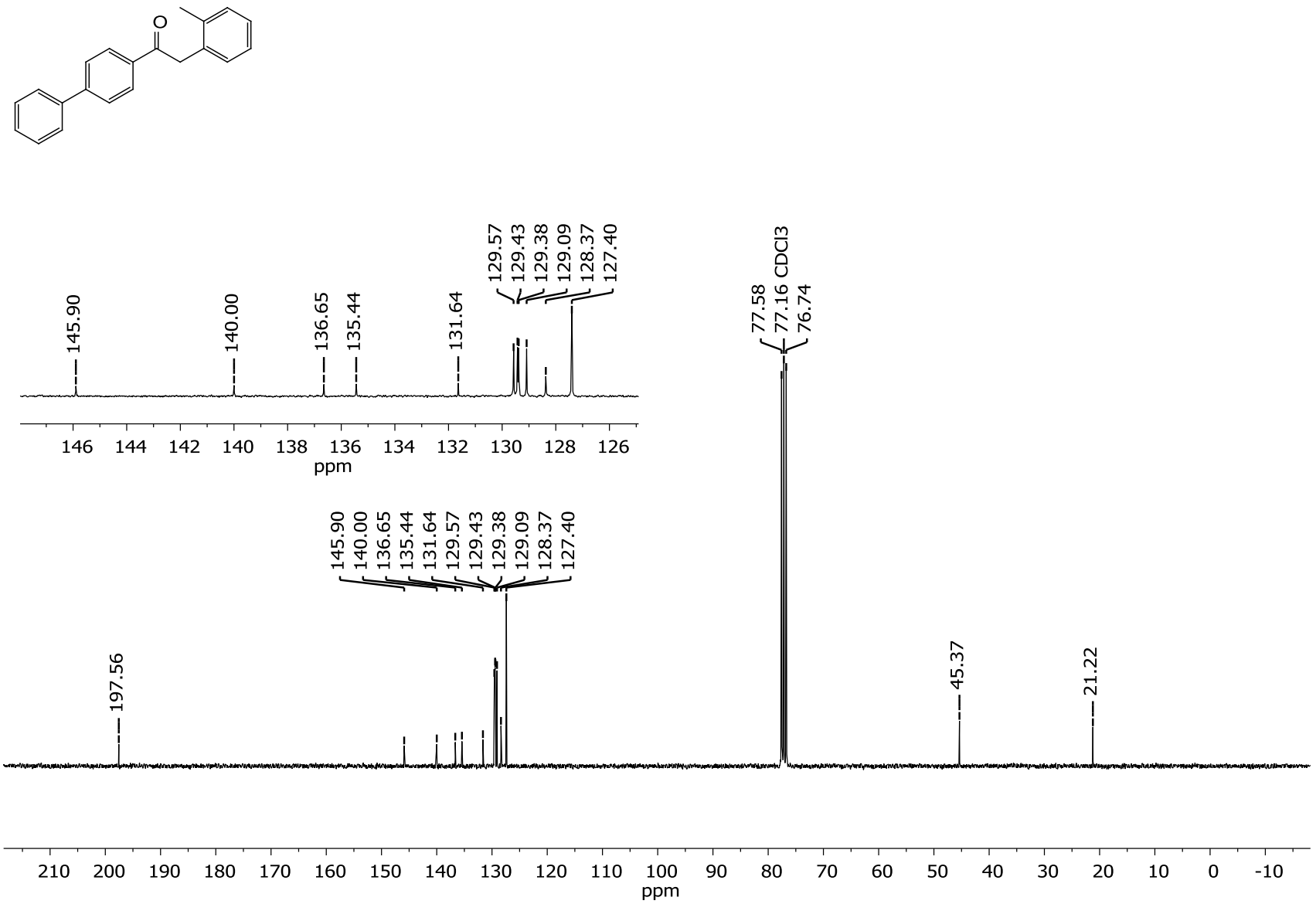

Figure S47. ^{13}C NMR spectrum of compound **5j** ($CDCl_3$, 75 MHz)

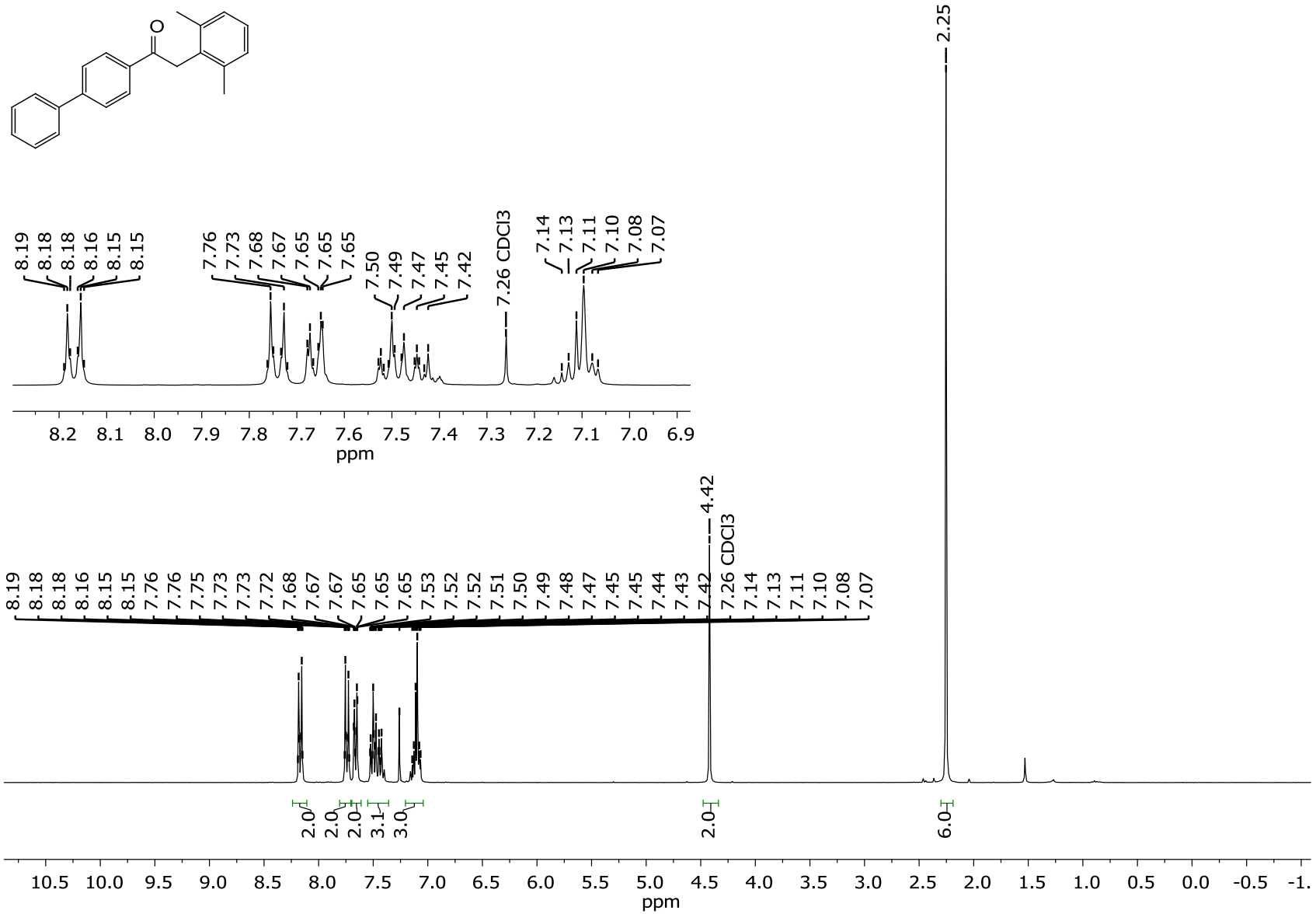

Figure S48. ^{1}H NMR spectrum of compound **5k** ($CDCl_3$, 300 MHz)

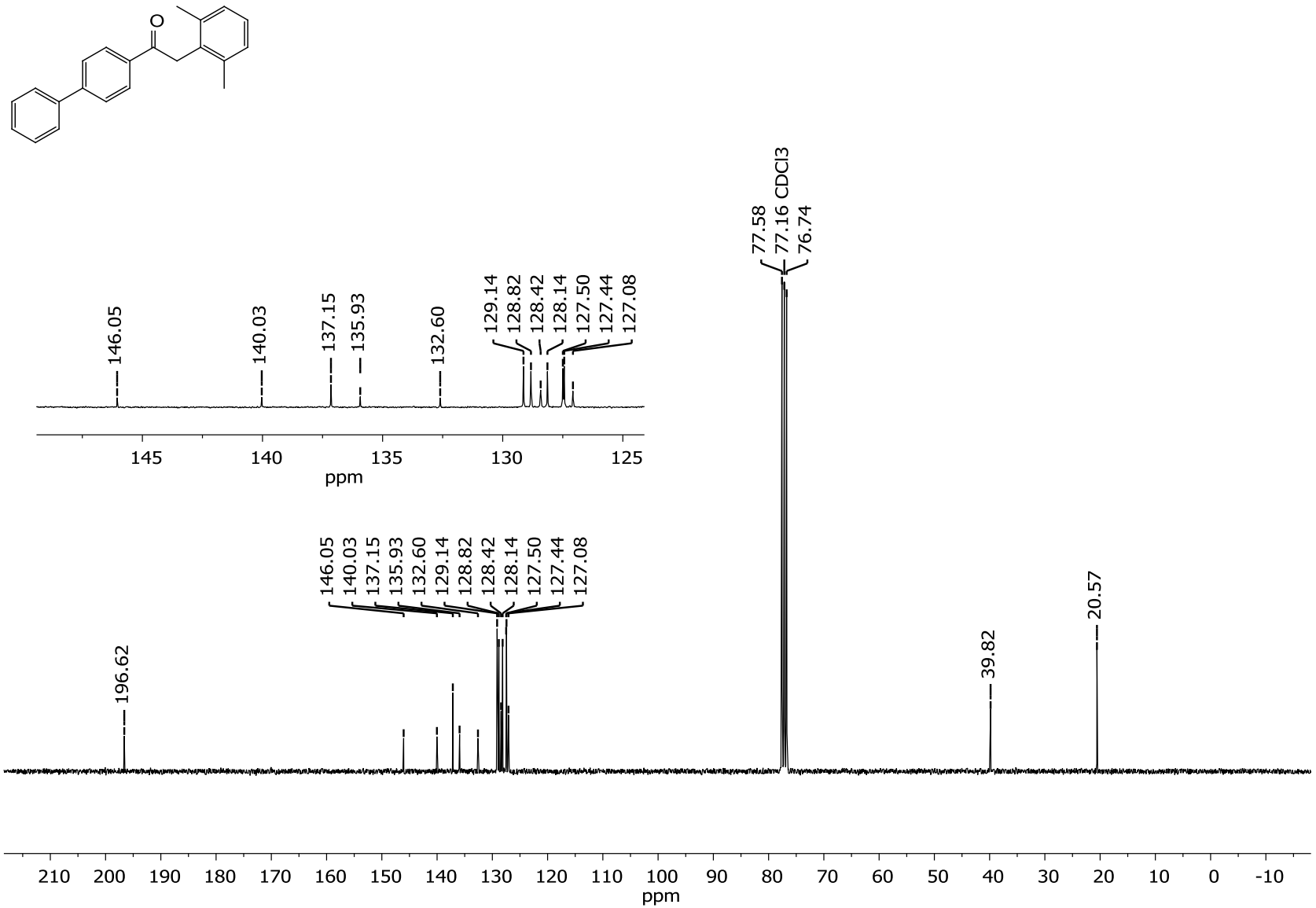

Figure S49. ^{13}C NMR spectrum of compound **5k** ($CDCl_3$, 75 MHz)

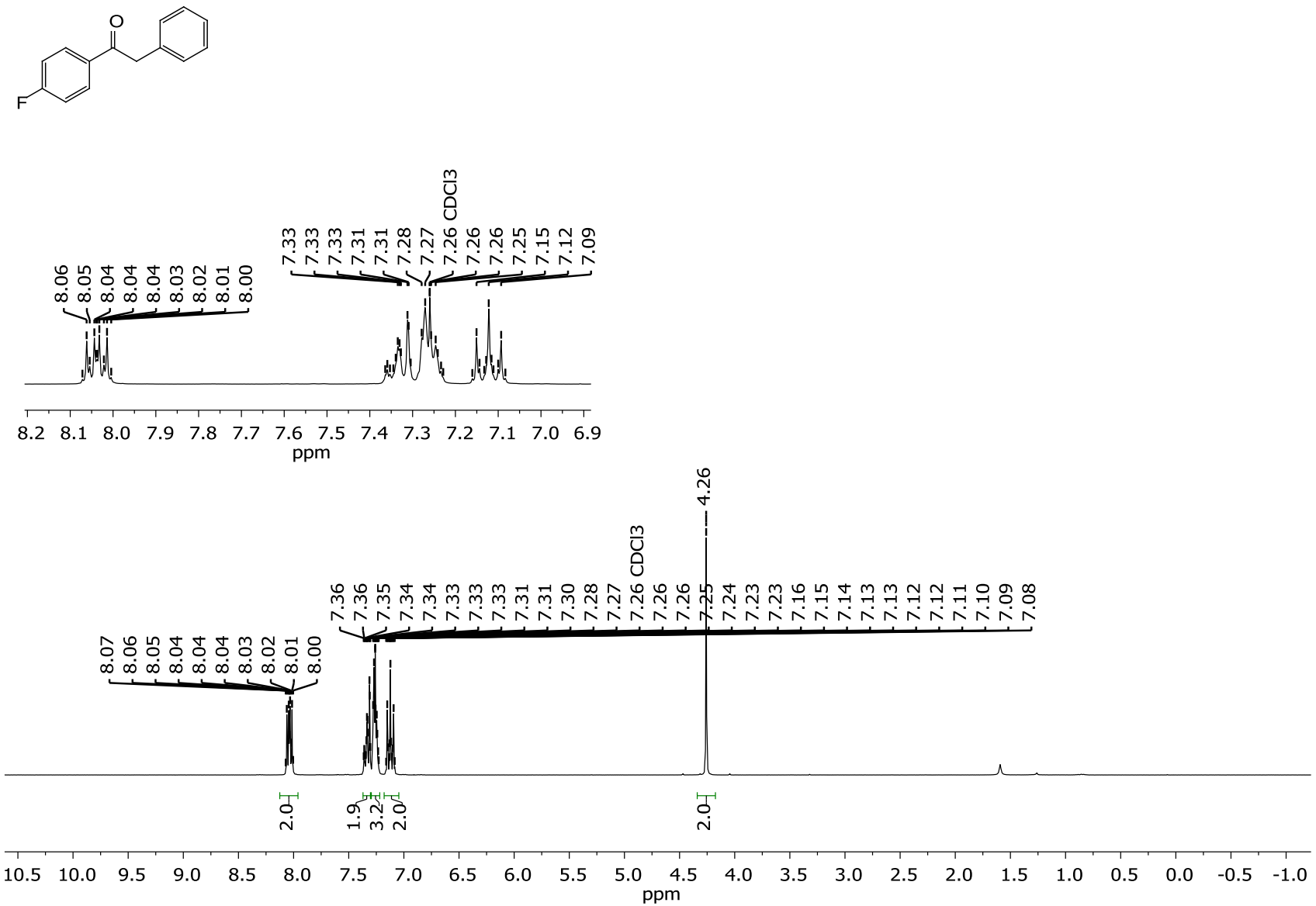

Figure S50. ^{1}H NMR spectrum of compound **5l** ($CDCl_3$, 300 MHz)

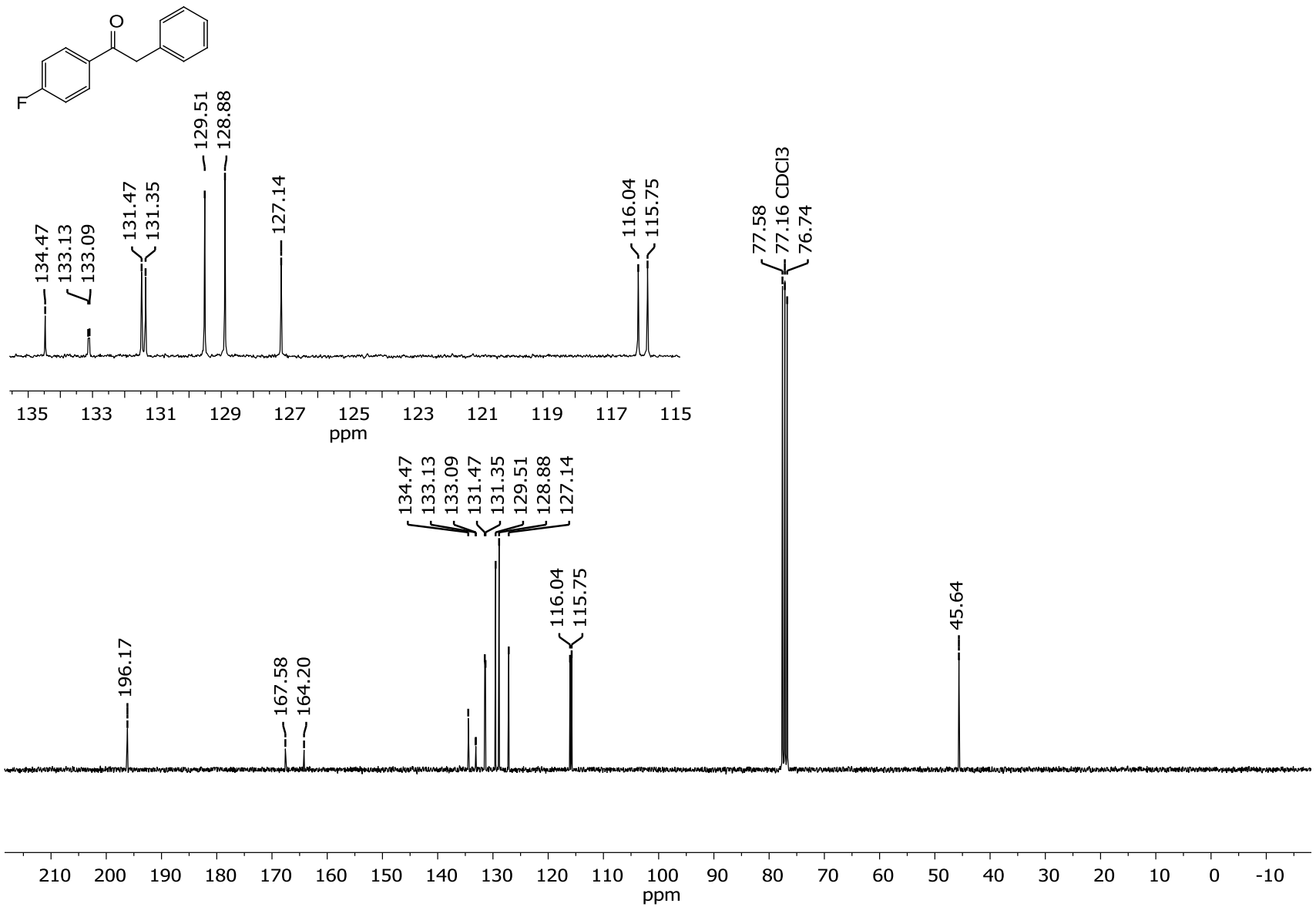

Figure S51. ^{13}C NMR spectrum of compound **5l** ($CDCl_3$, 75 MHz)

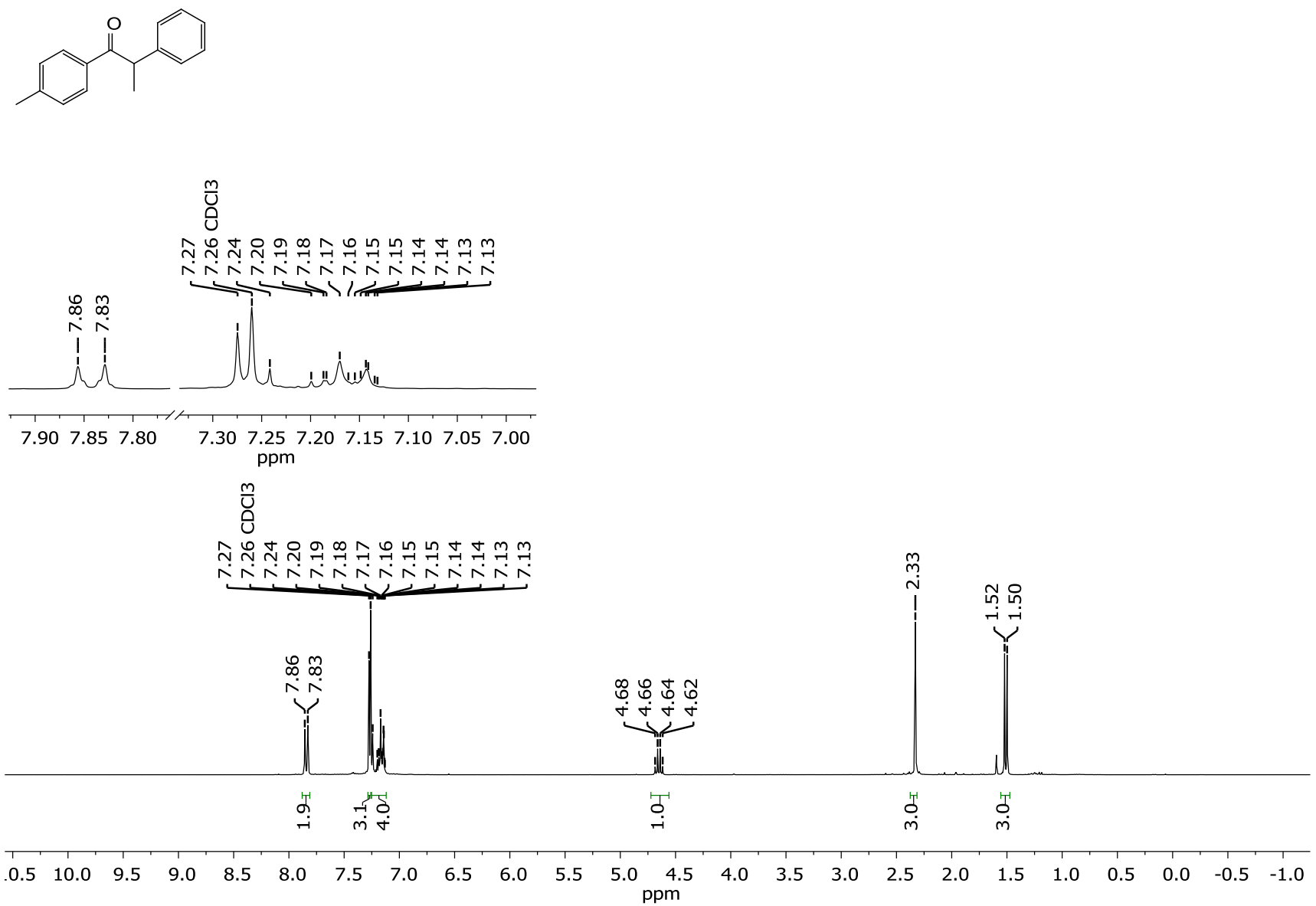

Figure S52. ^{1}H NMR spectrum of compound **5m** ($CDCl_3$, 300 MHz)

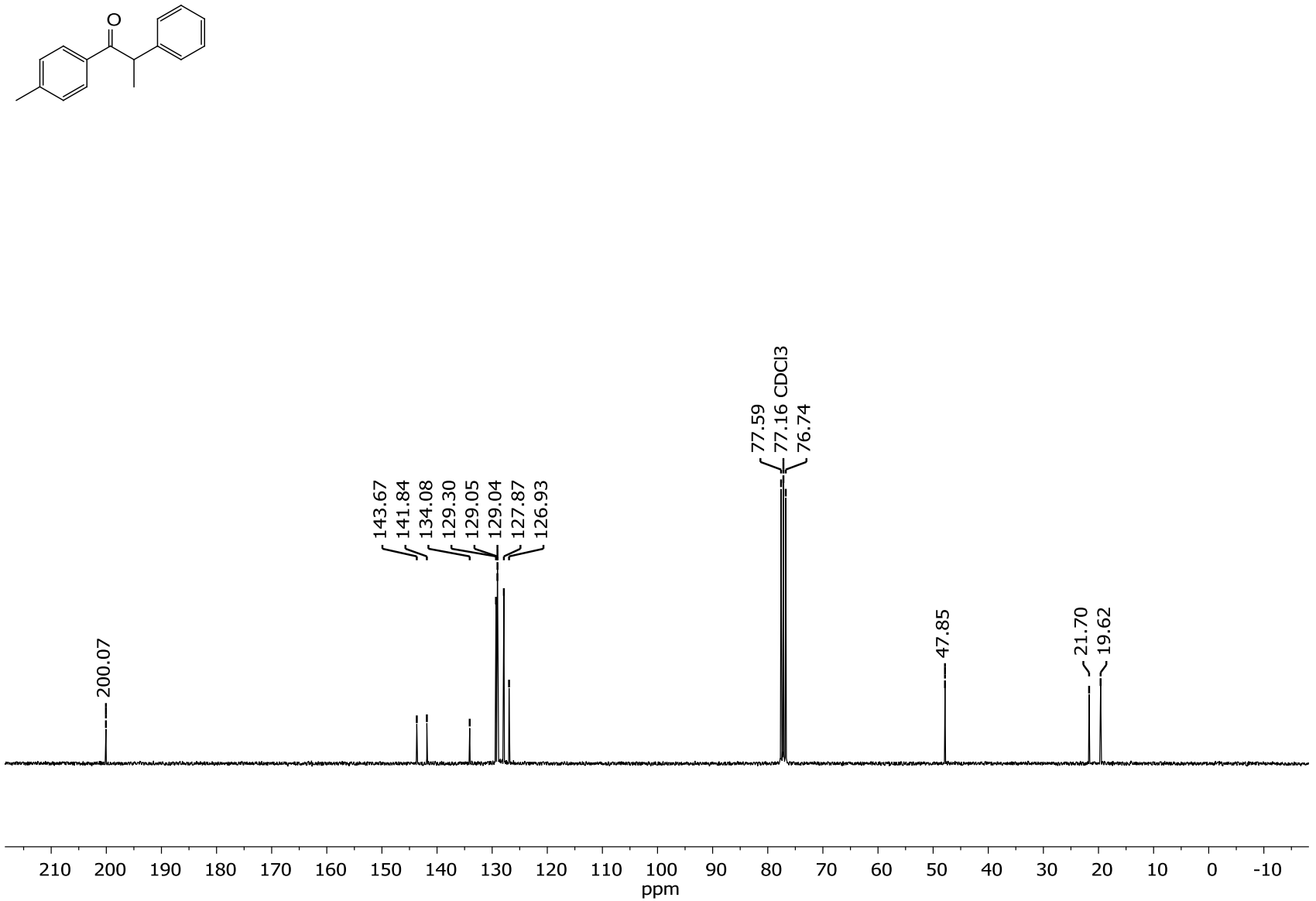

Figure S53. ^{13}C NMR spectrum of compound **5m** ($CDCl_3$, 75 MHz)

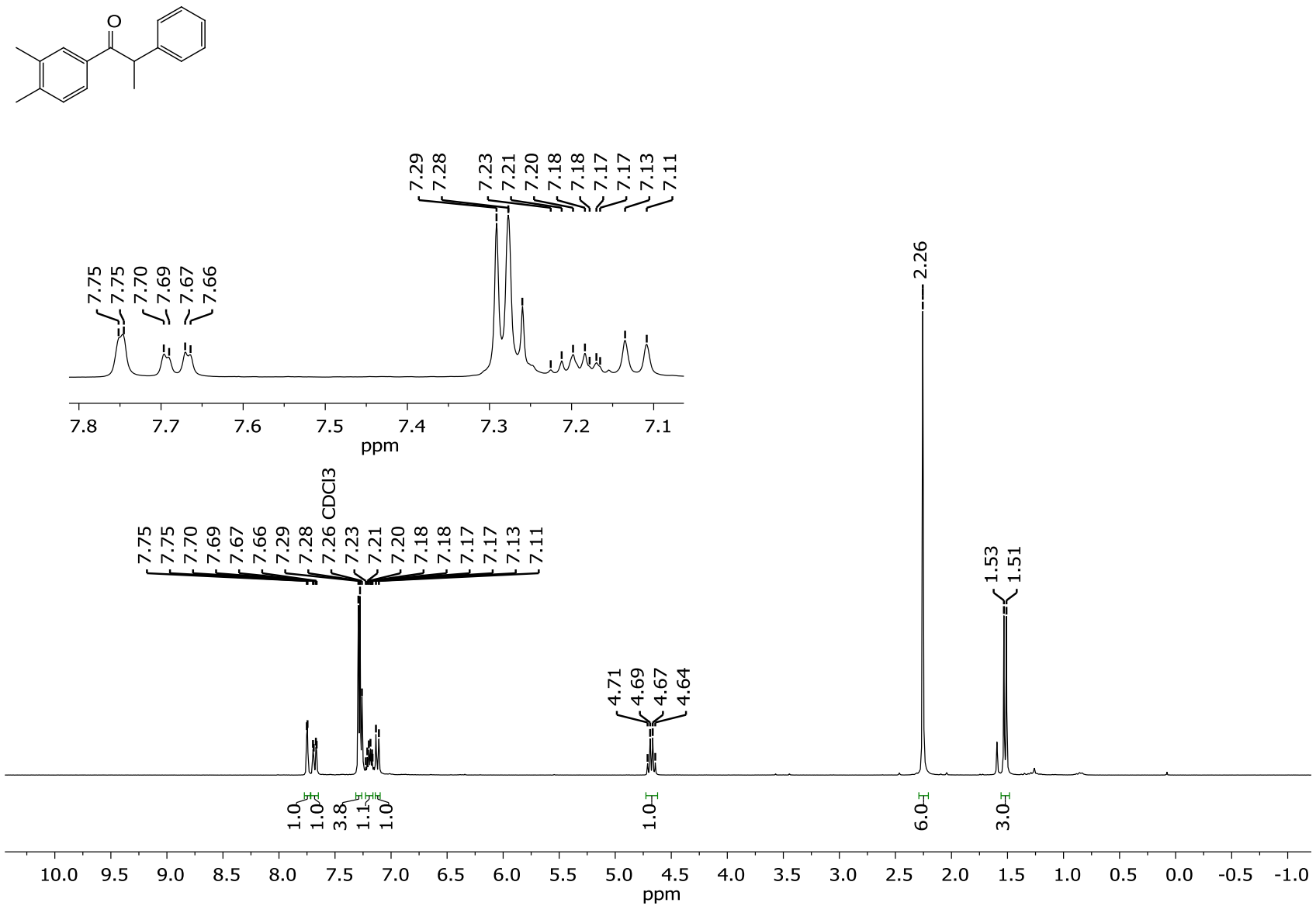

Figure S54. ^{1}H NMR spectrum of compound **5n** ($CDCl_3$, 300 MHz)

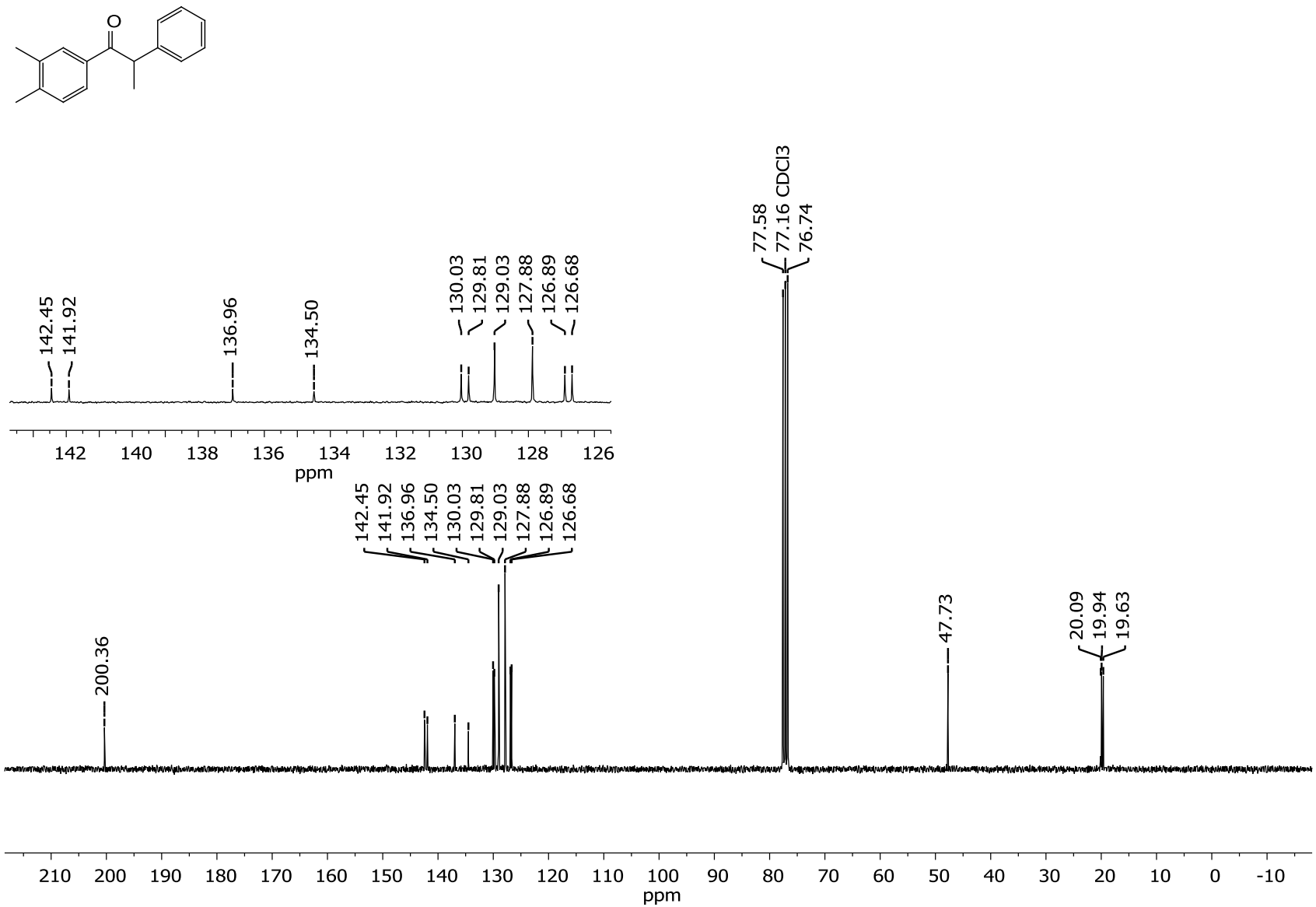

Figure S55. ^{13}C NMR spectrum of compound **5n** ($CDCl_3$, 75 MHz)

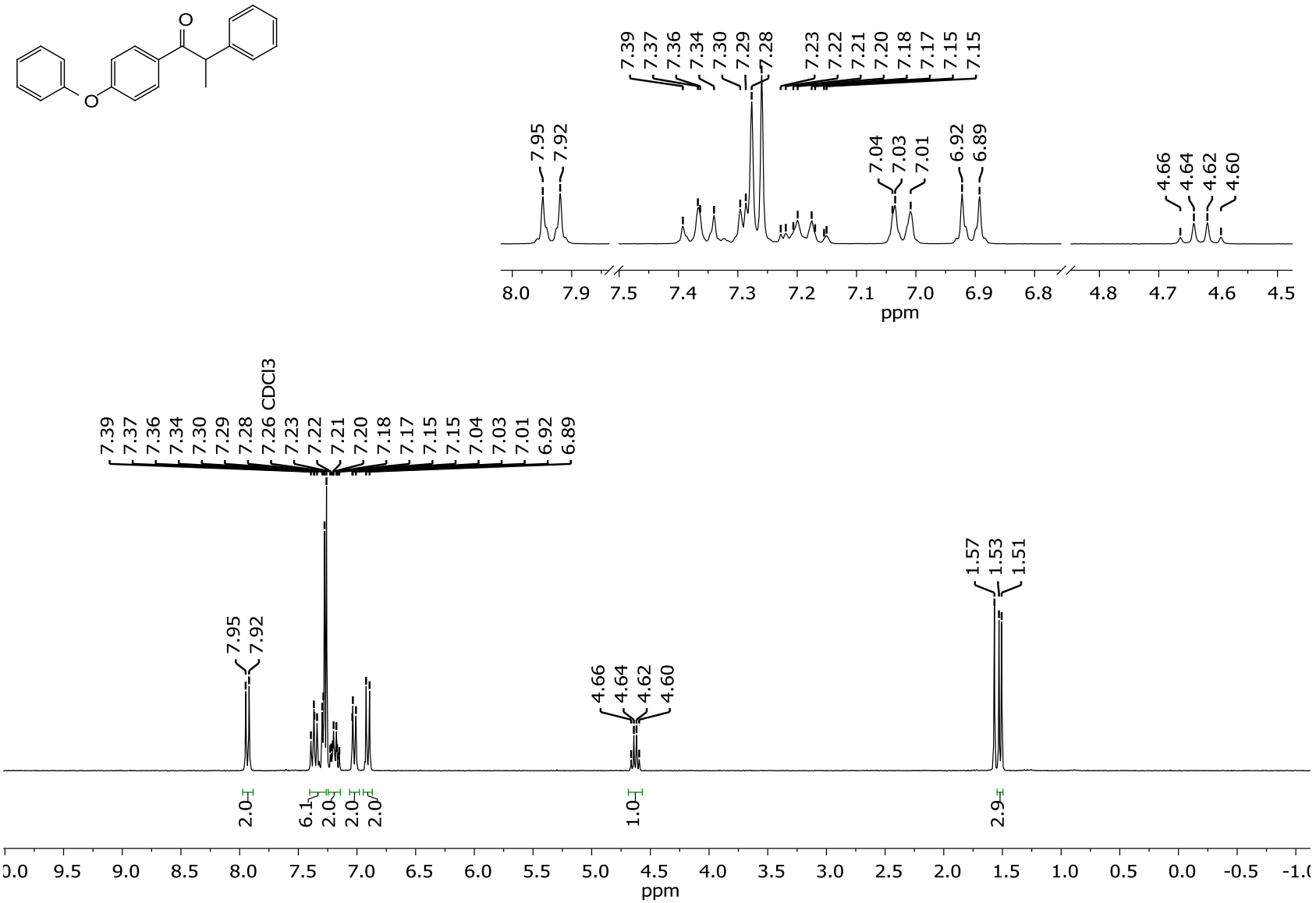

Figure S56. ^{1}H NMR spectrum of compound **5o** ($CDCl_3$, 300 MHz)

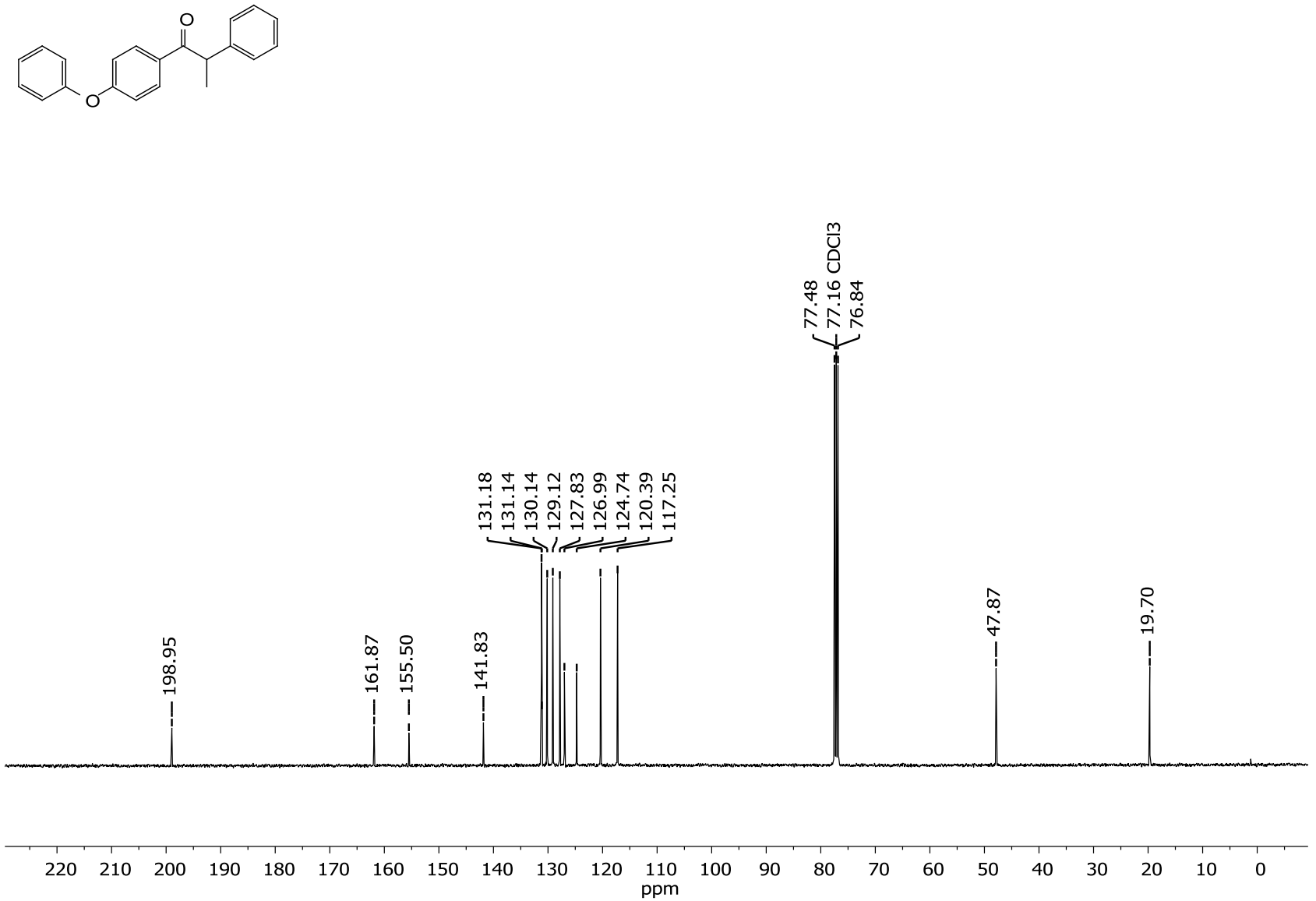

Figure S57. ^{13}C NMR spectrum of compound **5o** ($CDCl_3$, 100 MHz)

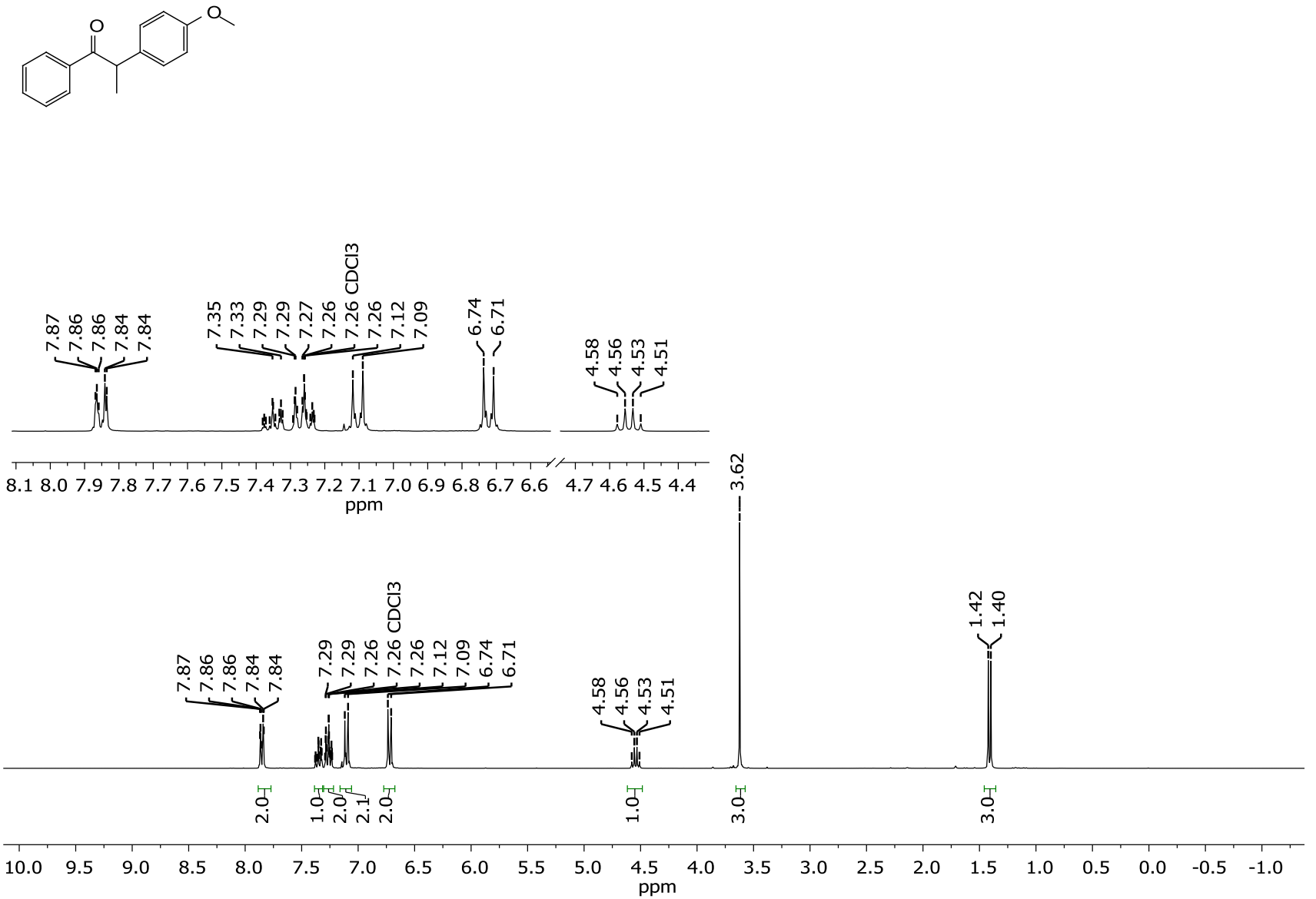

Figure S58. ^{1}H NMR spectrum of compound **5p** ($CDCl_3$, 300 MHz)

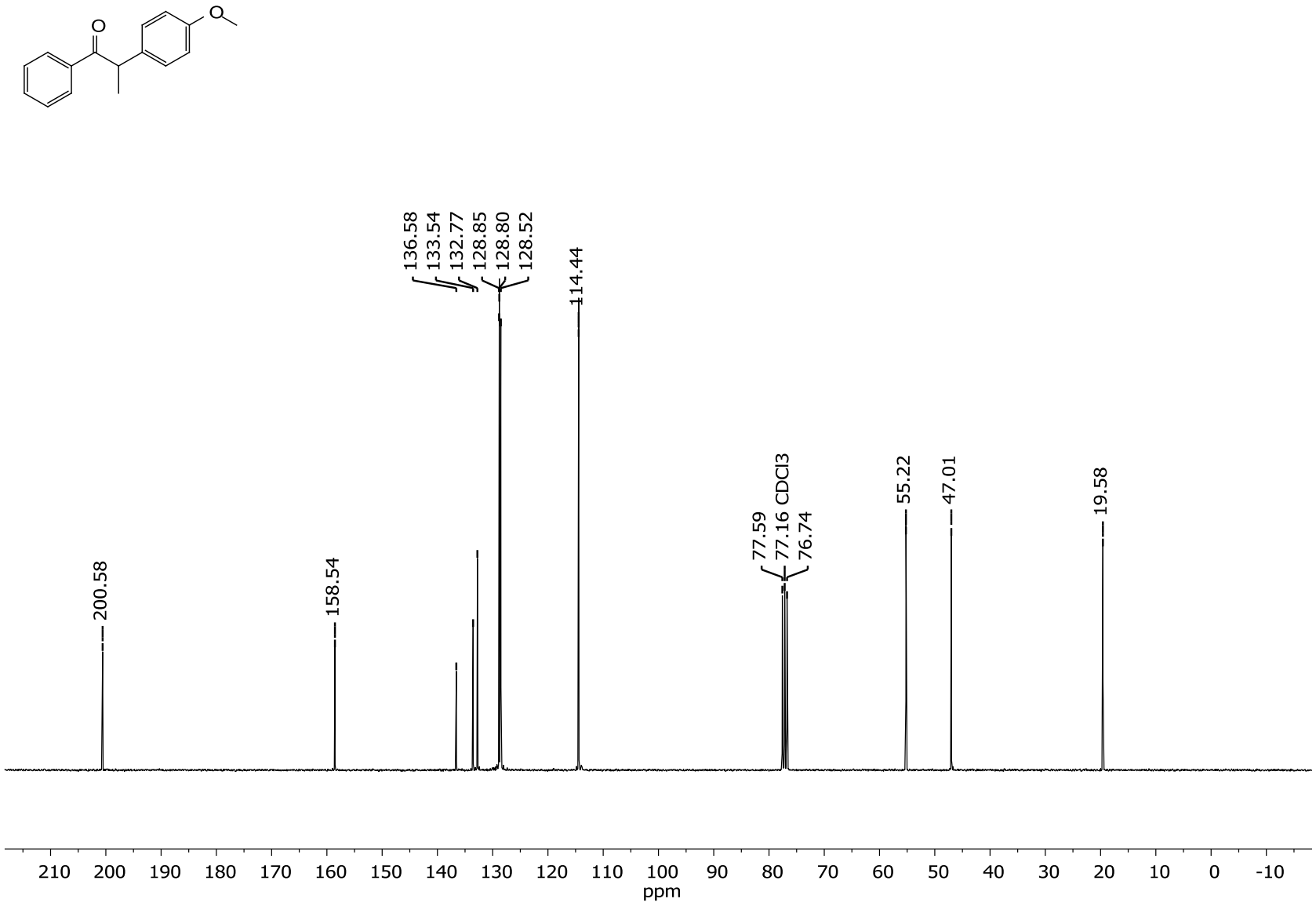

Figure S59. ^{13}C NMR spectrum of compound **5p** ($CDCl_3$, 75 MHz)

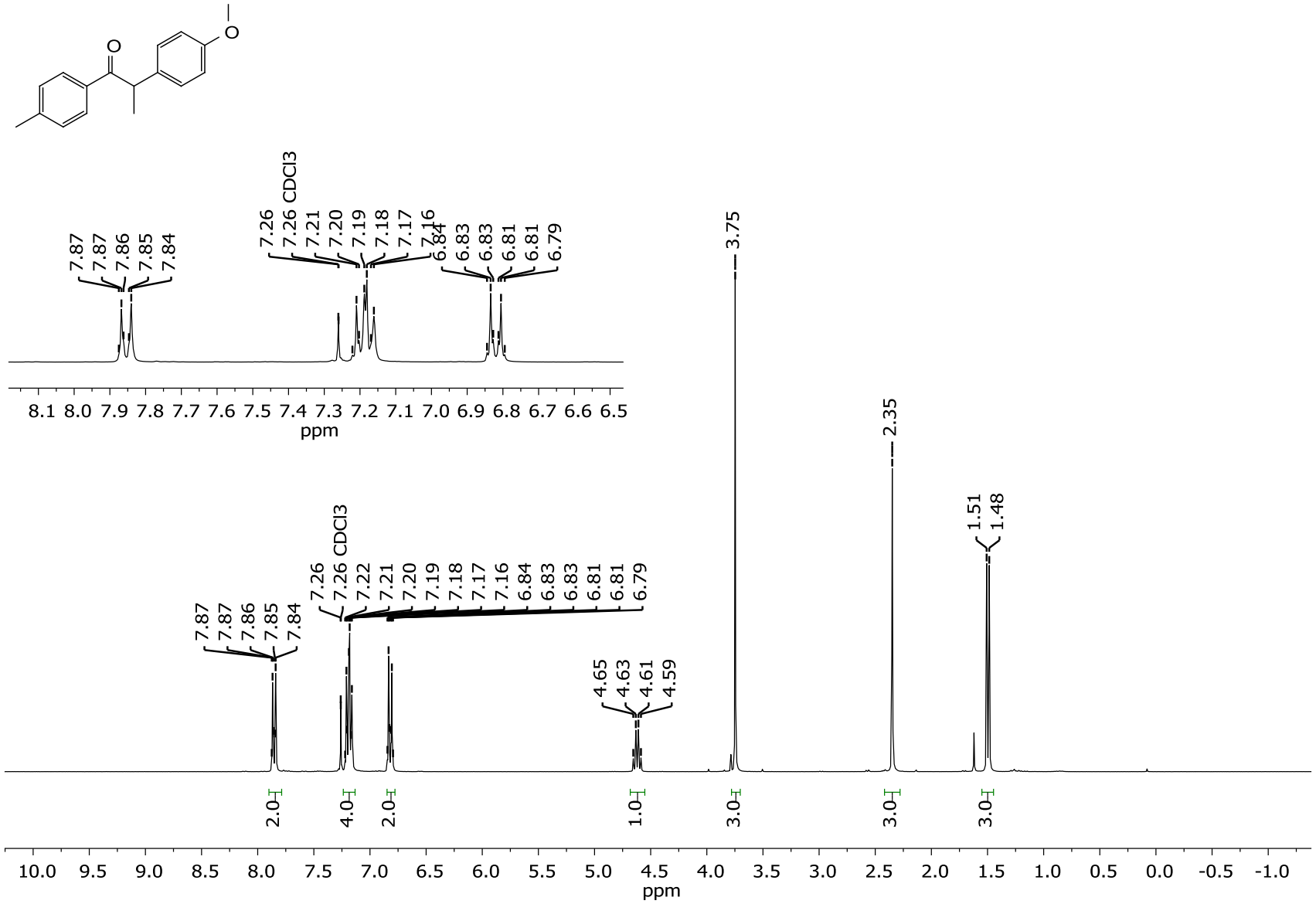

Figure S60. ^{1}H NMR spectrum of compound **5q** ($CDCl_3$, 300 MHz)

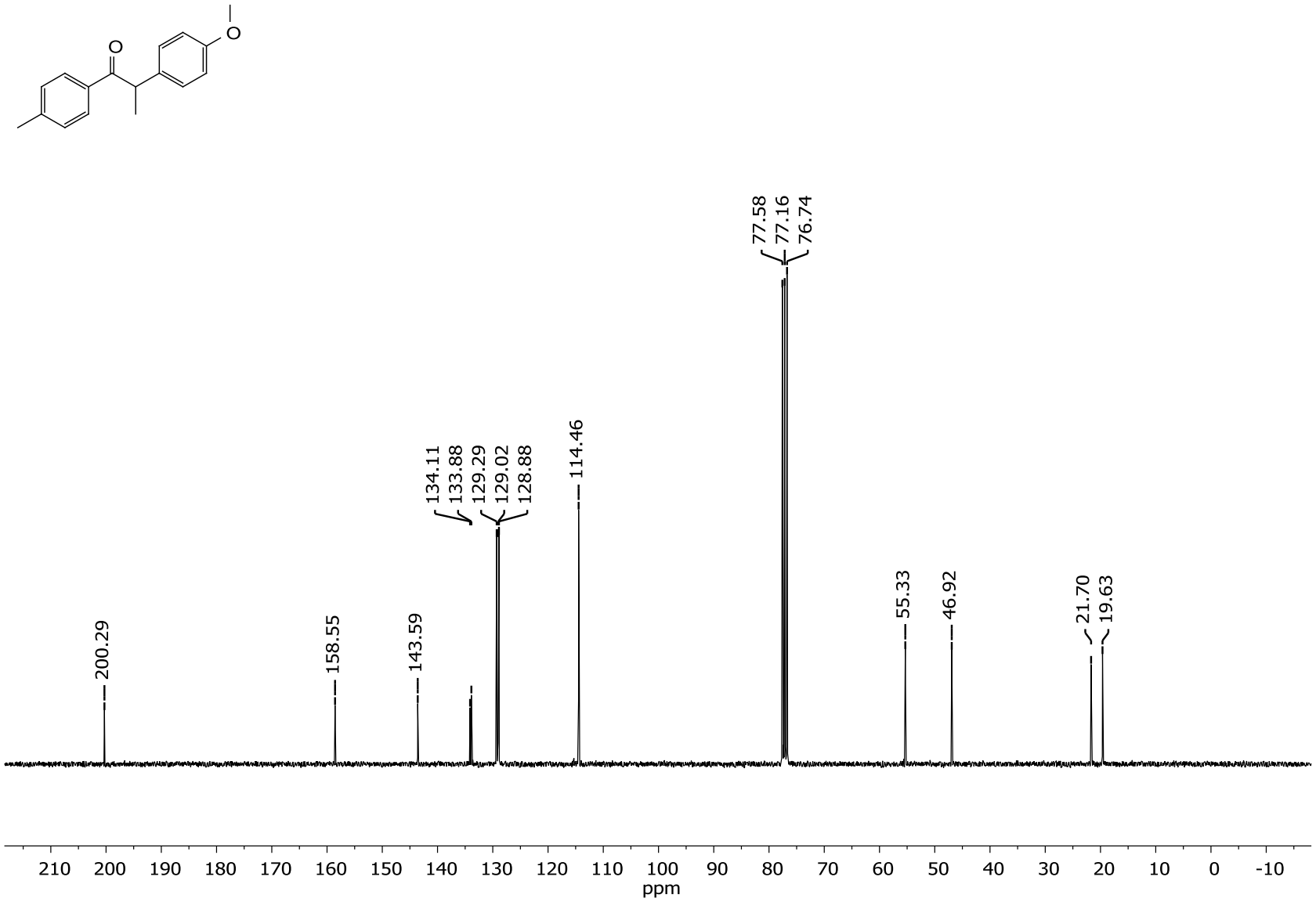

Figure S61. ^{13}C NMR spectrum of compound **5q** ($CDCl_3$, 75 MHz)

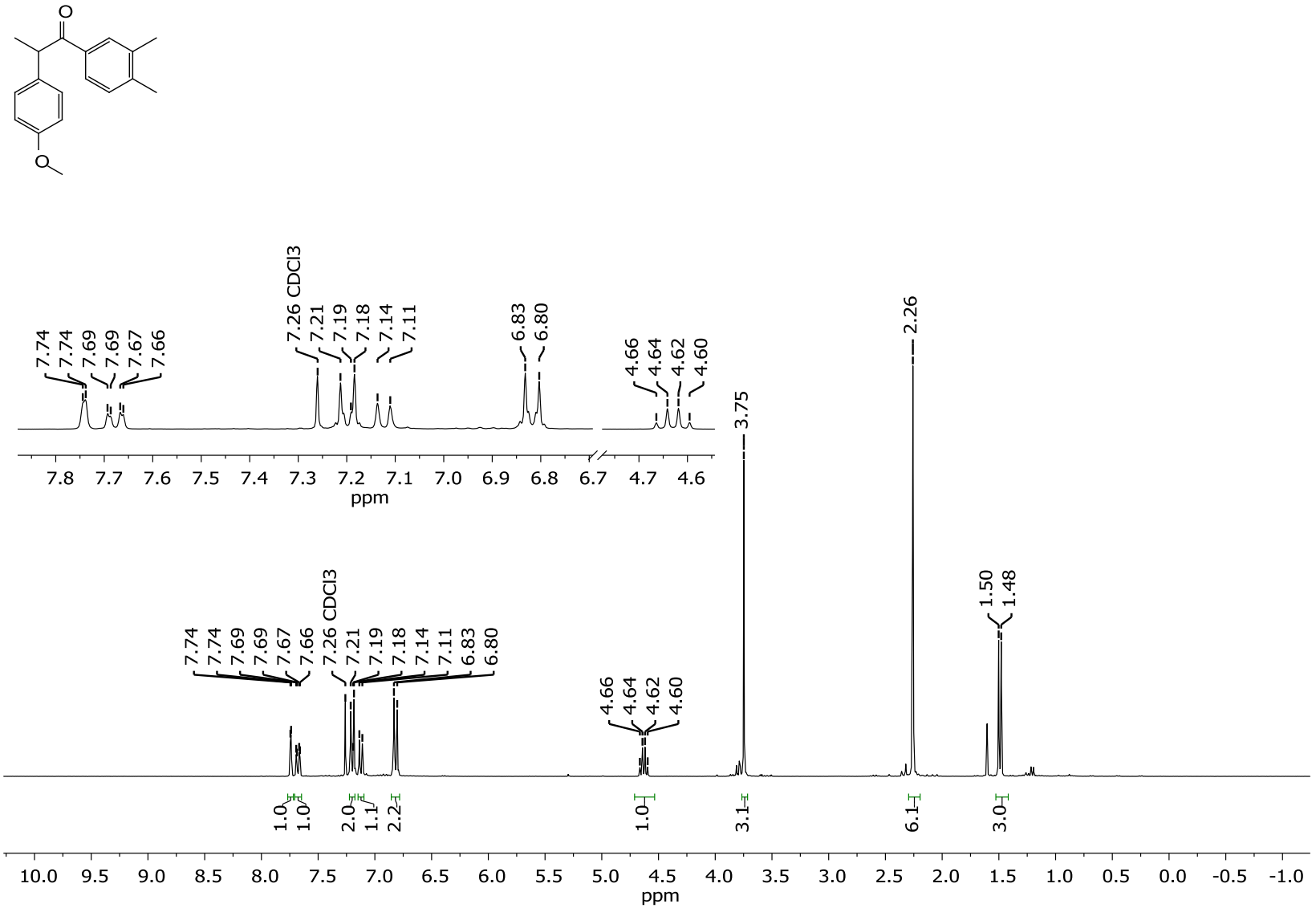

Figure S62. ^{1}H NMR spectrum of compound **5r** ($CDCl_3$, 300 MHz)

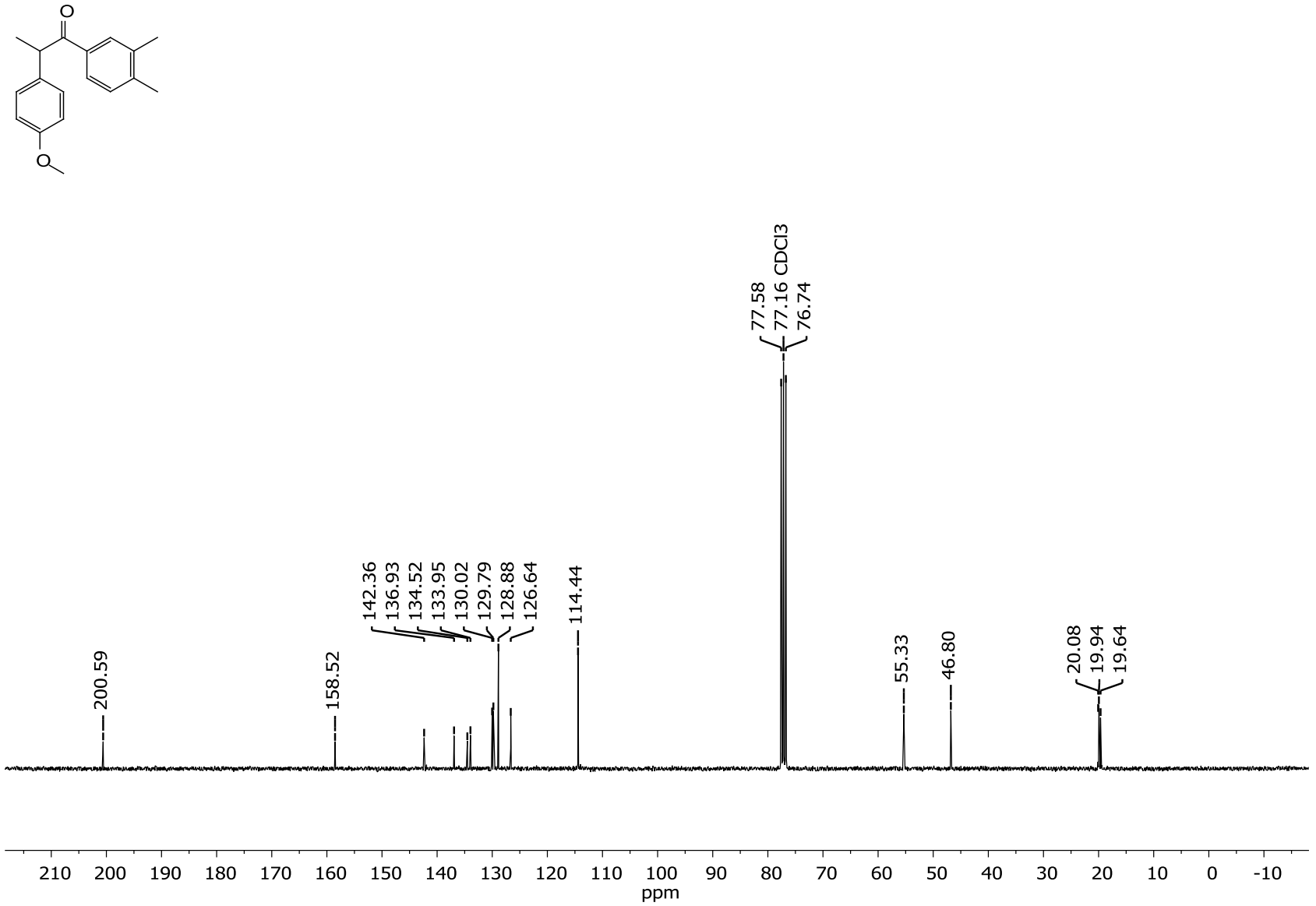

Figure S63. ^{13}C NMR spectrum of compound **5r** ($CDCl_3$, 75 MHz)

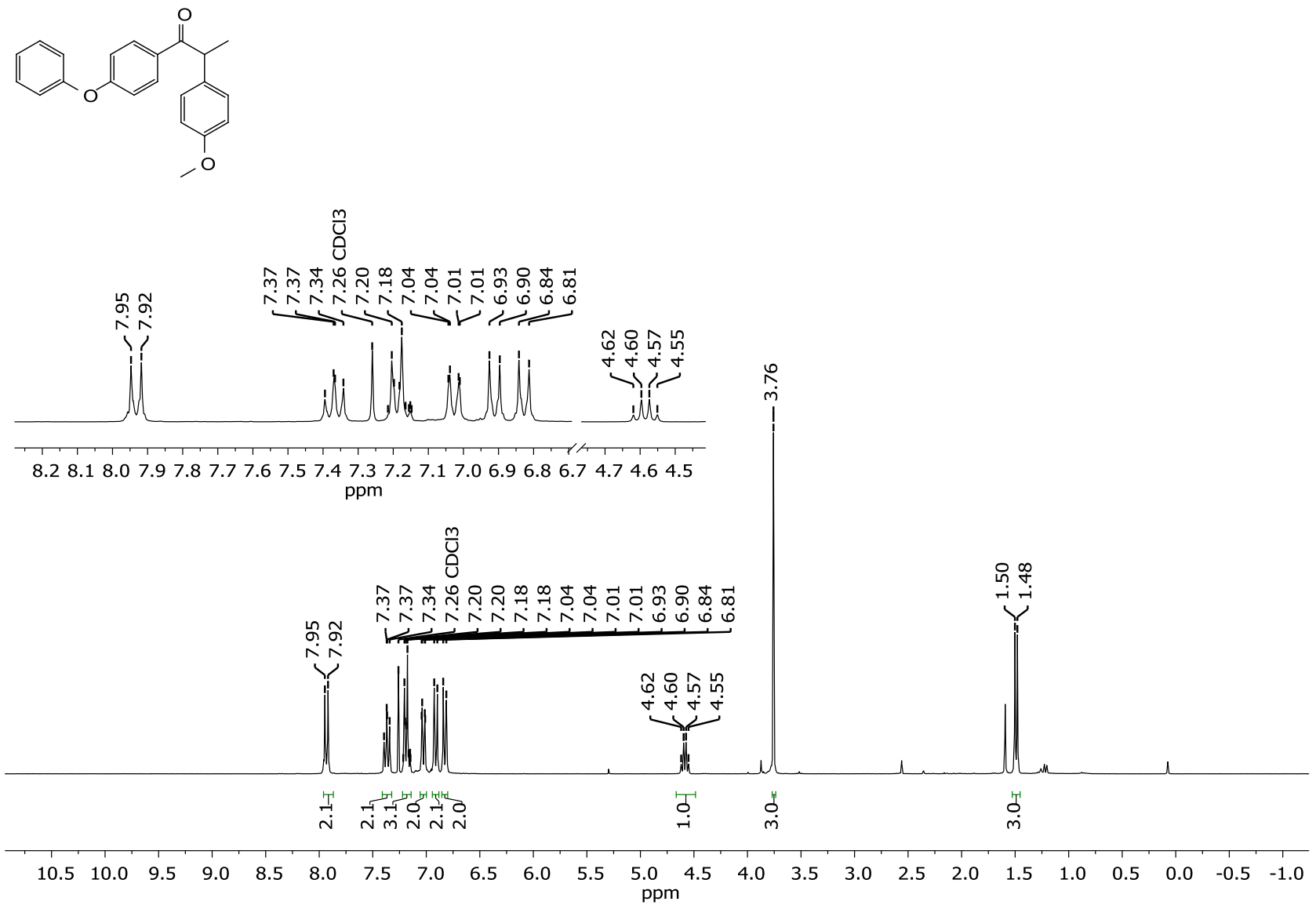

Figure S64. ^{1}H NMR spectrum of compound **5s** ($CDCl_3$, 300 MHz)

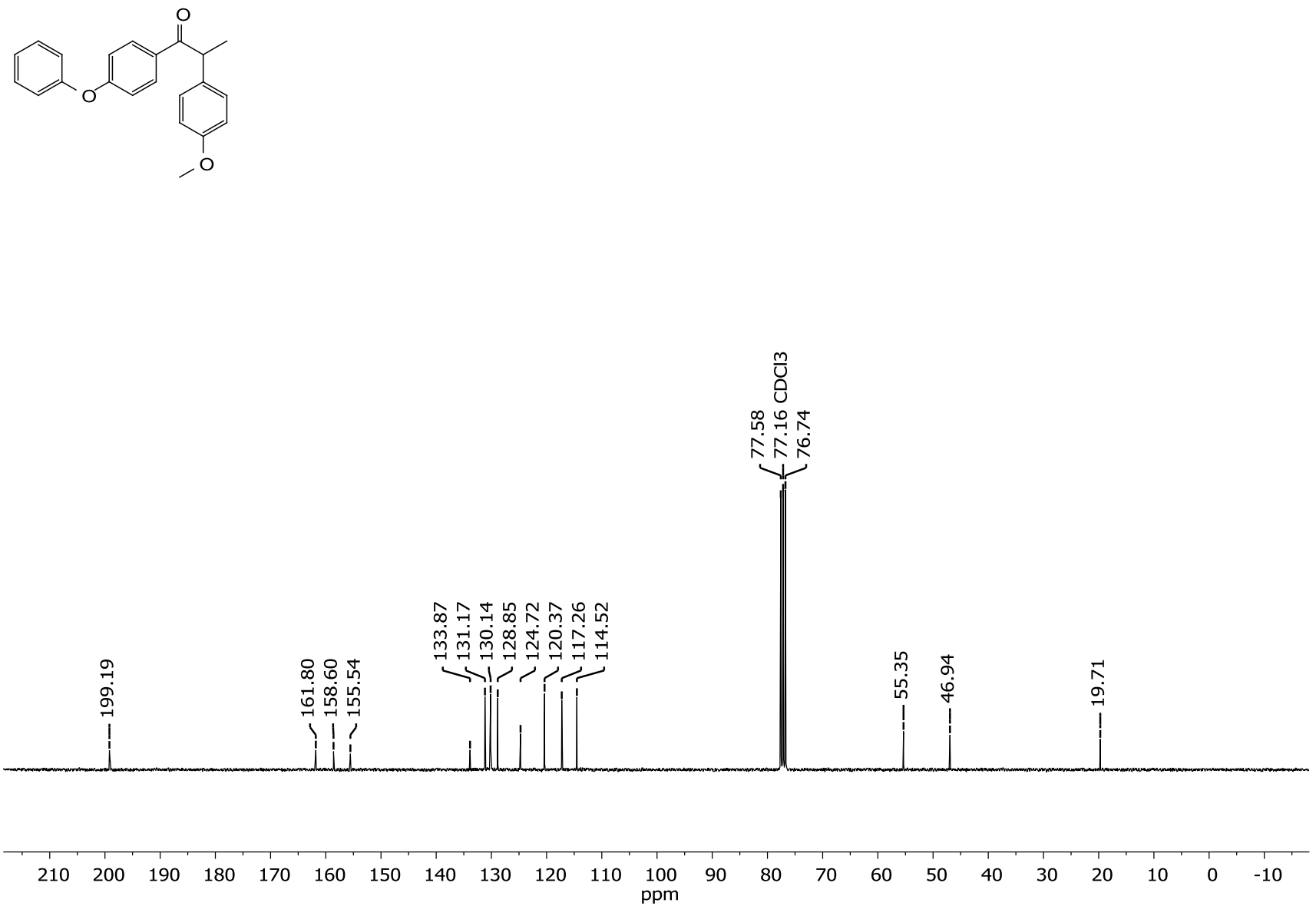

Figure S65. ^{13}C NMR spectrum of compound **5s** ($CDCl_3$, 75 MHz)

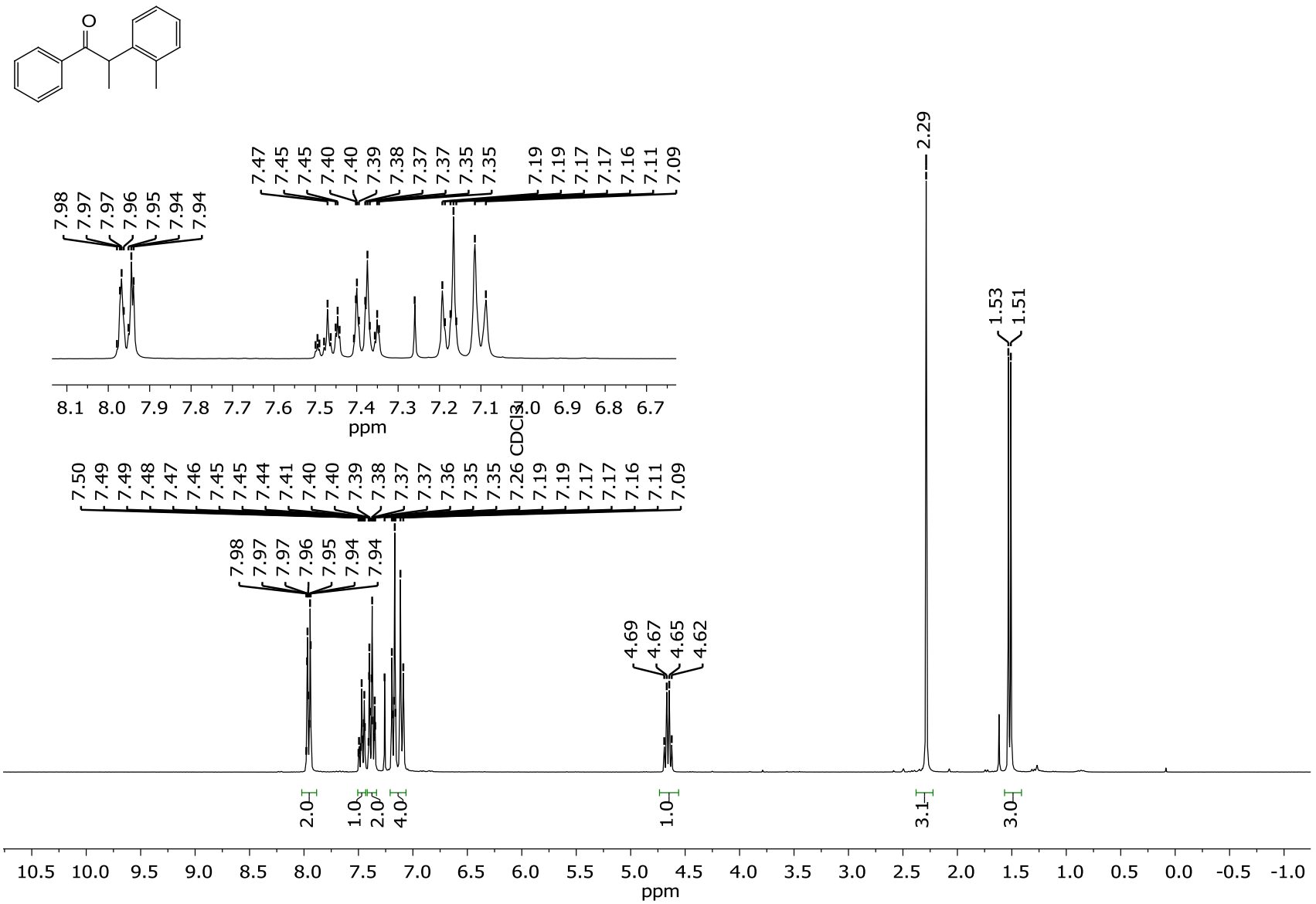

Figure S66. ^{1}H NMR spectrum of compound **5t** ($CDCl_3$, 300 MHz)

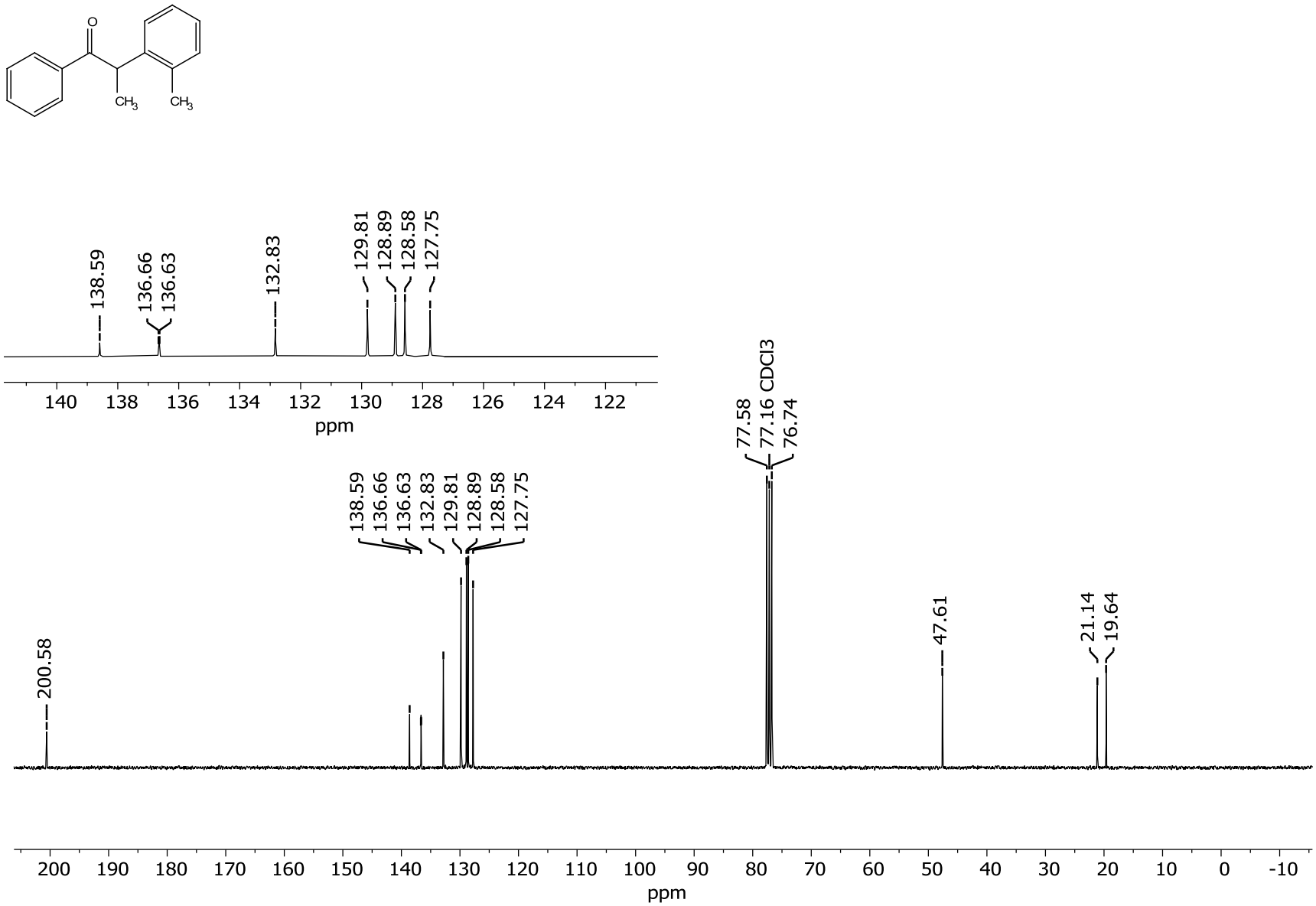

Figure S67. ^{13}C NMR spectrum of compound **5t** ($CDCl_3$, 75 MHz)

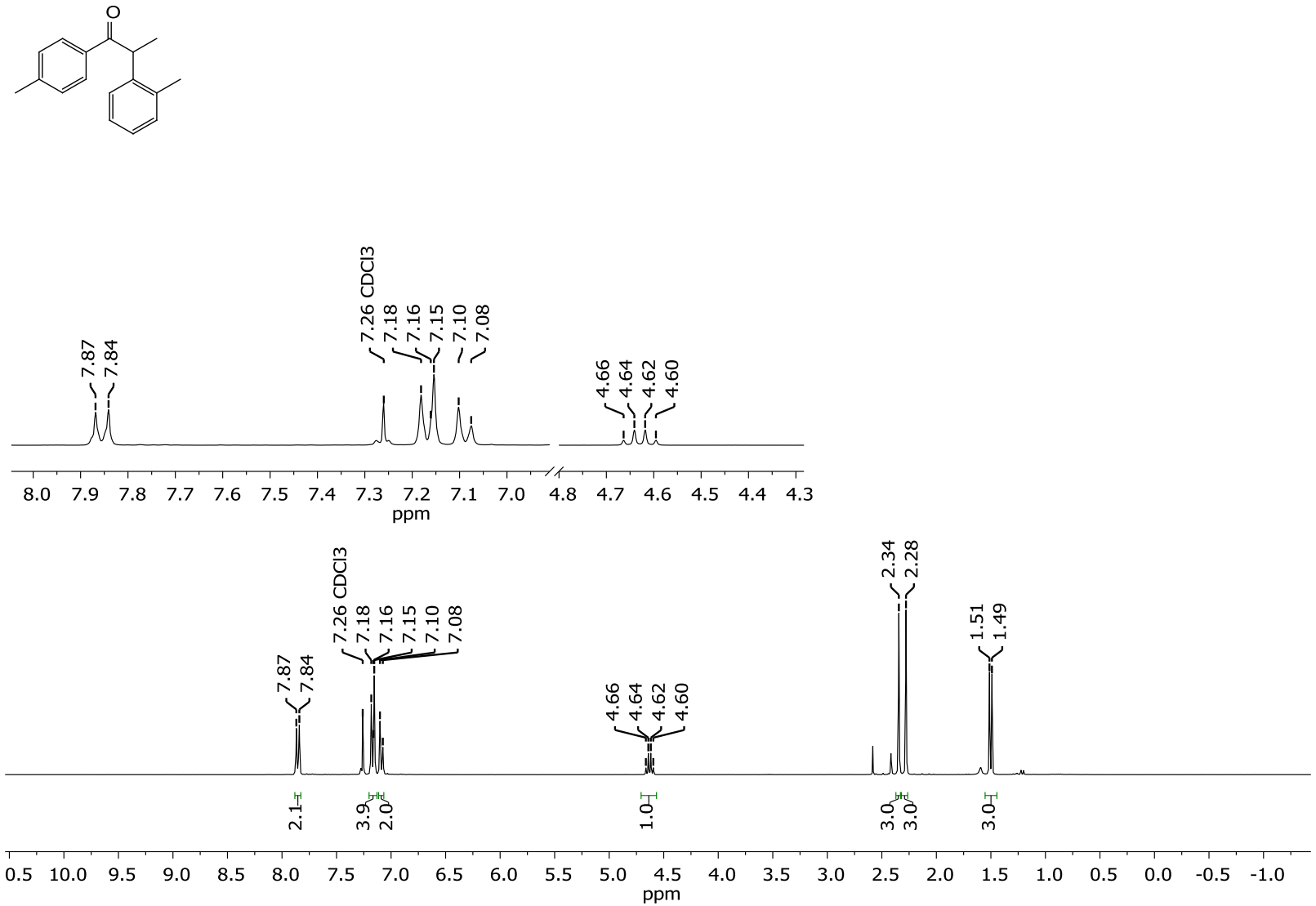

Figure S68. ^{1}H NMR spectrum of compound **5u** ($CDCl_3$, 300 MHz)

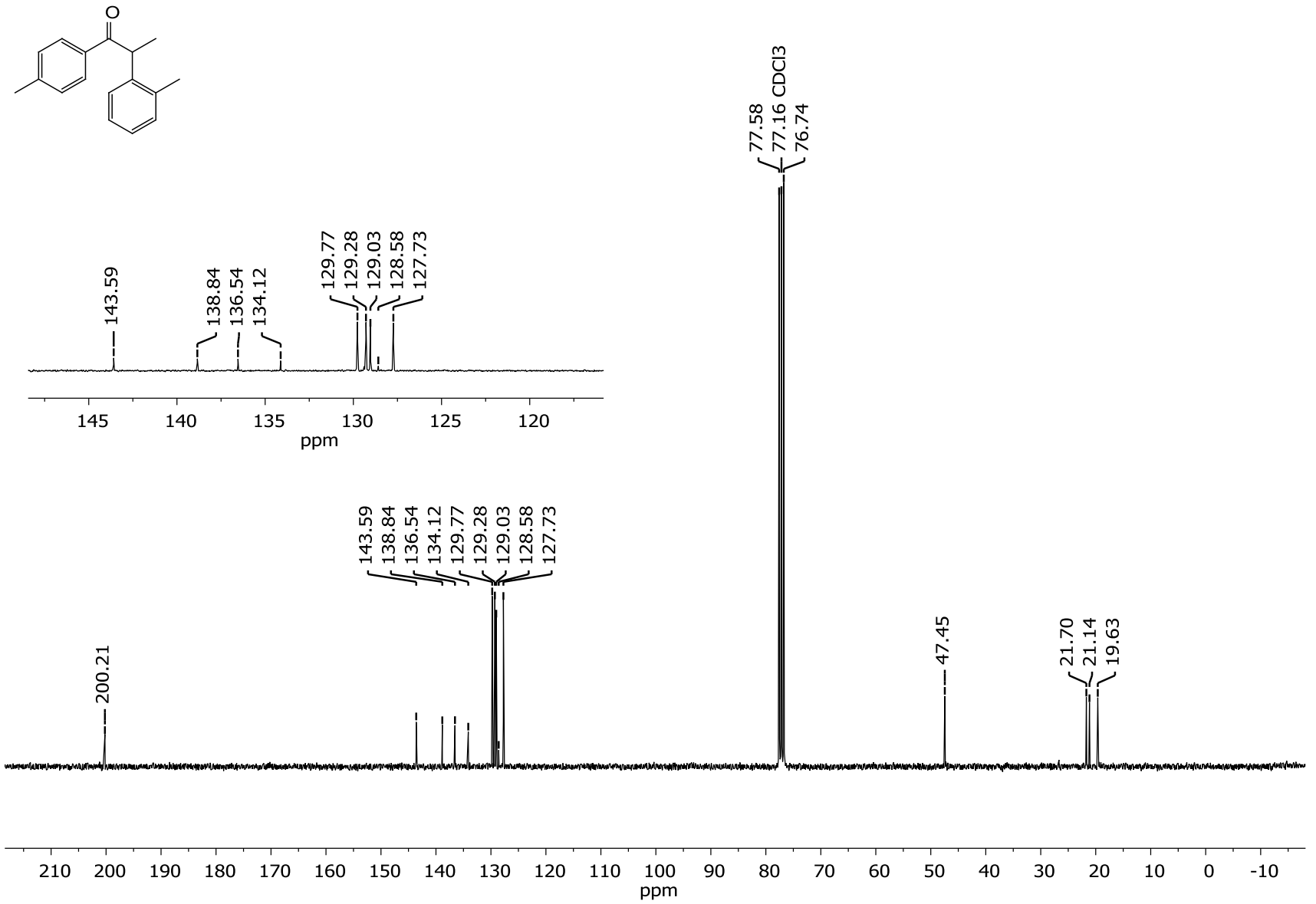

Figure S69. ^{13}C NMR spectrum of compound **5u** ($CDCl_3$, 75 MHz)

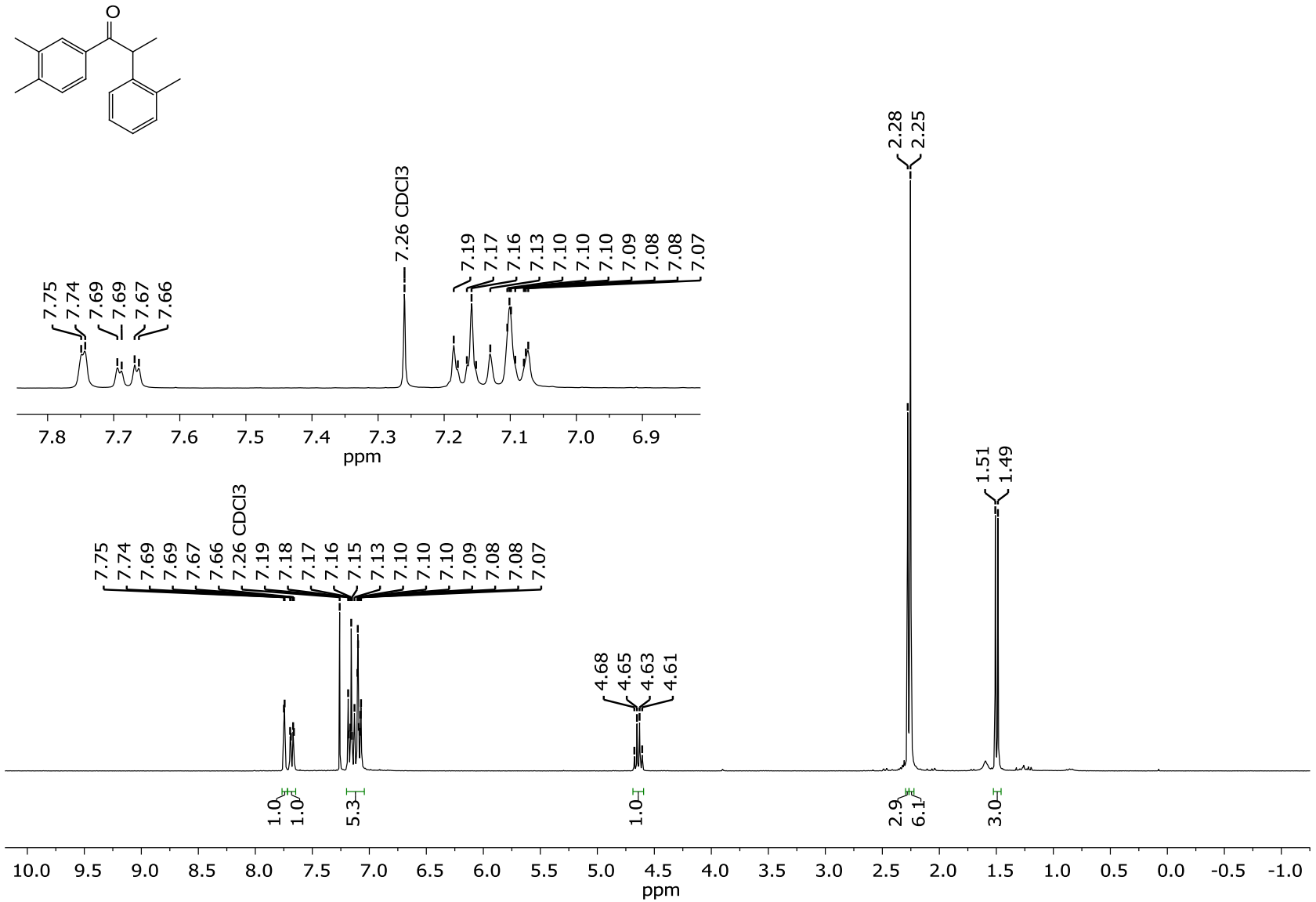

Figure S70. ^{1}H NMR spectrum of compound **5v** ($CDCl_3$, 300 MHz)

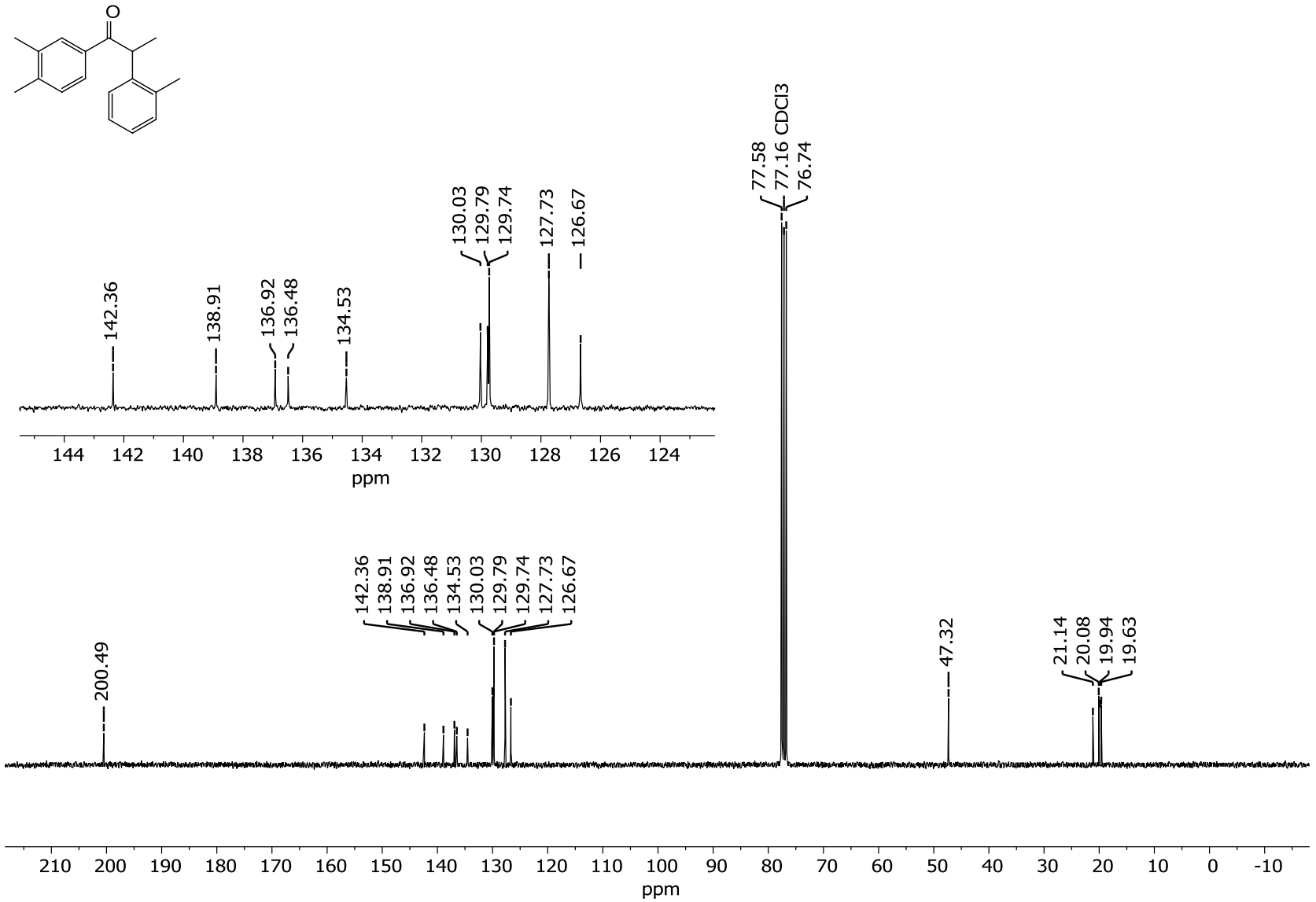

Figure S71. ^{13}C NMR spectrum of compound **5v** ($CDCl_3$, 75 MHz)

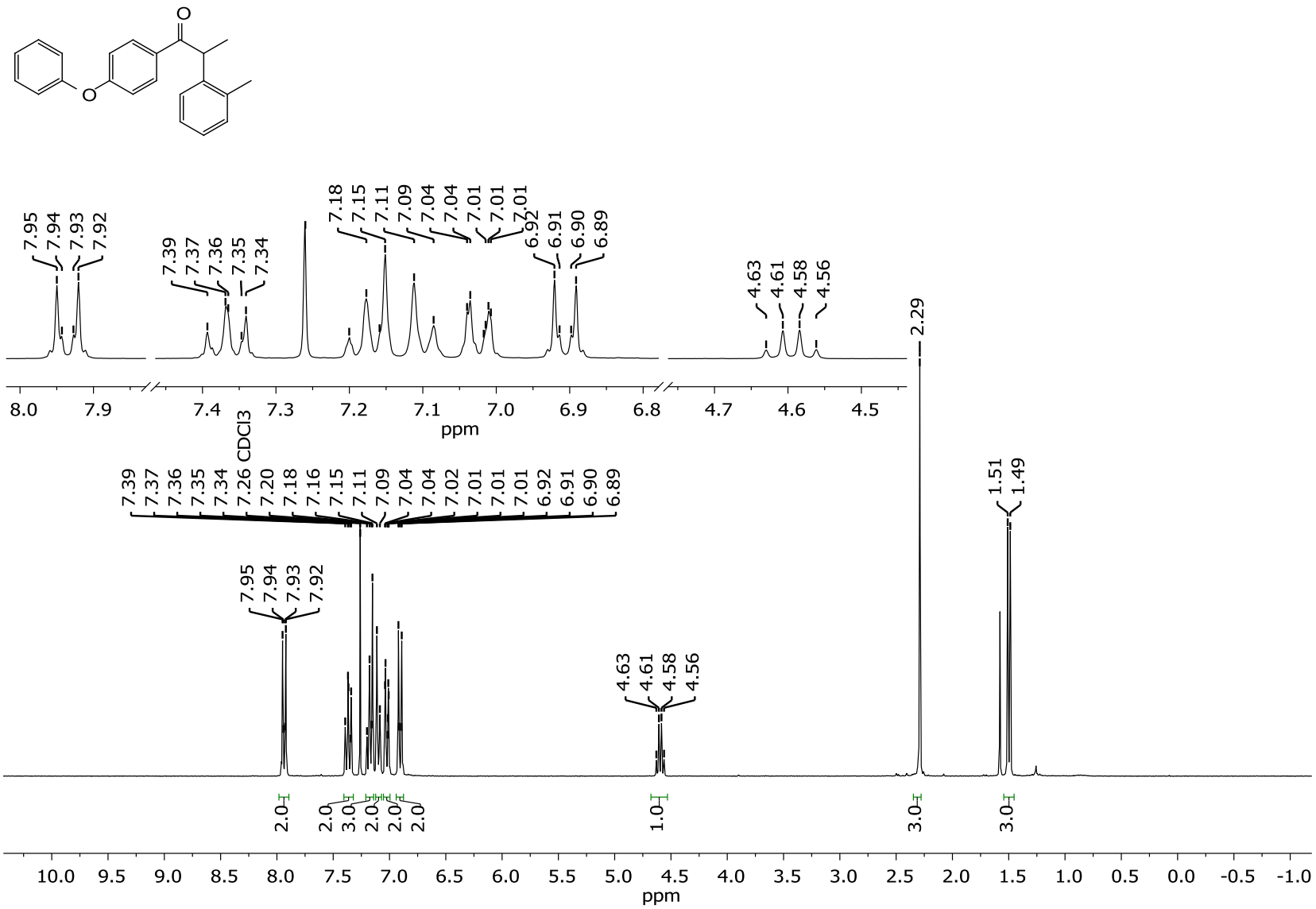

Figure S72. ^{1}H NMR spectrum of compound **5w** ($CDCl_3$, 300 MHz)

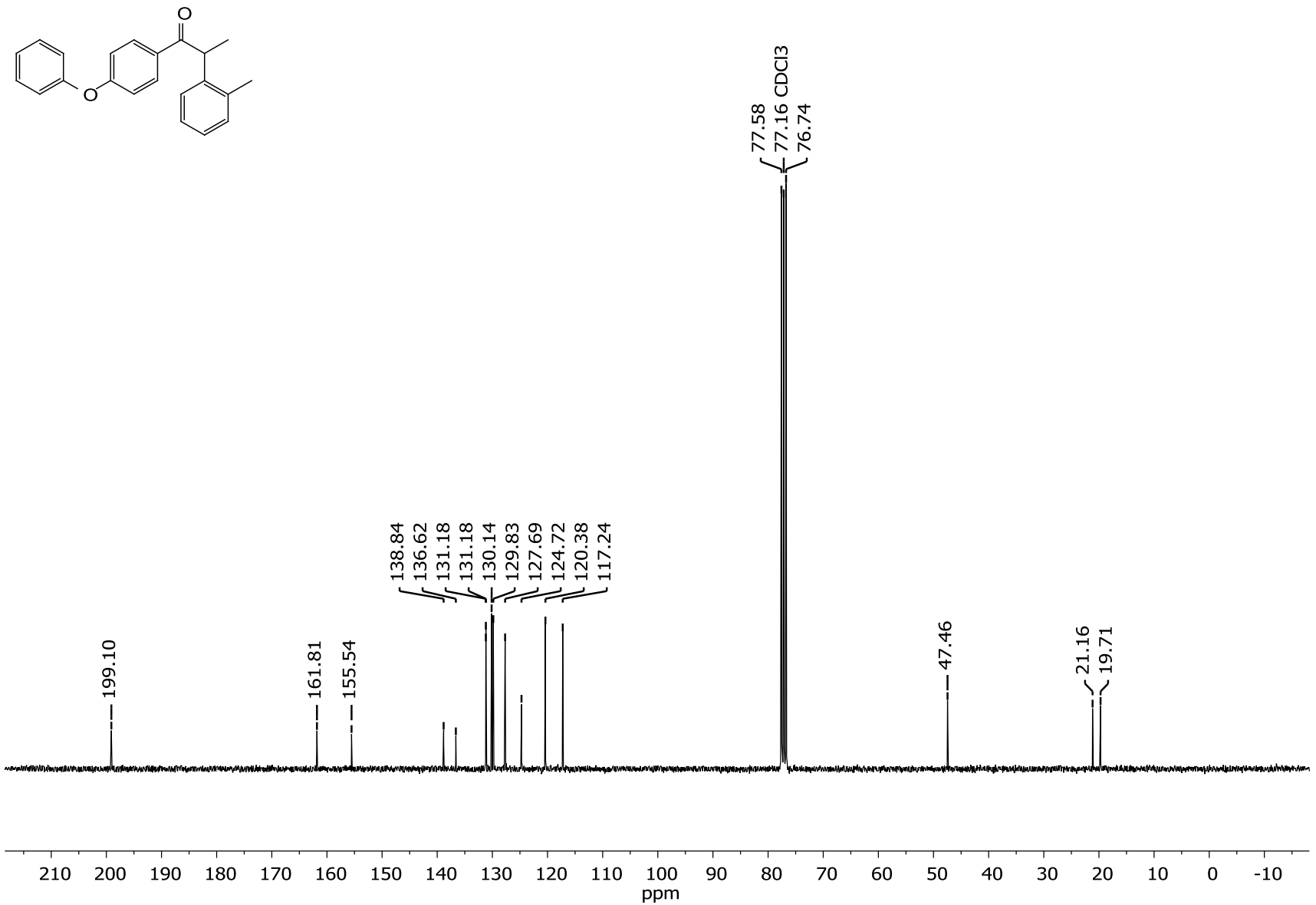

Figure S73. ^{13}C NMR spectrum of compound **5w** ($CDCl_3$, 75 MHz)

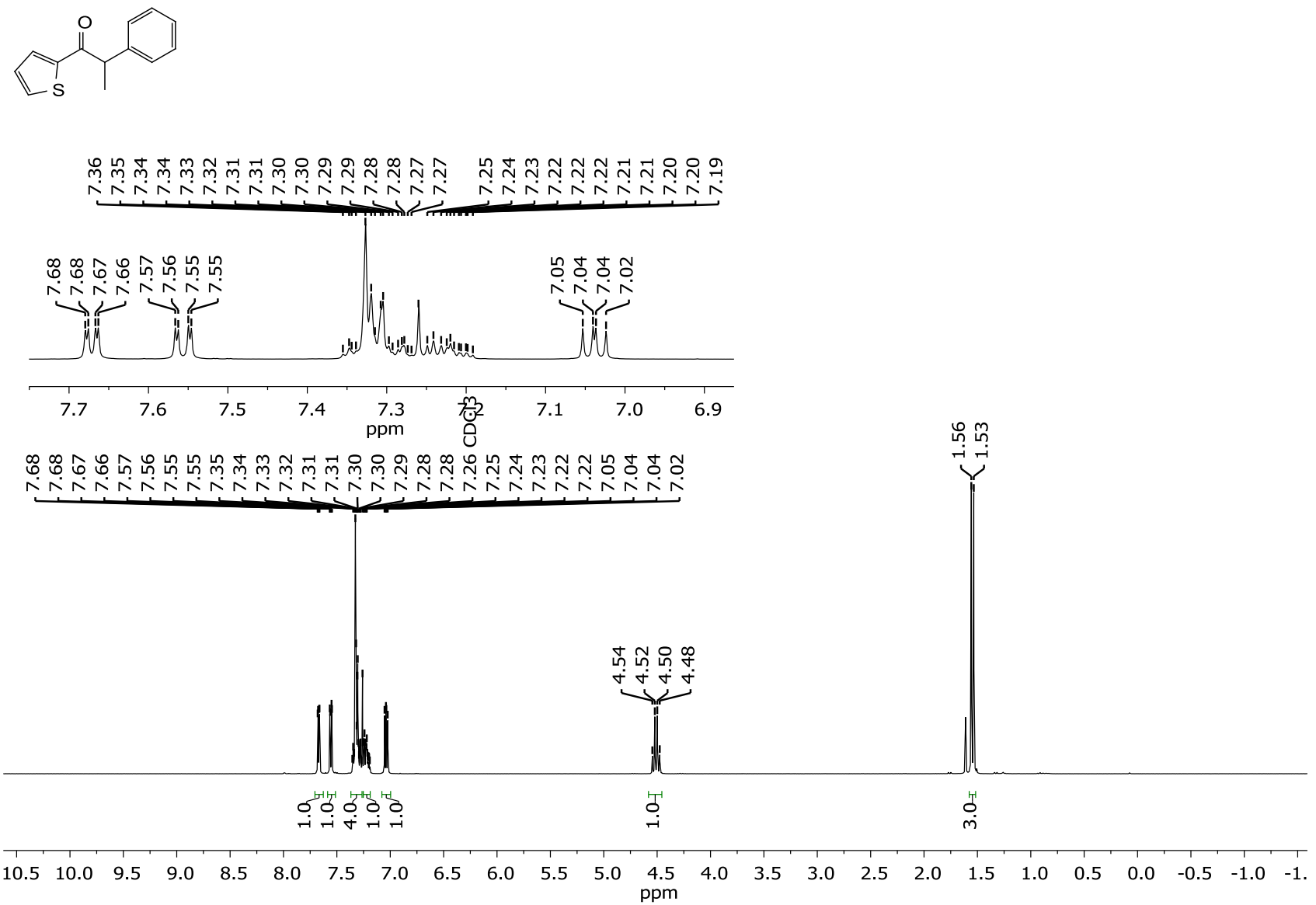

Figure S74. ^{1}H NMR spectrum of compound **5x** ($CDCl_3$, 300 MHz)

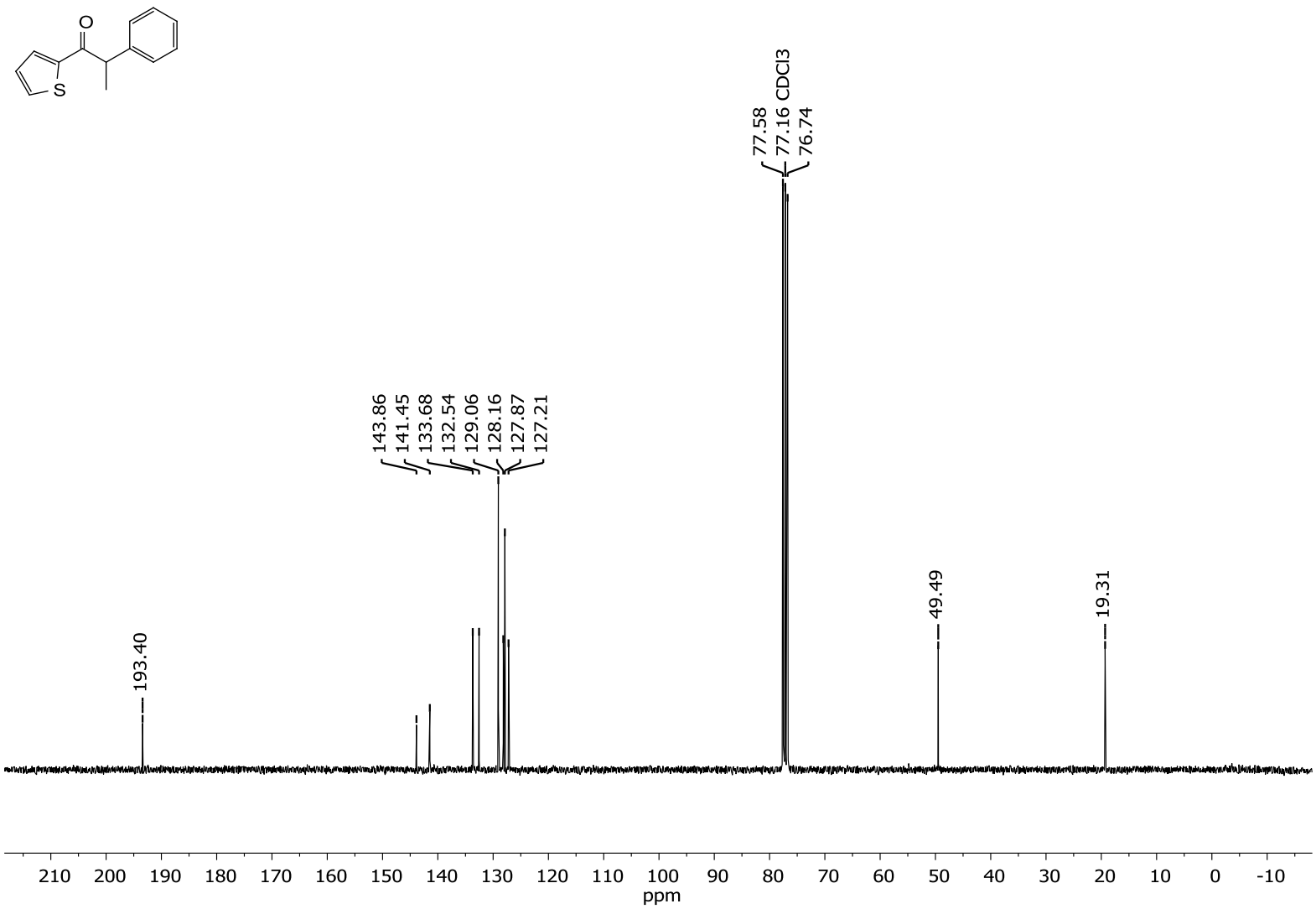

Figure S75. ^{13}C NMR spectrum of compound **5x** ($CDCl_3$, 75 MHz)

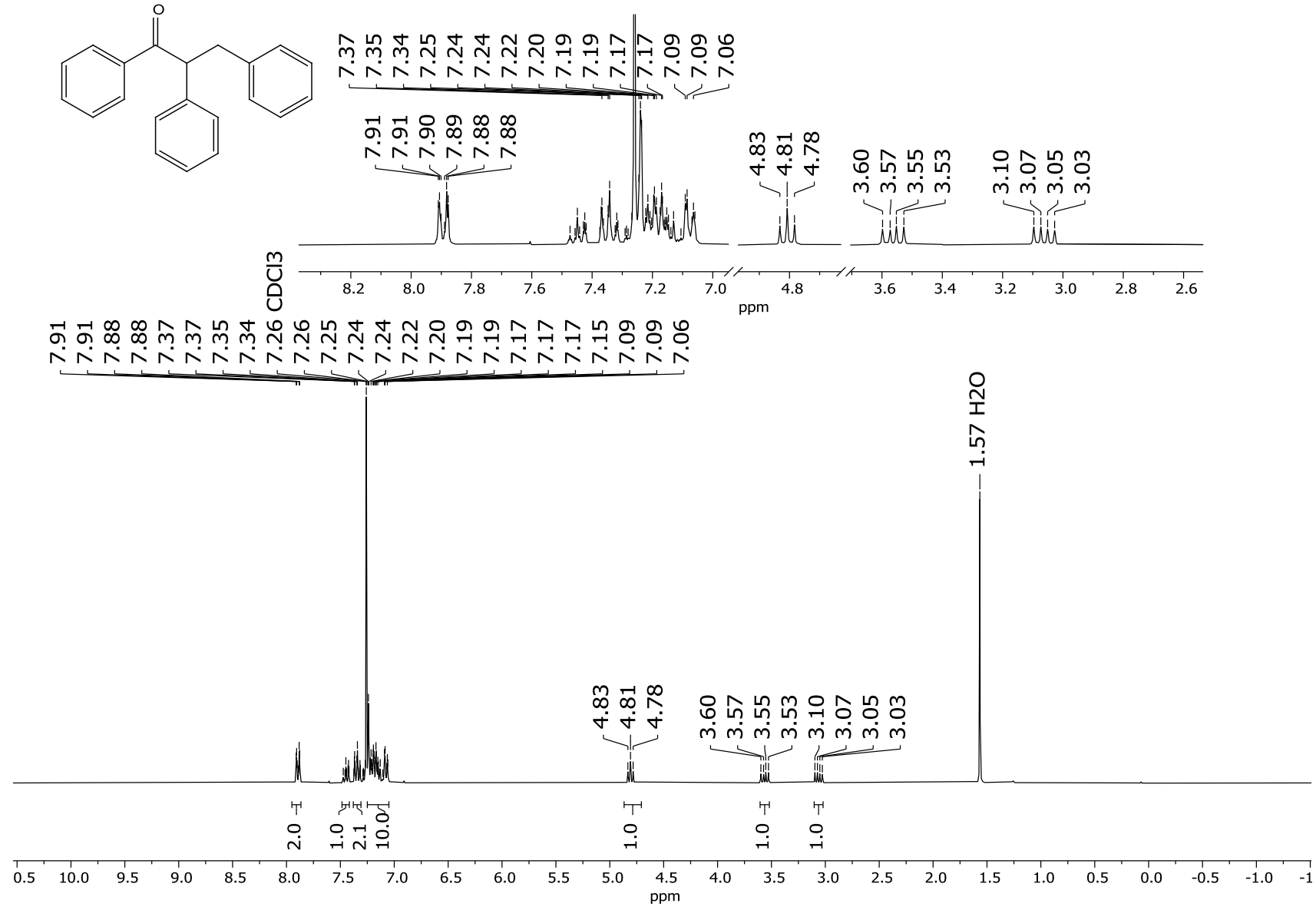

Figure S76. ^{1}H NMR spectrum of compound **5y** ($CDCl_3$, 300 MHz)

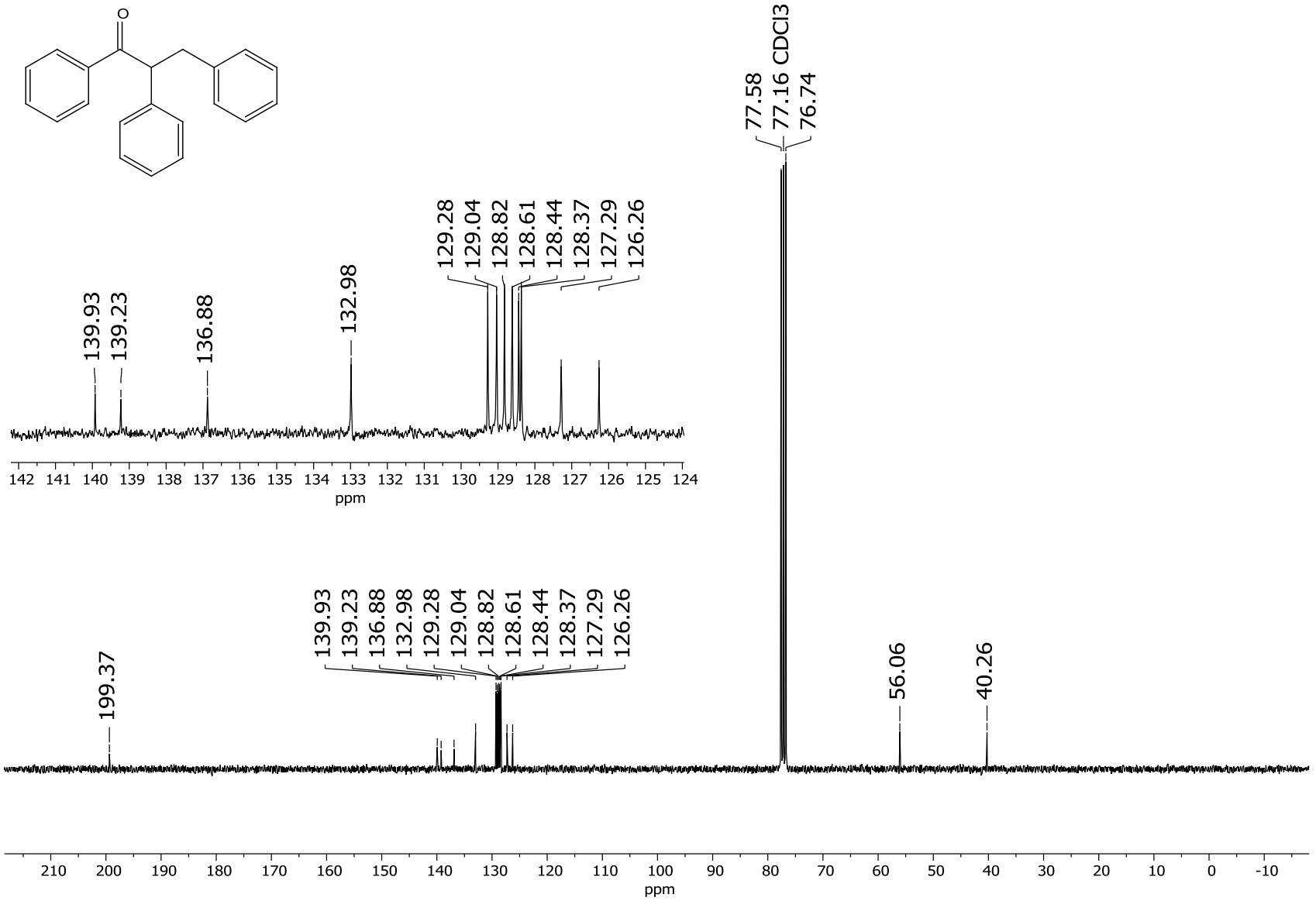

Figure S77. ^{13}C NMR spectrum of compound **5y** ($CDCl_3$, 75 MHz)

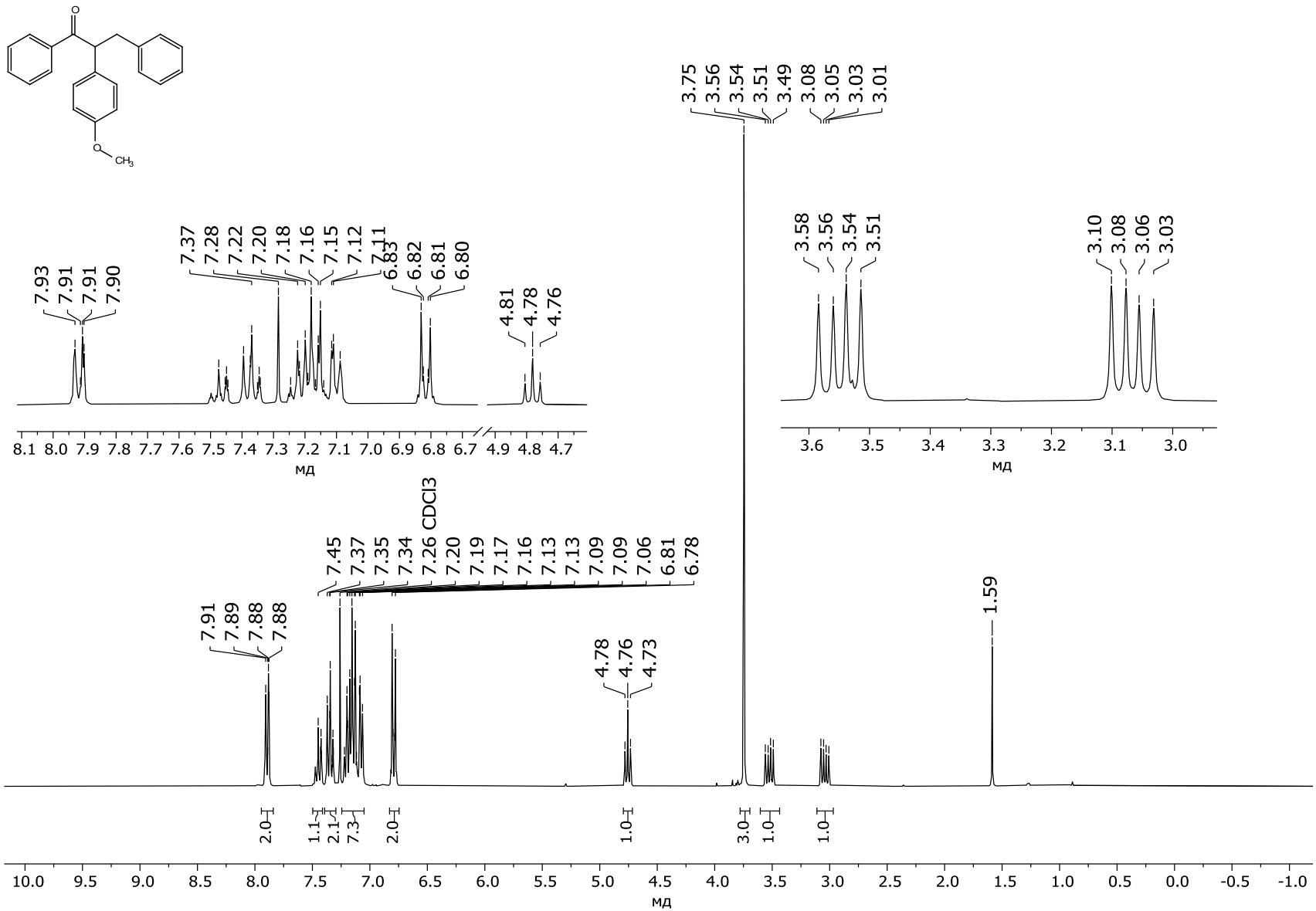

Figure S78. ^{1}H NMR spectrum of compound **5z** ($CDCl_3$, 300 MHz)

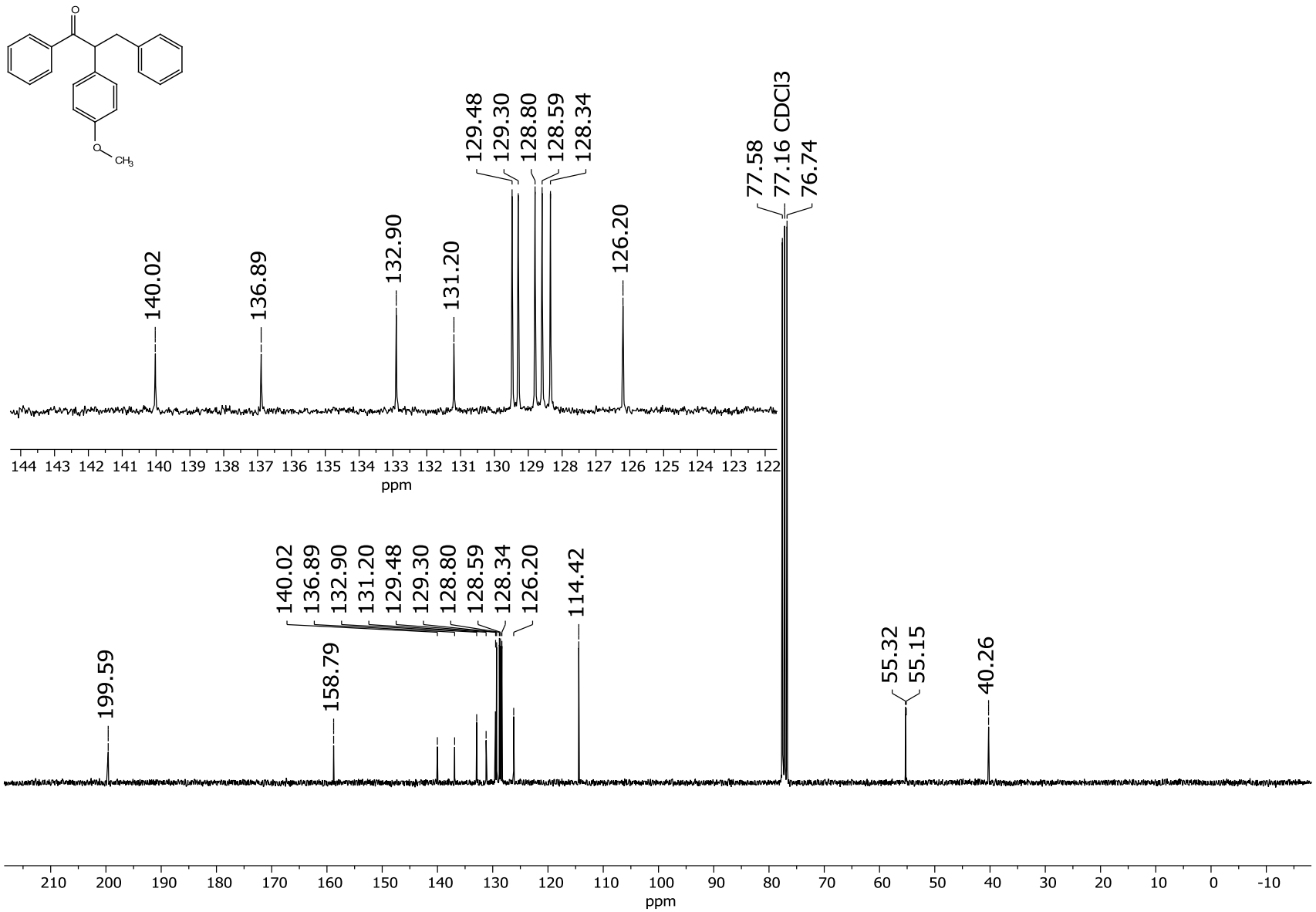

Figure S79. ^{13}C NMR spectrum of compound **5z** ($CDCl_3$, 75 MHz)

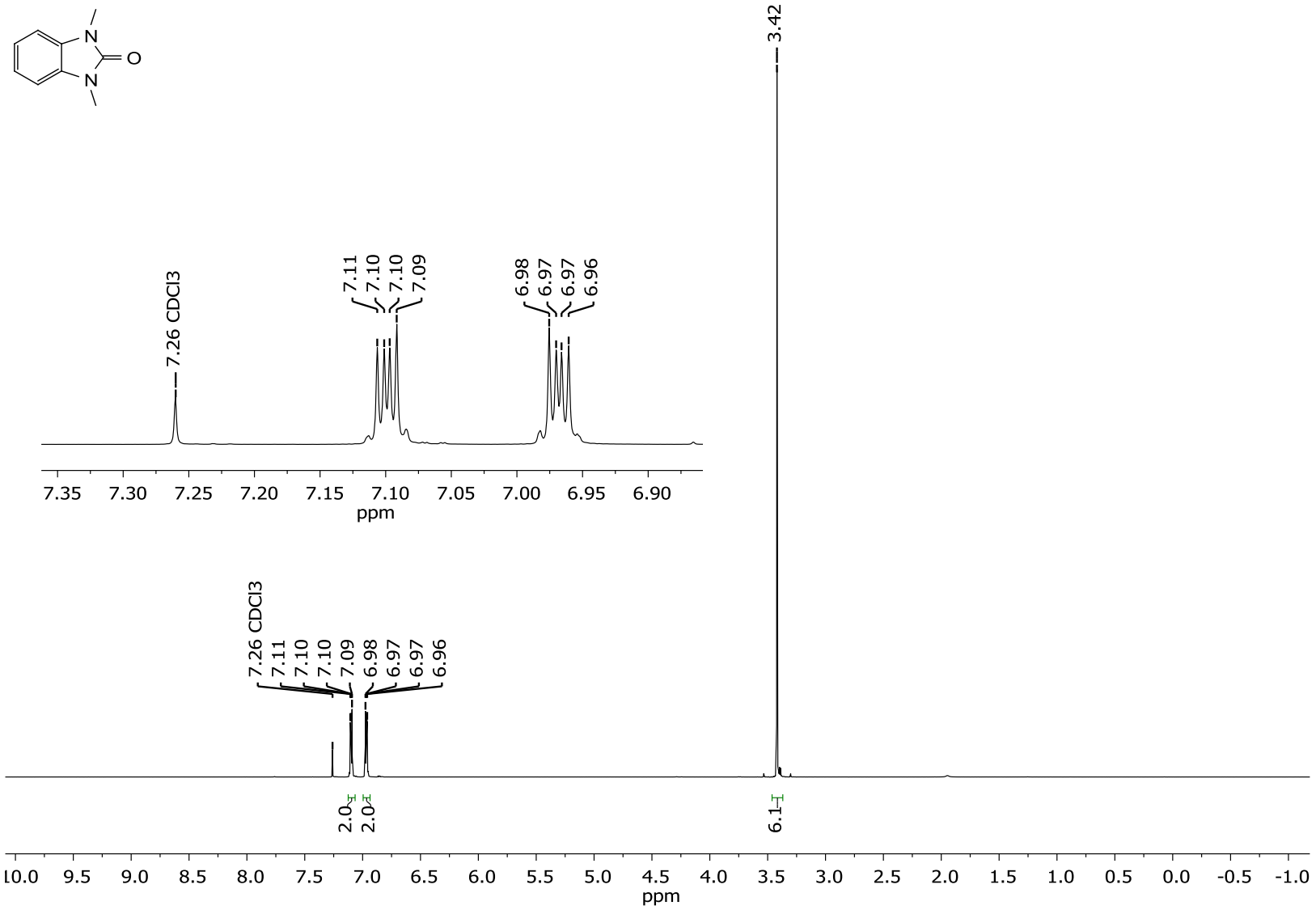

Figure S80. ^{1}H NMR spectrum of compound **6a** ($CDCl_3$, 600 MHz)

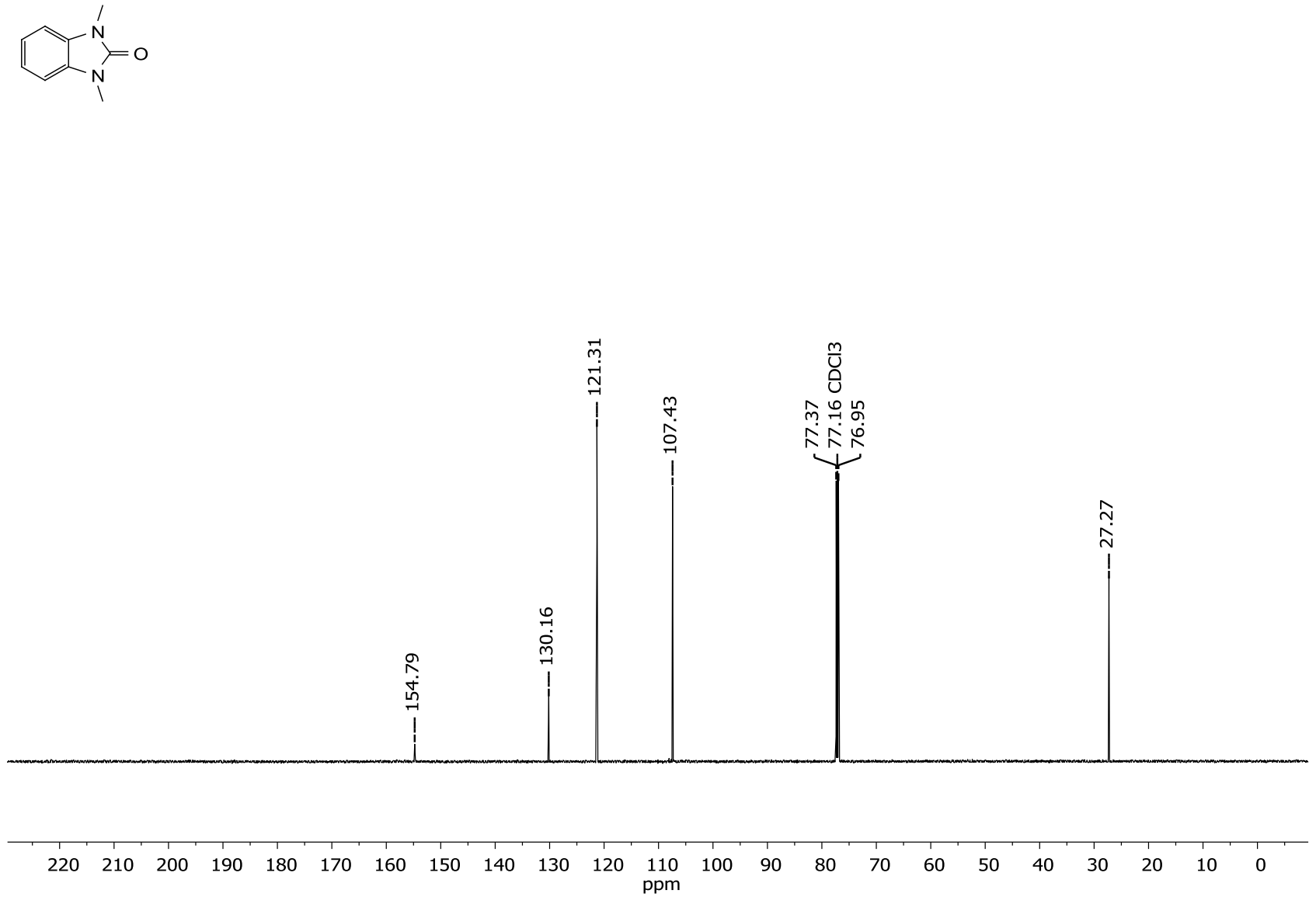

Figure S81. ^{13}C NMR spectrum of compound **6a** ($CDCl_3$, 150 MHz)

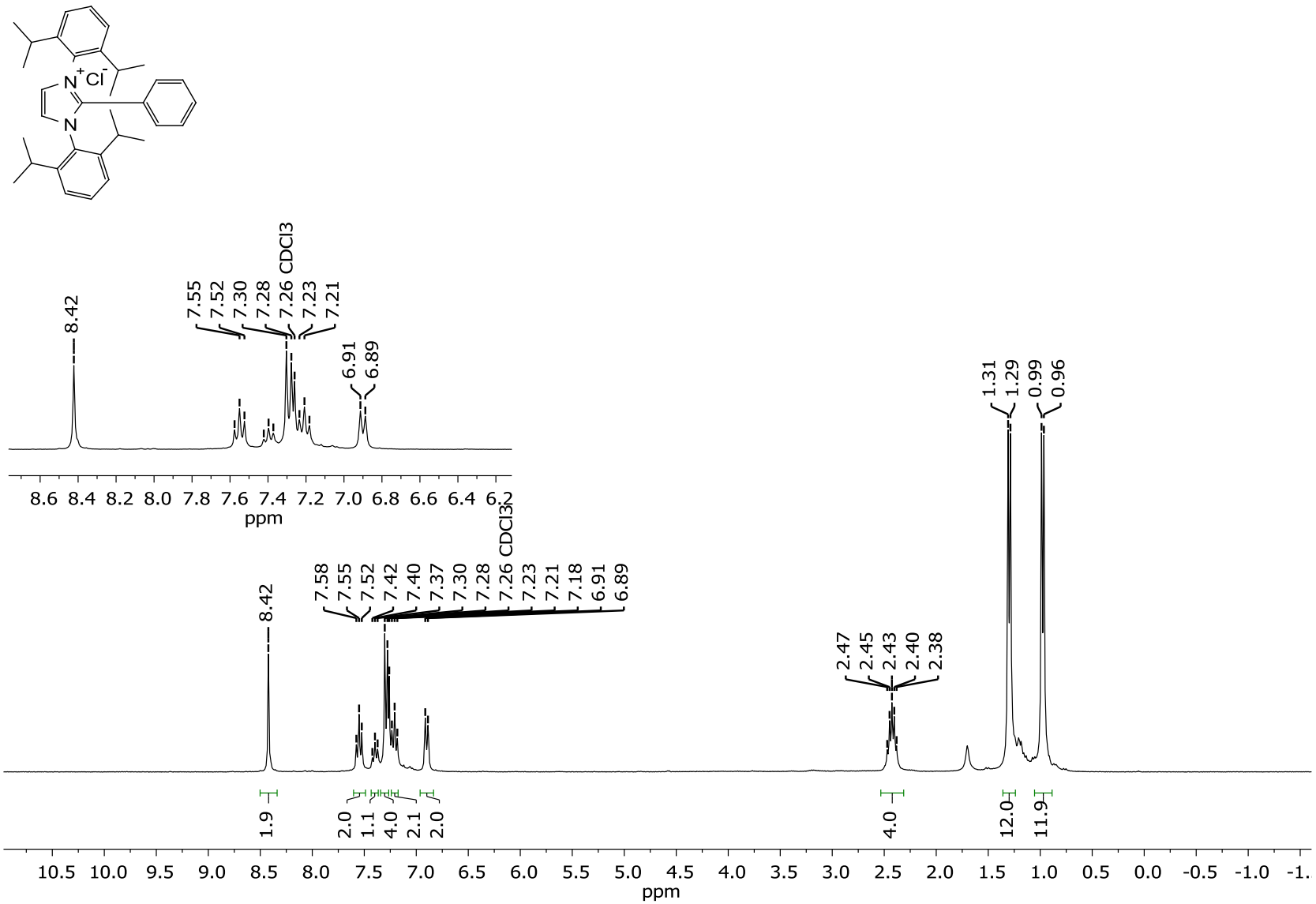

Figure S82. ^{1}H NMR spectrum of compound **7b** ($CDCl_3$, 300 MHz)

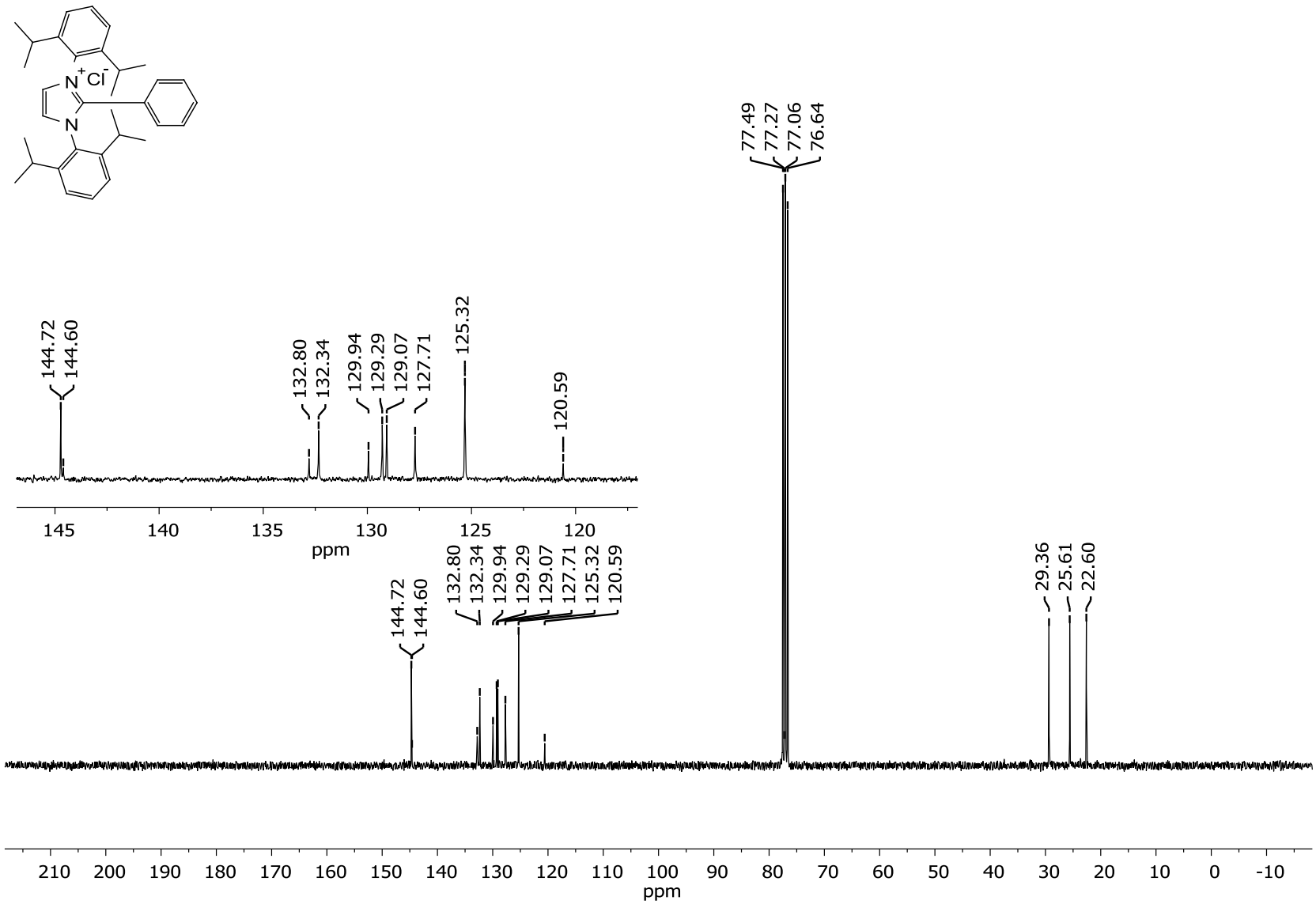

Figure S83. ^{13}C NMR spectrum of compound **7b** ($CDCl_3$, 75 MHz)